Stony Brook University

Effects of Marine Environments and Cyclic Loading

on Carbon Fiber-Vinyl Ester Composites

A Dissertation Presented

by

Arash Afshar

to

The Graduate School

in Partial Fulfillment of the

Requirements

for the Degree of

Doctor of Philosophy

in

Mechanical Engineering

Stony Brook University

December 2014

Stony Brook University

The Graduate School

Arash Afshar

We, the dissertation committee for the above candidate for the

Doctor of Philosophy degree, hereby recommend

acceptance of this dissertation.

Dr. Maen Alkhader
Dissertation Advisor, Mechanical Engineering

Dr. Fu-Pen Chiang
Committee Chair, Mechanical Engineering

Dr. T. A. Venkatesh
Outside Member, Material Science & Engineering

Dr. Chad S. Korach
Co-Advisor, Mechanical Engineering, University of Mount Union

This dissertation is accepted by the Graduate School

Charles Taber
Dean of the Graduate School

Abstract of the Dissertation

Effects of Marine Environments and Cyclic Loading

on Carbon Fiber-Vinyl Ester Composites

by

Arash Afshar

Doctor of Philosophy

in

Mechanical Engineering

Stony Brook University

2014

Fiber-reinforced composites are increasingly being employed in advanced composite based military marine crafts as they can assist in achieving cost savings, weight reductions and increased stealth capabilities. In these crafts, composites are considered for a wide range of applications, such as for superstructures, decks, bulkheads, masts and propellers, among others. However, in marine applications, composites are often exposed to aggressive environments, which include: ultraviolet radiation, salt water and cyclic loadings, to name a few. With time, such harsh elements can individually and cooperatively degrade the mechanical properties of fiber-reinforced polymer composites, diminishing their structural integrity and durability. Accordingly, ensuring the long-term reliability of composite marine crafts is instrumentally tied to characterizing the damaging effects of marine environments on fiber composites, particularly the synergistic effects as they are more severe, harder to anticipate and are not well-understood. Therefore, this work experimentally investigates the cooperative damaging effects of the long-term combined exposure to UV radiation,

moisture and cyclic (i.e. fatigue) loading on the structural integrity of the marine composite (carbon fiber reinforced vinyl-ester composite). Results demonstrate that UV radiation and moisture have synergistic deleterious effects on carbon fiber-vinyl ester composites and when combined with cyclic loading can accelerate and amplify the accumulated damage and reduce the composites' life.

Dedication

In dedication to my beloved mother and father and my beloved brothers, Babak and Ali, for supporting me all the way.

Acknowledgements

I would like to sincerely thank Professor Maen Alkhader and Professor Chad Korach for advising my research and dissertation, and their patience, insightful comments, and immense knowledge.

I would like to express my sincere gratitude to Professor Fu-Pen Chiang for introducing this project to me and for the continuous support of my research.

I would also like to thank my fellow labmates and friends Richard Anger, Heng-Tseng and Sumantu Lyer.

I gratefully thank Dr. Airan Perez, ONR Corrosion Program Officer, for supporting this work under ONR grant N00014-11-10816. I would like also to thank Dr. Yapa Rajapakse, ONR Solid Mechanics Program Officer, for his encouragement of this work.

Contents

Chapter

Tables

Table

Figures

Figure

Chapter 1

INTRODUCTION

1.1 Literature review

Carbon fiber-vinylester composites are good candidates for the marine industry and offshore structures. This is due to the high strength-to-weight ratio and the corrosion resistance of these materials. Carbon fibers are hydrophobic materials and the aqueous environment does not change their mechanical properties. Vinylester resin is also corrosion-resistant and has the ability to withstand water absorption. However, the mechanical properties of carbon fiber-vinylester composites can be deteriorated when they are exposed to different environmental conditions like moisture and ultraviolet radiation. The effect of moisture on the mechanical properties of fiber-reinforced polymeric composites has been investigated extensively in recent years [3, 4, 5, 6]. The mechanical properties of glass fiber-reinforced composites may significantly deteriorate due to moisture absorption, while this is not the case for carbon fiber-reinforced composites. This is due to the fact that carbon fibers, unlike glass fibers, are hydrophobic materials. Moisture can be absorbed into the fiber-matrix interface and replace or weaken resin/fiber chemical bonds. Moisture reduces the strength of fiber-matrix interfaces via irreversible hydrolysis and plasticization. In composite materials with brittle matrix, the damage mode can be changed from being matrix-dominated before moisture absorption to a fiber-matrix interfacial mode after saturation. This may lead to a sig-

nificant variation in the strength of the composite. In a composite with a very brittle matrix, the moisture's plasticizing effect might cause a small increase in the toughness of the material [1, 2]. The transverse strength is a mechanical property that is mostly sensitive to moisture absorption.

The weight gain of the specimen immersed in sea water is lower than the one immersed in pure water. This is due to the fact that the polymer can be considered a semi-permeable membrane and the osmotic pressure reduces the driving force for moisture absorption.

The hydrostatic pressure does not have a significant effect on the quantity of moisture absorption. The increased driving force for moisture absorption due to high pressure will be eliminated by the simultaneous reduction in free volume by hydrostatic pressure.

The effect of ultraviolet radiation on polymeric composites has been studied by different researchers [7, 8, 9]. UV light is not able to deeply penetrate composite laminates, and as a result, most of the matrix remains undamaged and fibers maintain their bonds to the matrix. Composite stiffness varies slightly due to UV radiation, as changes induced by UV radiation is a surface phenomena, while modulus is a bulk material property. In many polymers, UV irradiation initiates chain scissions, which produce small free molecules. These molecules are capped by oxygen and can be removed from the specimen, resulting in polymer weight loss. In the near-vacuum state, there is not enough oxygen to remove the small molecules from the specimen. Thus, broken bonds may be renewed, and no weight loss will be observed [10]. The energy of UV photons is almost the same as the energy of polymer covalent bonds, which is about 290-460 kJ/mole. UV photons initiate photo-oxidative reactions, which deteriorate the material by changing its chemical structure [11, 14]. Molecular chain scission and/or chain cross-linking are typically produced by photo-oxidative reactions. Chain scission reduces the molecular weight of the polymer, and lowers strength and heat resistance. Chain cross-linking increases the brittleness of the polymer, which

may result in micro-cracking. The thermal shock can intensify the effect of UV irradiation on one-ply glass/epoxy composite laminate. The UV radiation could initiate micro cracks at the irradiated surface of specimens, which can be propagated during thermal shock. No crack is observed in the case of the multi-ply glass/epoxy or graphite/ epoxy laminates due to higher thermal shock resistance of thick specimens [10].

The synergistic effects of ultraviolet radiation and moisture have also gained much attention in recent years. UV irradiation produces micro cracks on the surface of polymer composites, facilitating the ingression of moisture into the laminate. Moisture is able to dissolve and remove products of photo-oxidation reactions from a UV-irradiated surface and provide a fresh surface for further degradation by UV radiation [12, 13, 14, 15, 16, 17]. The effects of combined exposure on the mechanical properties can be more deleterious compared to individual exposures. The transverse strength is the most susceptible property and decreases substantially compared to virgin specimens, which were not exposed to any environmental conditions [14].

Based on the loading direction, different modes of damage may occur between the fiber and matrix interface. If loading direction is parallel to the fiber direction, and in the presence of strong fibers, one of these scenarios may occur [18]:

(a) No slip will occur at the fiber-matrix interface.

(b) Unbounded fibers constrained in the matrix by strain mismatches due to the initial pressure occurred by different thermal expansion, but have a tendency towards frictional slip.

(c) Fibers have weakly bonded to the matrix under initial radial tension, but they might be debonded due to the stress concentration near the tip of growing matrix crack.

In the case of weak fibers, fiber fracture occurs during the progressive fiber pull-out [19].

When the loading direction is normal to the fiber direction [20, 21, 22, 23, 24], an interface

crack between fiber and matrix is growing in three distinctive stages:

a) In presence of small debonding (smaller than 30° angles) both stress σ_{rr} and $\sigma_{r\theta}$ appears as singular in mathematical models and the crack is working in mixed mode (dominated by mode I).

b) In the interval between 60° and 70° when a contact zone is detected, only $\sigma_{r\theta}$ reaches a singular value, the crack is working in a pure shear mode.

c) At the interval between 60° and 70°, the direction of maximum circumferential stress at the neighborhood of the crack tip is approximately normal to the applied load direction. As a result, the crack corresponding to a debonding in this interval may leave the interface and penetrate the matrix.

The fracture energy of fiber-reinforced composite can be investigated by the work of fracture technique in the flexural test [25, 26]. Fracture energy λ_I corresponds to the initiation of crack propagation, while the work of fracture technique measures λ_F, an average of released energy during a whole fracture process. The work of fracture is dependent on the strain rate and fiber volume fraction, which can be explained by the investigation of the microstructure of fracture surfaces. A larger fiber pull-out is observed in smaller strain rates, thus, a higher work of fracture is needed. However, the fracture initiation energy is not strain-dependent.

Many researchers have studied the fracture of functionally graded materials in prior decades [27, 28, 29, 30, 36, 37]. Finite element analysis can be used to study crack propagation in plates made of functionally graded materials[28, 38]. The strain energy release rate G and the J-contour integral are approximately equal when Γ approaches to the crack tip (where Γ is the contour of integration). In the three-point bending test, the crack is working in mode I when it grows in the direction of material property variation and is working in both mode I and mode II when it propagates perpendicular to the direction of the material property variation [29, 30].

In the aerospace industry and offshore applications, composite materials are frequently subjected to cyclic mechanical loading and varying environmental conditions. The effect of cyclic loading on composite materials has been extensively studied in recent decades [31, 32, 33, 34, 35]. The modes of damage in composite laminates due to fatigue loading can be divided into four categories: fiber breakage, matrix cracking, fiber-matrix decohesion and delamination. In low stiffness fiber composites like glass-epoxy, the limiting strain for the matrix material defines the fatigue limit. However, this is not true for high stiffness fiber composites (e.g. carbon-epoxy)[39]. The fatigue damage during compressive loading is more detrimental than that during tensile loading, as the role of the matrix and the fiber/matrix interface becomes more significant [40, 41]. The worst-case fatigue loading scenario is tension-compression, which produces the maximum damage to fiber-reinforced composite materials [40].

Fatigue models based on cumulative damage have been investigated by several researchers [42, 43, 44, 45, 46]. In homogeneous materials, the damage accumulates at a slow rate in the beginning of the fatigue life, and then, a dominant crack grows in a direction normal to the loading direction. On the other hand, in composite materials, the heterogeneous characteristic of composites lead to the presence of many modes of fatigue damage. Extensive matrix cracking appears at the early stages of fatigue life. In the intermediate stage, damage is growing at a relatively slow and steady rate, which is related to the stable crack growth along the fiber-matrix interface. Finally, the damage grows rapidly again during the last stage of the fatigue life due to the failure of fibers [47, 49]. Generally, in fiber-reinforced composite laminates, matrix cracking and delamination occur early in the fatigue life. On the other hand, fiber-matrix debonding and fiber failure accumulate slowly at the beginning of the fatigue life and accumulate rapidly when the specimen approaches the final failure [50, 51].

In Glass Fiber Reinorced Palstic (GRP) specimens, the strength-log life curves are characterized by gradual accumulation of damage until the composite material fails due to the level of loading. On the contrary, Carbon Fibre-Reinforced Plastics (CRFP) specimens experience a small reduction in strength during fatigue life until the final failure of fibers [48, 49].

The fatigue behavior of unidirectional fiber-reinforced composites has been studied by many researchers [52, 53, 54, 55, 56]. It has been shown that the final fracture of off-axis samples, due to fatigue loading, occurs along the fiber direction. In on-axis samples, two different scenarios may occur. In composites with strong fiber-matrix interfaces, the final failure occurs in the form of fiber breakage. On the other hand, matrix splitting along the fiber direction is a final failure mode of composites with weaker fiber-matrix interfaces.

Typically, the strength of the fiber-matrix interface is an important factor in the damage accumulation of graphite/epoxy laminates during the fatigue life [50, 51]. The fiber-matrix interface can be changed by fiber surface treatment and fiber sizing or by altering the polymeric resin. At high loading levels, the presence of longitudinal cracks in the laminates with weaker fiber-matrix interfaces prevents stress concentration on the fibers and leads to a longer fatigue life. However, at low loading levels, the presence of longitudinal splitting reduces the effective length of fibers, which results in a shorter fatigue life [51].

Further investigation of the flexural fatigue behavior of fiber-reinforced plastic composites [57, 58, 59] is critical for the marine and aerospace industries, as bending loading is a dominant force on relevant structures. In hybrid glass-carbon fiber-reinforced epoxy matrix composites, reduction in material strength and elastic modulus is due to the flexural fatigue, which is dependent on the fatigue loading level. However, the damage accumulation in the stiffness during the fatigue life is dissimilar to accumulated damage in the strength [60]. For cross-ply ($0^\circ/90^\circ$) carbon

fiber-reinforced epoxy laminates with high resistance to interlaminar fracture, the fatigue limit is defined by the compressive stress of the 0° layers. However, for laminate with low resistance to interlaminar fracture, the fatigue limit significantly decreases, as the mode of failure changes to delaminations between 0° and 90° plies of the laminate during fatigue loading [61]. In flexural fatigue with constant displacement amplitudes, the maximum applied force will decrease during the fatigue life, showing a continuous degradation of the bending modulus [62].

Several researchers have studied the effects of environmental degradation on the fatigue life of composite materials [42, 63, 64, 65, 2]. The loss in tensile strength and modulus due to cyclic loading in an aqueous environment is greater than that in the air. For any type of moist environment, when the S-N curves of glass-reinforced vinylester composites are normalized to their respective Ultimate Tensile Strength (UTS), they will collapse on top of one another. This indicates that the environmentally aged and virgin specimens experience a similar fatigue failure mechanism [2]. It has been shown that the flexural failure stress of a cross-ply carbon fiber/epoxy composite laminate, environmentally degraded by exposure to UV radiation and condensation, is equivalent to the failure stress of a virgin composite laminate subjected to 50,000 cycles of mechanical fatigue at 50% of its UTS [65].

1.2 Organization of this dissertation

In chapter 2, experimental measurements of the mechanical properties of unidirectional carbon fiber-vinylester composite laminates after long-term, indoor immersion (laboratory-controlled) and outdoor exposure are presented. Additionally, a comparison of these two conditions will be discussed. In chapter 3, a method is presented to model changes in the mechanical properties of carbon fiber/vinyl ester composite laminates degraded by ultraviolet radiation and moisture. This

model predicts changes in the mechanical properties associated with the thickness direction of composite laminates for a given exposure time. In the chapter 4, a fatigue damage model is developed to predict degradation in the stiffness and strength of unidirectional carbon fiber-vinylester composites. Describing and modelling different modes of fatigue damage in aged and virgin carbon fiber-vinyl ester composites are presented here. In chapter 5, uni-axial cyclic loading is applied to composite coupons after environmental condition exposure, the effects of which will be determined by modulus evolution during the fatigue life and post-fatiguing three-point bending test. In chapter 6, the deterioration in the integrity and protective abilities of marine coating systems, due to the long-term combined exposure to UV, sea water and flexural cyclic loading, is investigated.

Chapter 2

Effect of Long-Time Environmental Exposures

2.1 Introduction

Composites used in infrastructure and structural applications can be exposed to environmental conditions, initiating degradation in the composite due to stress, UV radiation, moisture and chemical effects. Combined exposure of UV radiation and sea water creates synergistic degradation, and is generated from cyclic exposure to the individual conditions. In this work, three separate exposure systems are used to age carbon fiber-reinforced vinylester composites: UV radiation, salt spray, and humidity environmental chambers; full sample immersion in salt and sea water conditions; and outdoor exposure in a tidal pond. Characterization of the time-dependent changes in the mechanical strength and modulus of the coupons is performed for each environment. Comparison between the conditions will be discussed in the context of long-term outdoor exposure with accelerated laboratory conditions.

2.2 Experimental setup

Carbon fiber-reinforced vinylester unidirectional composite laminates (Graphtek LLC) were used in these experiments, Table 2.1. Composite laminate sheets with nominal thickness of 1.4 mm were machined using a diamond wet saw into 12.5 x 77 mm (width x length) coupons with [0]

and [90] fiber directions.

Table 2.1: Material properties

Property	Carbon Fiber	Vinyl Ester
Longitudinal modulus (GPa)	220	3.2
Transverse modulus (GPa)	22	3.2
Tensile strength (MPa)	3,530	88
Poisson's ratio	0.29	0.29
Glass transition temperature (C)	N/A	130

Three-point bending tests were performed on the composite samples following the ASTM D790 standard, using a screw-driven mechanical loading frame (TiraTest 26005) with a 0.5 kN load cell. Support geometry followed ASTM D790, with the support span set for 60 mm resulting in a span/thickness ratio of ~ 43. A cross-head rate of 4.25 mm/min was used to produce a strain rate of 0.01 mm/min (see Fig. 2.1).

The energy release rate was determined using the Double Edge Notch (DEN) specimens in a hydraulic mechanical loading frame (Instron 8501). A gauge length of 102 mm was used with the edge notches in the center of the gauge. A cross-head rate of 2 mm/min. was employed, and the load at first failure was recorded. Tensile modulus of an un-notched specimen was measured with the incrementally increasing load, and recording the corresponding strain to compute the tangent modulus.

2.3 Exposure conditions

The first group of samples were exposed to 800 and 2000 hours of combined and individually-accelerated aging, respectively, before characterization utilizing two chambers: i) Moisture and heat in a Tenney Benchmaster BTRS temperature and humidity chamber, and ii) UV radiation/condensation in a Q-Lab QUV/se accelerated weathering chamber. UV radiation simulates natural sunlight using

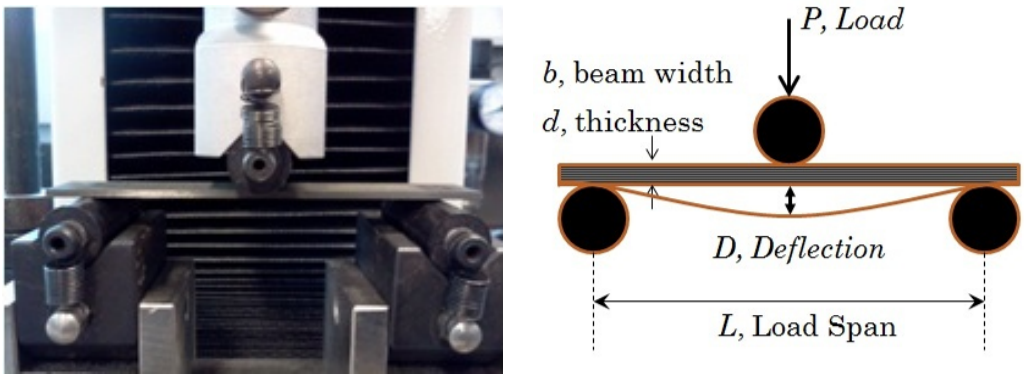

(a) (b)

Figure 2.1: Setup of three-point bending test

fluorescent UV bulbs at a 340 nm wavelength. Intensity is monitored by real-time UV irradiance sensors. Temperature is controlled using a blower. Condensation is provided with water evaporation, which condenses on the sample surfaces. One-half of the samples are rotated between the two chambers every 24 hours to create a combined effect between controlled constant temperature and humidity and the cyclic UV radiation/condensation condition. The conditions in the chambers remained constant for the duration of the exposure. In the combined temperature and humidity chamber, moisture was set at 85% relative humidity (RH) and temperature at 35C. In the QUV chamber, the UV radiation and condensation conditions cycled every 3 hours. For the UV cycle, the UV irradiance was set at 0.6 W/m2 at 60C, and the condensation cycle was set at a temperature of 50 C (see Fig. 2.2).

The second group of samples were immersed in distilled water, salt water, and sea water for six months and one year durations at room temperature, in closed containers and in a dark environment. The third group of samples were mounted on a frame with four different levels, which was placed in a tidal pond for six months and one year. Based on the position of the samples on the ladder frame, samples were exposed to varying amounts of sea air (containing sunlight and

humidity) and sea water. The four levels of the frame are as follows: The upper level (Row 1) samples always remained out of water and the samples were exposed to the sea air only for the entire duration. The samples in the second level (Row 2) were exposed to 18 hours of sea air and 6 hours of sea water immersion for each day; two cycles of 9 hours of sea air followed by 3 hours of sea water. The samples in the third level (Row 3) were exposed to 6 hours of sea air and 18 hours of sea water immersion for each day; two cycles of 3 hours sea air followed by 9 hours of sea water. The samples in the lower level of the frame (Row 4) are immersed for the entire duration in sea water. Five specimens per condition were used in the experiments (see Fig. 2.3).

(a)

(b)

(c)

Figure 2.2: Environmental Chambers:(a) Heat and Humidity (b) Salt Spray

(c) UV-Condensation

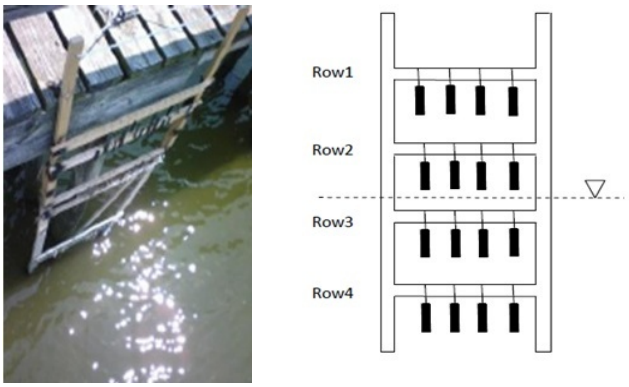

Figure 2.3: The ladder frame in tidal pond

2.4 Specimen weight changes as a function of duration

Weight measurements of the composite samples were made every 48 hours for the environmental chambers. Percent weight change was calculated by taking the difference between the original sample weight and the measured weight at specific times, divided by the original weight and multiplied by 100. The results indicate that samples constantly exposed to moisture and salt spray all had eventual mass gain, reaching a steady-state due to moisture uptake. There was a significant difference between the specimens in the combined UV-salt spray condition versus those in the constant moisture condition, particularly for the salt spray cases (Fig. 2.4). The decrease in mass after a peak value of 500 hours for the combined UV-salt spray cases indicates loss of surface material due to degradation and erosion of the matrix.

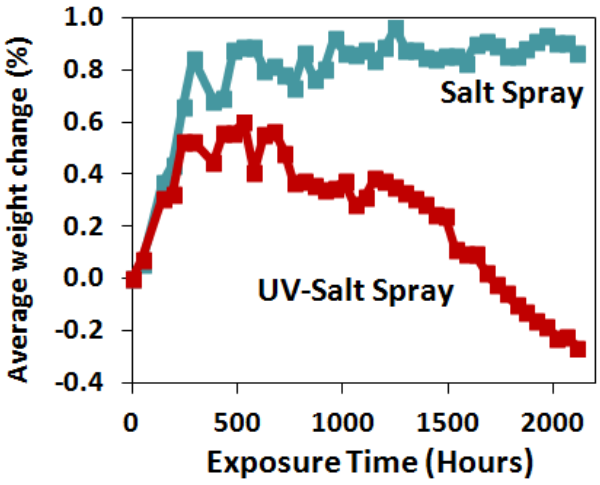

Figure 2.4: Average sample weight change for constant salt spray and combined UV-salt spray exposed carbon fiber / vinylester composites. Decrease in UV-salt spray sample weight after 500 hours due to photodegradation material losses.

2.5 Characterization of the time-dependent changes

Here, characterization of the time-dependent changes in the mechanical strength and modulus of the carbon fiber/vinylester coupons is performed for different environmental conditions. Comparison between the conditions will be discussed in the context of long-term outdoor exposure and indoor immersion with accelerated laboratory conditions.

The bending modulus of samples can be obtained as:

$$E = \frac{L^3 m}{4bd^3} \tag{2.1}$$

where L is the load span, b is the width of the sample, d is the thickness of the sample and m is the slope of load displacement curve, which is shown in Fig. 2.5.

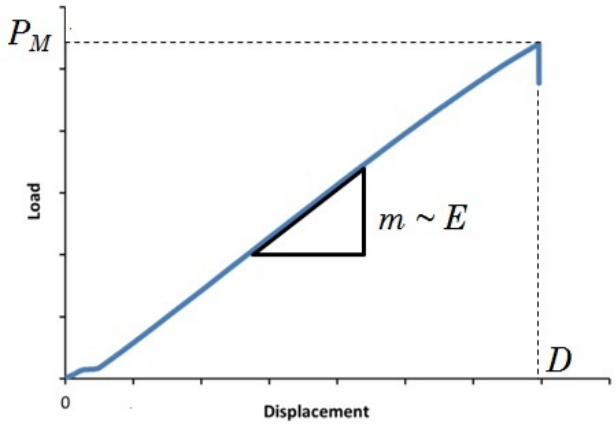

Figure 2.5: Schematic load-deflection curve

Based on the ASTM D790 standard, bending strength of samples can be obtained with:

$$\sigma_f = \frac{3P_M L}{2bd^2}\left[1+6(\frac{D}{L})^2-4(\frac{d}{L})(\frac{D}{L})\right] \tag{2.2}$$

where P_M is the fracture load and D is the deflection. Two additional terms are added to the fracture strength formula of simply supported beams. These terms are correction factors in the case of large deformation, which is assessed when the deflection to the load span ratio is more than 1:10. In this case, higher load levels occur in the supports, which alter the moment in the simply supported beam. Samples with 0 degree fiber orientation usually experience a large deformation in the flexural test, while this is not the case for samples with 90 degree fiber orientations.

2.5.1 Mechanical flexural response

Samples (all [0] fiber direction) exposed to different environmental exposures have been characterized by three-point bending to determine flexural modulus and residual strength (ASTM D790) [71]. All exposure conditions showed an insignificant difference in the flexural modu-

lus when compared to the unconditioned specimens, and within experimental error, Fig. 2.6 and Fig. 2.8. Results showed that the flexure strength decreases up to 18% for both indoor immersion and outdoor exposure, Fig. 2.7. There is a minimal difference in residual flexural strength of samples immersed in distilled, salt and sea water. The data from outdoor exposure shows that higher degradation is occurred in flexural strength of samples immersed in sea water for a longer period of time. No significant changes in flexural modulus and flexural strength have been observed between 6 month and 1 year of indoor immersion or outdoor exposure. On the contrary, in the environmental chamber, a substantial decrease in flexural strength of samples with 2000 hours of exposure time compared to 800 hours of exposure time has been observed, Fig. 2.9. This may due to the elevated temperatures in the laboratory chambers (50 to 60 C) when compared to the temperatures of immersion (21C) and of outdoor environments.

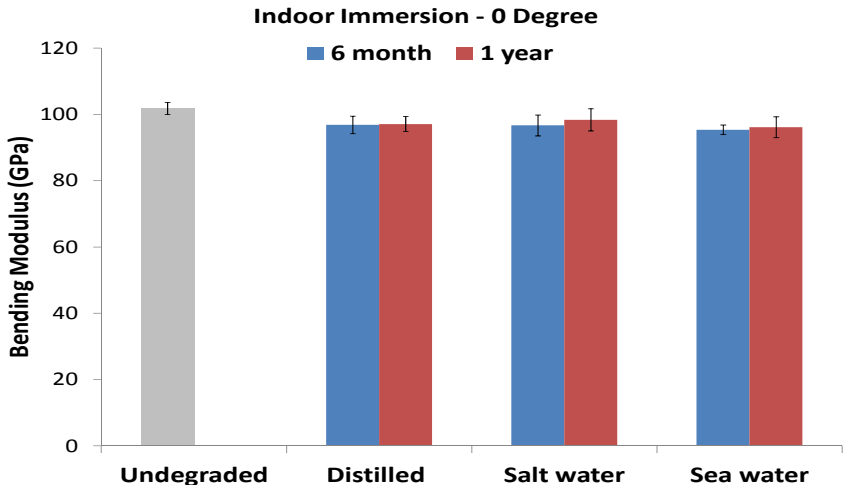

(a)

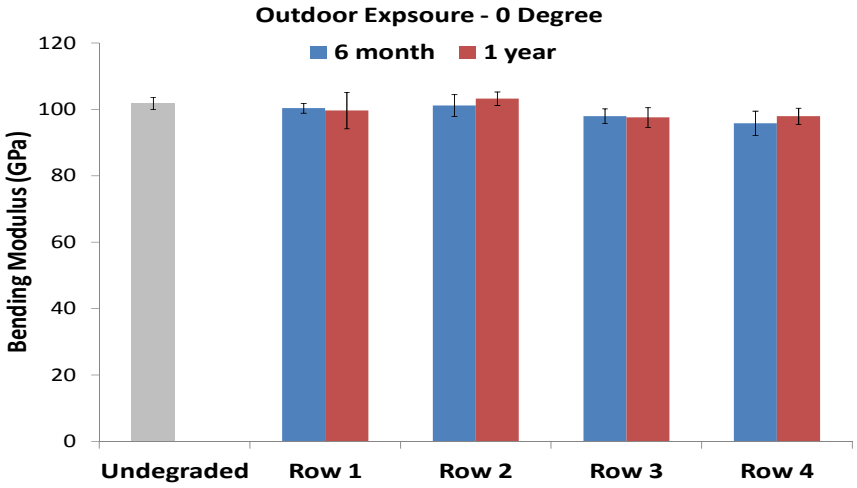

(b)

Figure 2.6: Flexural modulus degradation due to (a) indoor immersion (b) outdoor exposure

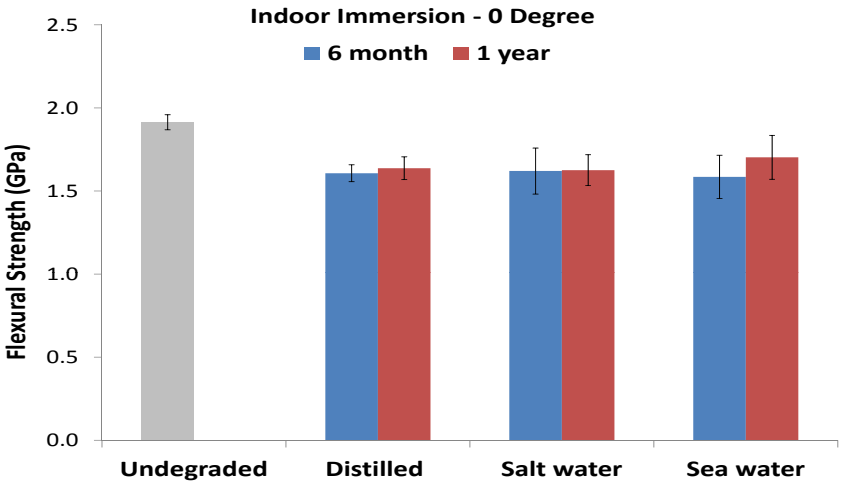

(a)

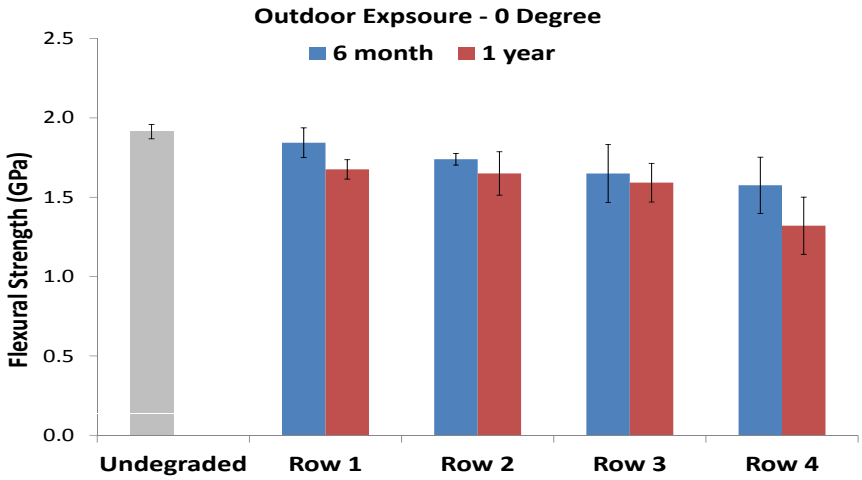

(b)

Figure 2.7: Flexural strength degradation due to (a) indoor immersion (b) outdoor exposure

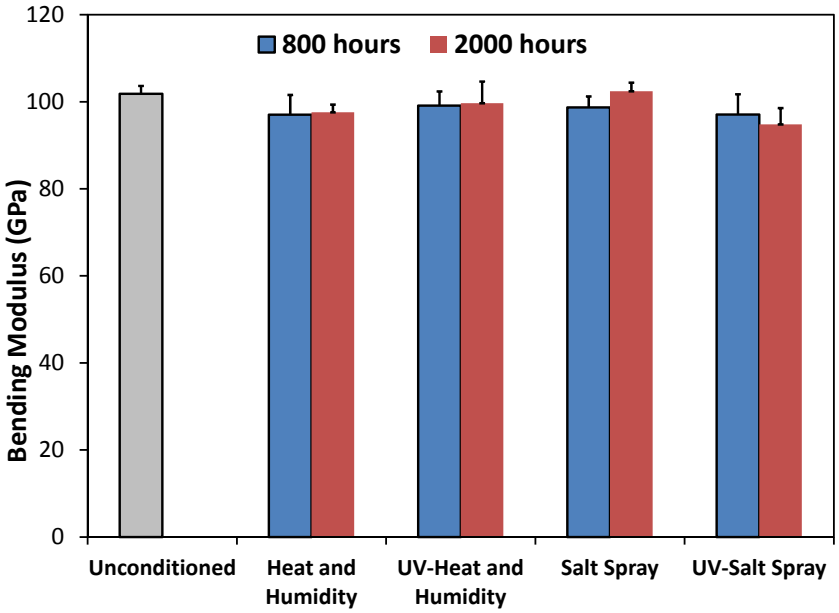

Figure 2.8: Flexural modulus degradation in the environmental chamber

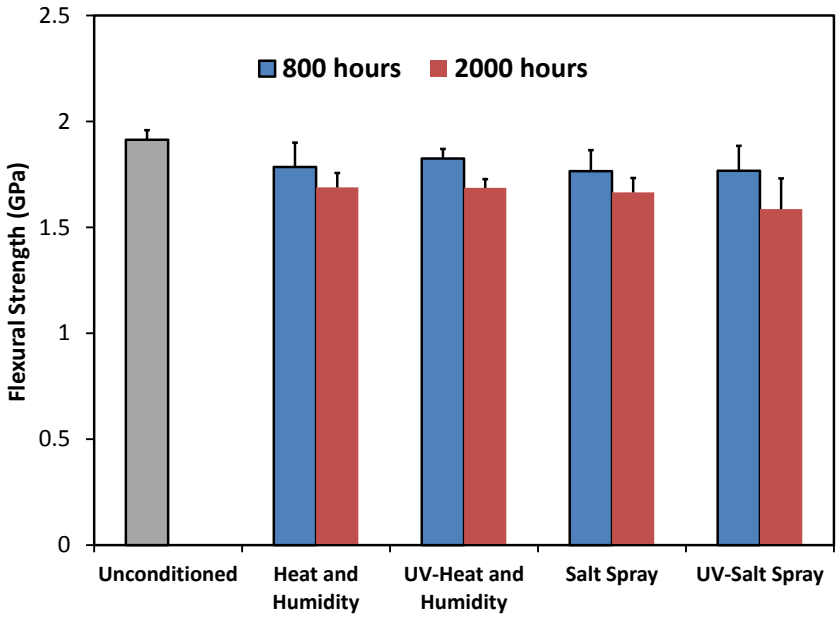

Figure 2.9: Flexural strength degradation in the environmental chamber

2.5.2 Fracture strength

The energy release rate of longitudinal fracture of samples from the tidal pond after a 6-month outdoor exposure and indoor immersion were characterized with the method used in [120], which utilizes the shear-lag model. Samples were all 0° fiber composites with double-edge notches (DEN), machined across the fibers with a diamond saw. All exposure conditions showed a decrease in the energy release rate compared with the unconditioned specimens (Fig. 2.10). To compute the energy release rate, the tensile modulus of an un-notched specimen was measured with strain gauges, which were then used to compute the tangent modulus (determined to be 120 GPa). Cases which were fully immersed in sea water showed a decrease of 65% in their energy release rates.

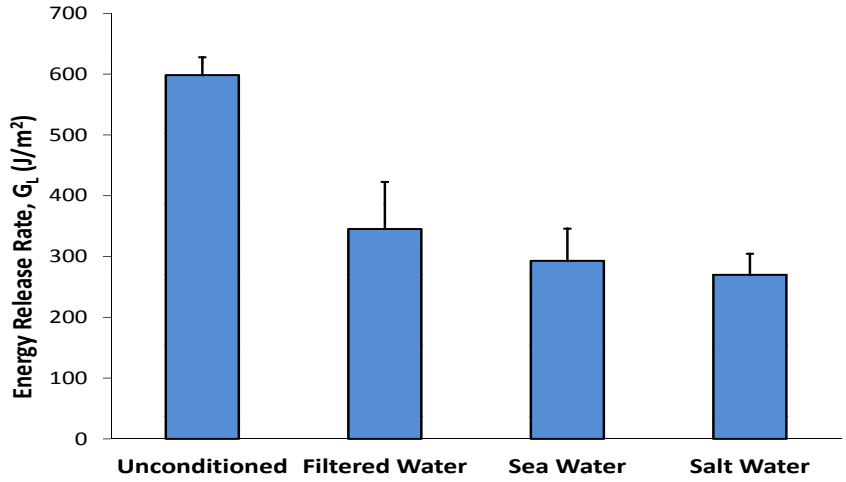

(a)

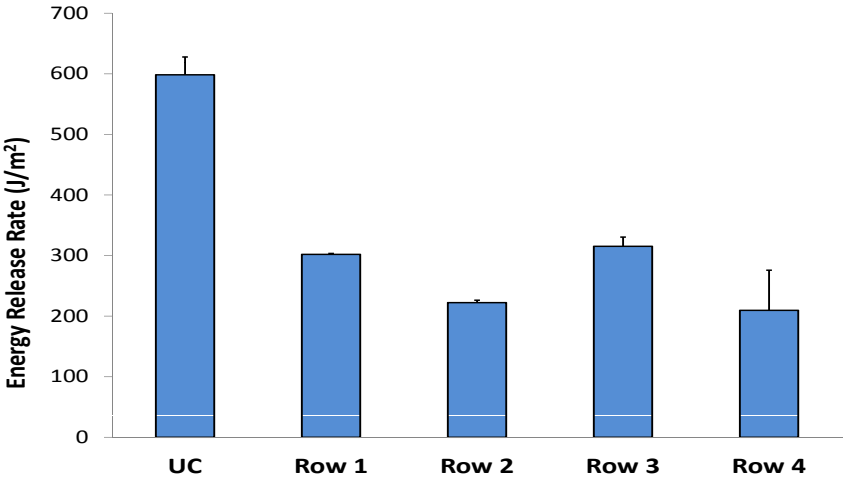

(b)

Figure 2.10: The energy release rate for longitudinal fracture of samples degraded by a 6-month (a) indoor immersion (b) outdoor exposure

2.6 Conclusion

Carbon fiber-reinforced vinyleseter unidirectional composites were characterized by long-term outdoor exposure to UV radiation, humidity and sea water; indoor immersion in distilled, salt and sea water; and exposure to UV radiation, salt spray, and humidity in accelerated weathering chambers. The current study shows that the effect of various types of exposure on the flexural modulus of [0] fiber direction samples is minimal. However, the flexural strength has been diminished significantly. This might be due to degradation of the fiber-matrix interface via hydrolysis and plasticization during moisture absorption, which deteriorates the load transfer mechanism between the matrix and fibers. Extensive micro-cracking on the surface of the composite samples induced by UV radiation is another factor in the reduction of flexural strength of samples exposed long-term to UV radiation. The energy release rate was computed for 0 DEN samples in tension. While a decrease in the energy release rate was found to occur for all samples subjected to different environmental exposure in a tidal pond, full immersion in sea water leads to the largest decrease in the energy release rate.

Chapter 3

Environmental Damage in Composites

3.1 Introduction

Fiber-reinforced polymer (FRP) composites, by virtue of their ability to provide higher stiffness- and strength-to-weight ratios, lower radar signatures, and better resistance to electro-chemical corrosion, as compared to metals, are increasingly used in new classes of naval crafts. In the move towards composites, marine industries have adopted carbon fiber-reinforced vinyl ester composite, as vinyl ester is more tolerant to marine elements, such as UV radiation and moisture, than are many other epoxies and polymers. UV radiation and moisture, individually and synergistically, adversely affect polymers through various, and often, interacting mechanisms. UV radiation, through photo-oxidation, molecular chains sessions, and chain cross-linking, can increase polymers' brittleness and introduce micro-cracks, which negatively affect the structural properties of fiber composites (e.g., reduction in elastic properties and strength). Moisture, on the other hand, diffuses into FRP composites and, through plasticization and hydrolysis, can damage the composites matrix and fiber-matrix interfaces, effectively reducing the composite's strength. The aforementioned corrosive and erosive elements (UV radiation and moisture) have limited damaging effects on carbon fiber-reinforced vinyl-ester laminates. Therefore, this composite, even after long-term exposure to marine environmental elements, exhibits confined surface damage that has

negligible effects on most properties of the composite. However, as this surface damage coincides with the location of maximum flexural stresses, it can critically impact the flexural properties of the composite for marine applications; particularly, as composites used in marine applications are often subjected to out of plane loads. Although potentially critical, the damaging effects of marine environments on the flexural properties of carbon fiber vinyl-ester composites have not yet been fully characterized. Hence, this work aims to characterize the effects of long-term exposure to UV radiation and moisture on the flexural properties of carbon fiber vinyl-ester composites.

3.2 Experimental details

Carbon fiber-reinforced vinyl ester unidirectional composite laminates (Graphtek LLC) were used for all experiments and conditions (see Table 2.1). Composite laminate sheets with a nominal thickness of 1.4 mm were machined (using a diamond wet saw) into 12.5 $\times$ 77 mm coupons for flexural testing with two fiber directions: [0] and [90]. Samples were exposed to 1000 hours of individual and combined radiation/condensation in a Q-Lab QUV/se accelerated weathering chamber. UV radiation simulates natural sunlight by using fluorescent UV bulbs at a 340 nm wavelength. UV irradiance was set to 0.6 W/m2 at 60 C. Intensity is monitored by real-time UV irradiance sensors, while the temperature is controlled using a blower. Condensation cycles are characterized by 50 C temperature-controlled settings in which water evaporation leads to condensation on sample surfaces. For the combined exposure condition, the UV radiation and condensation cycles alternated every 3 hours in the chamber to provide a synergistic effect of both environmental conditions. Three-point bending tests were performed on the composite samples following the ASTM D790 standard, using a screw-driven mechanical loading frame (TiraTest 26005) with a 0.5 kN load cell. Support geometry followed ASTM D790, with the support span

set to 60 mm, resulting in a span/thickness ratio of ~ 43. A cross-head rate of 4.25 mm/min. was used to give a strain rate of 0.01 mm/min. The fiber volume fraction was determined to be 56% based on the image analysis of polished cross-sections. Three to five specimens per fiber orientation and condition were used in these experiments.

The surface microscopy was performed by Hitachi Scanning Electron Microscopy (see Fig. 3.1) and Keyence Digital Microscopy (see Fig. 3.2).

Figure 3.1: Hitachi Scanning Electron Microscope

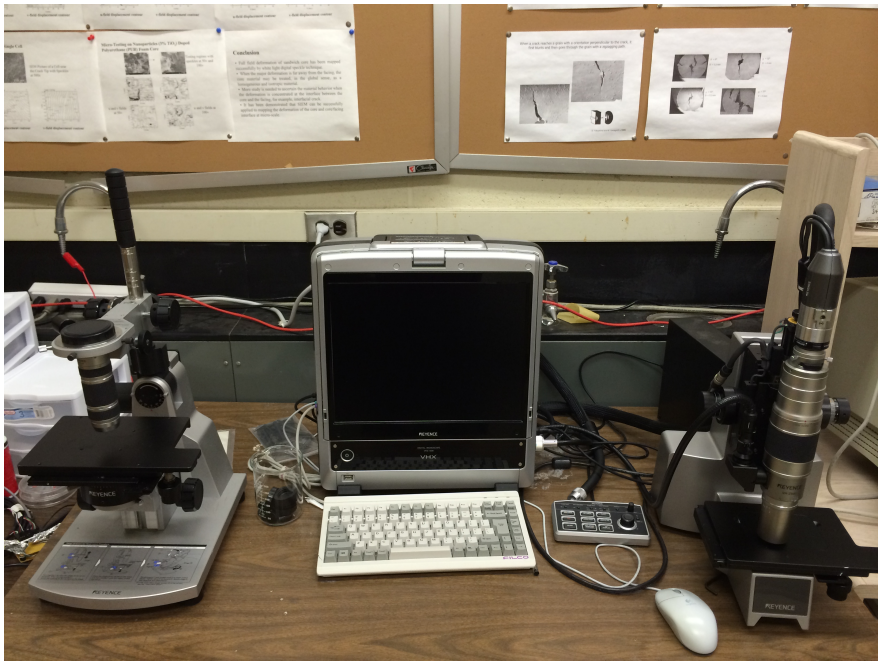

Figure 3.2: Keyence Digital Microscope

3.3 Laminate mechanical properties

The flexural properties of virgin and environmentally aged carbon fiber vinyl ester composites, based on the assumption of uniform degradation, are given in Tab.3.1. E_L is a longitudinal modulus, E_T is a transverse modulus, Ult_L represents longitudinal strength, and Ult_T denotes transverse strength. The exposure time for all conditions is set to 1000 hours.

Table 3.1: Mechanical properties of carbon fiber-vinyl ester composite laminates

Property	Virgin	UV	Moisture	UV and Moisture
$E_L(GPa)$	101.8±1.8	102.8 ±1.45(1%)	97.7±1.7(−4%)	99.6±4.9(−2%)
$E_T(GPa)$	7.01±0.197	6.638±0.19(−5%)	6.83±0.14(−3%)	6.53 ±0.04(−7%)
$Ult_L(MPa)$	1822.5±45.4	1733.1 ±60.1(−5%)	1784.9 ±25.2(−2%)	1705.86±41.2(−6%)
$Ult_T(MPa)$	103.9±5.4	91.8 ±5.6(−12%)	95.5 ±5.2(−8%)	72.66±3.11(−30%)

The effects of different environmental conditions on the longitudinal modulus of carbon fiber-vinyl ester composites are small. This is due to the fact that the longitudinal modulus is

primarily a fiber-dominant property and the mechanical properties of carbon fibers are not degraded by UV radiation and moisture.

Other mechanical properties are degraded with different types of exposures. UV exposure initiates photo-oxidative reactions and produces micro-cracks on the surface of polymeric composites. Longitudinal strength (-6%), transverse modulus (-7%) and transverse strength (-12%) are reduced by UV irradiation. Moisture also has a detrimental effect on the mechanical properties of carbon fiber-vinyl ester composites by weakening fiber-matrix interfaces. Transverse strength is the property that is most highly degraded by moisture absorption(-8%). The synergistic effects of UV radiation and condensation produce maximum damage in the longitudinal strength, transverse strength and traverse modulus of samples. The damage in samples' transverse strength due to combined exposure (-30%) is higher than the the sum of the damage induced by individual exposures. Since the combined UV radiation/moisture exposure has the most detrimental effect on the mechanical properties of carbon fiber-vinyl ester composites, the investigation of different modes of environmental damage for this type of exposure is critical. As aforementioned, the maximum damage due to combined exposure to corrosive and erosive elements occurs in the transverse strength of samples. Modeling the transverse modulus through the thickness of the aged composite laminates provides us with a feasible method of finding the bending stress distribution and true failure stress of the specimens.

3.4 Lamina mechanical properties

The aging-induced damage's effect on the structural integrity of the carbon fiber-vinyl ester laminate is observed through changes in the specimens flexural stiffness and strength, which are computed via laminate theory and 3-point bend tests. With aging, stiffness of the laminate, along

with thickness, become heterogeneous and usually follow steeply varying functions that are hard to measure. Accordingly, it is customary to define effective (average) elastic properties at the lamina level and determine their values with 3-point bend tests. To assist in this step, we invoke the observation that damage zones have sub-lamina length scales and assume that damage uniformly affects the exposed external lamina. Applying these assumptions to laminate theory results in differing values of lamina properties, specifically stiffness and ultimate strength, listed in Tab. 3.2. Results demonstrate that, in general, transverse properties are more sensitive to aging than are the longitudinal properties. This observation is expected, as the longitudinally-oriented fibers, which are less susceptible to aging than is the vinyl-ester matrix, are the main contributors to the composites structural properties. In regards to the longitudinal properties, moisture caused a 10% drop in stiffness and strength, exhibiting worse aging effects than did UV radiation. In the case of transverse direction, Tab. 3.2 shows that UV radiation (-16% in stiffness and -22% in strength) is more damaging than is moisture (-8% in stiffness and -13% in strength) to composite laminates, however, the combined exposure to UV radiation and moisture produces the most damaging effects (-21% in stiffness and -40.5% in strength) when compared to that of individual environmental conditions.

Table 3.2: Mechanical properties of carbon fiber-vinyl ester composite laminas

Property	Virgin	UV	Moisture	UV and Moisture
$E_L(GPa)$	101.8	104.829 (3%)	89.378 (-12%)	95.134 (-7%)
$E_T(GPa)$	7.01	5.88 (-16%)	6.45 (-8%)	5.56 (-21%)
$Ult_L(MPa)$	1822.5	1767.3 (-3%)	1632.86 (-10.4%)	1629.47 (-10.6%)
$Ult_T(MPa)$	103.9	81.35 (-22%)	90.14 (-13.2%)	61.81 (-40.5%)

3.5 Modes of environmental damage in transverse modulus

The transverse modulus of an environmentally-aged unidirectional carbon fiber-vinyl ester composite laminate can be obtained with a modified Halpin-Tsai formulation [66]:

$$E_T(z) = \frac{1+\zeta(z)\eta c_f}{1-\eta c_f} E_m(z)$$
$$\eta = \frac{\frac{E_f}{E_m(z)} - 1}{\frac{E_f}{E_m(z)} + \zeta(z)} \tag{3.1}$$

where $E_T(z)$ is the transverse modulus of the aged sample in the thickness direction. E_f is the transverse modulus of fibers. $E_m(z)$ represents the transverse modulus of the matrix in the thickness direction. $\zeta(z)$ symbolizes a factor, which is dependent on the reinforcement, fiber-matrix load sharing mechanism, and loading condition. And $E_m(z)$ and $\zeta(z)$ will be defined in the following sections.

3.5.0.1 Damage in fiber-matrix interfaces

Moisture may penetrate into the fiber-reinforced polymeric composites via different mechanisms, including diffusion, the capillarity along the fibers, fiber-matrix interfaces, and transportation through microcracks [70]. Moisture can deteriorate the fiber-matrix interface via hydrolysis and plasticization. Figure 3.3 shows the effect of moisture on the fiber-matrix interface on the fracture surface of a sample with a 90 degree fiber orientation. The fiber-matrix interface debonding has a deleterious effect on the transverse modulus of unidirectional composite laminates. The fiber-matrix interface degradation can be dependent on the amount of moisture absorbed by the composite. Fibers have very weak bonds to the matrix on laminate surfaces due to moisture saturation. This damage can be intensified in the presence of UV radiation. The fiber-matrix bonds are stronger in the thickness direction of the laminate due to greater moisture content on the surface

than within the laminate. The effect of fiber-matrix debonding on the transverse modulus can be modelled by reducing the contribution of the fiber reinforcement to the transverse modulus of the composite laminate. To do so, $\zeta(z)$ can be defined as

$$\zeta(z) = \zeta_0(\alpha_1 - \beta_1 e^{c_1(1-\frac{h}{2|z|})}) \quad \frac{-h}{2} \leq z \leq \frac{h}{2} \tag{3.2}$$

where ζ_0 is a constant factor for virgin samples. h is the thickness of the composite plate and α_1, β_1 and c_1 are constants. A small amount of moisture diffusion occurs at the greatest depth of the composite laminate, thereby, fibers are fully bonded to the matrix at the middle plane of the laminate.

$$\zeta(z) = \zeta_0 \tag{3.3}$$

To satisfy the above condition, $\alpha_1 = 1$. Fibers are considered fully debonded from the matrix on the laminate surface due to moisture saturation and UV radiation. Therefore,

$$\zeta(h/2) = \zeta(-h/2) = 0 \tag{3.4}$$

To satisfy the above condition, $\alpha_1 = \beta_1$. The contribution of fiber-reinforcement to the transverse modulus can be simplified to:

$$\zeta(z) = \zeta_0(1 - e^{c_1(1-\frac{h}{2|z|})}) \quad \frac{-h}{2} \leq z \leq \frac{h}{2} \tag{3.5}$$

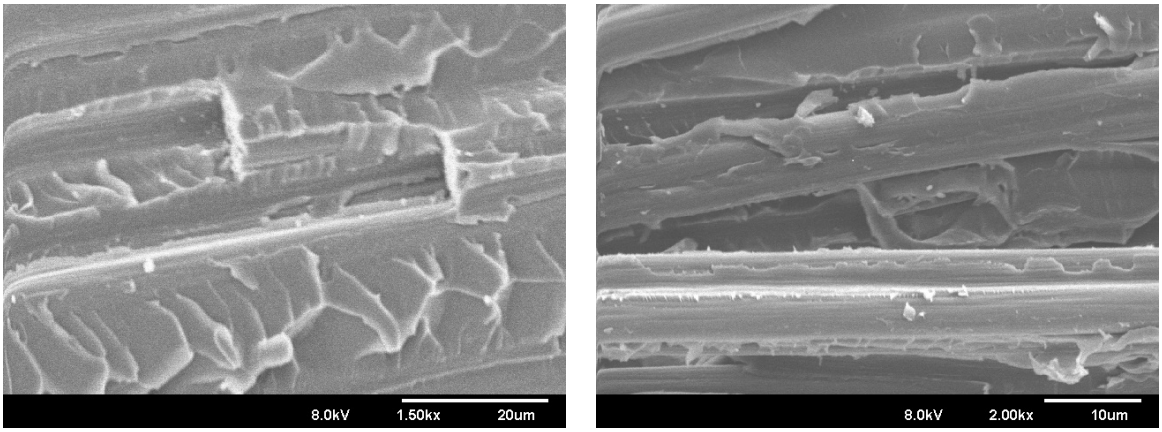

(a) (b)

Figure 3.3: The micrograph of the fiber-matrix interface in the fracture surface of samples with 90 degree fiber orientation using Scanning Electron Microscopy (a) Virgin (b) Aged

3.5.0.2 Damage in matrix

Ultraviolet radiation produces extensive micro-cracking on the surface of the composite laminate. The damage can be intensified in the presence of moisture. Figure. 3.4 shows the edge of a sample with 0 degree fiber orientation, which has been degraded by ultraviolet radiation and moisture. The damaging effects of ultraviolet radiation is primarily a surface phenomenon and degrade the mechanical properties of the thin, topmost layer on the surface of composite laminates. The matrix can also be degraded by moisture-induced micro-cracks due to plasticization. The matrix modulus, through the thickness of the laminate, can be expressed with a similar function as in equation Eqn. 3.6

$$E_m(z) = E_{0m}(\alpha_2 - \beta_2 e^{c_2(1-\frac{h}{2|z|})}) \quad \frac{-h}{2} \leq z \leq \frac{h}{2} \tag{3.6}$$

where α_2, β_2 and c_2 are constants. In the middle of the laminate, no UV penetration is expected. Therefore, the matrix is considered undamaged,

$$E_m(0) = E_{0m} \tag{3.7}$$

which results in $\alpha_2 = 1$. On the surface of the laminate, due to the extensive micro-cracking, the matrix is significantly degraded. Thus,

$$E_m(h/2) = E_m(-h/2) \approx 0 \tag{3.8}$$

The contribution of the matrix modulus in the transverse modulus can be rewritten as:

$$E_m(z) = E_{0m}(1 - e^{c_2(1-\frac{h}{2|z|})}) \quad \frac{-h}{2} \leq z \leq \frac{h}{2} \tag{3.9}$$

The schematic profiles of ζ and the matrix modulus in the thickness direction of the composite laminate are given in Fig. 3.5. As discussed earlier, a thin layer of matrix on the surface of the aged specimen is extensively degraded by combined exposure to UV radiation and moisture. This thickness can be measured by surface microscopy of the aged sample (see Fig. (3.6)) and was measured to be about $30 - 60\mu m$. The degradation of the thin, topmost layer, aforementioned, is the primary cause for the rapid decrease in the contribution of the fiber reinforcement and matrix modulus to the transverse modulus near the surface of the specimens.

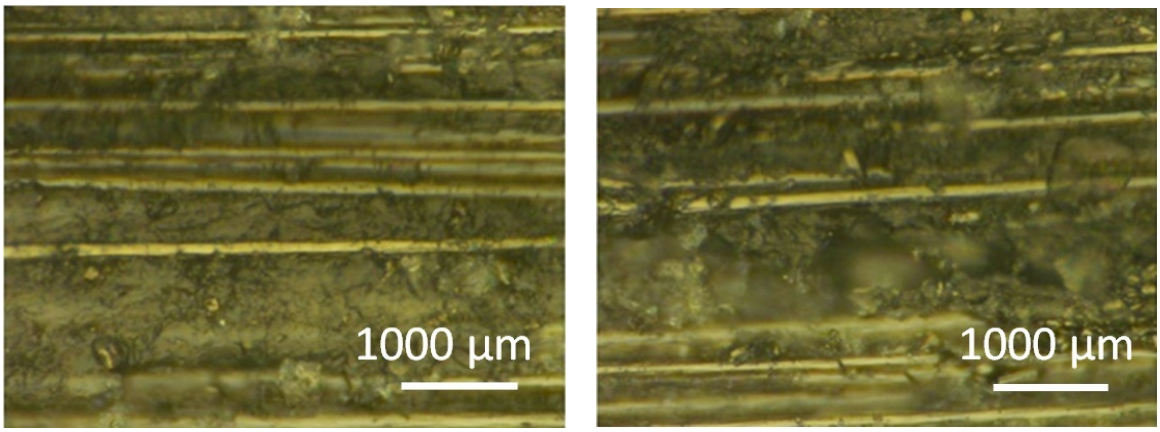

(a) (b)

Figure 3.4: The micrograph of the edge of samples with 0 degree fiber orientations via digital microscopy (a) Virgin (b) Aged

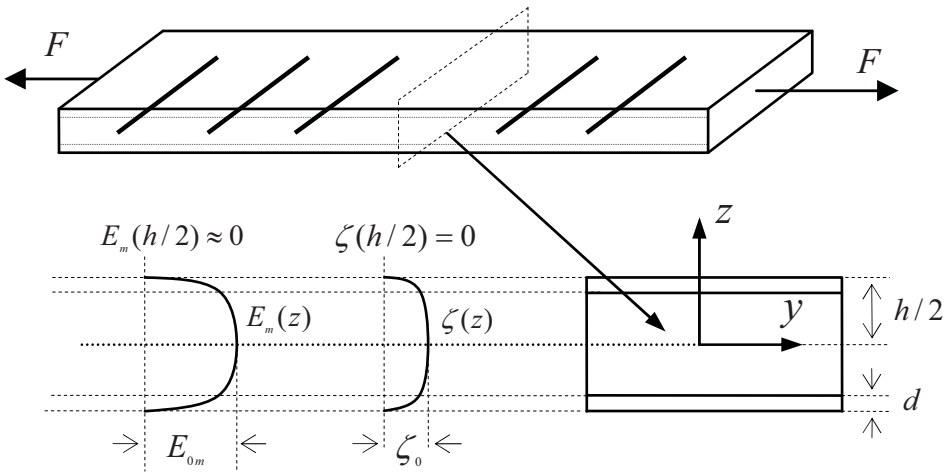

Figure 3.5: Schematic profiles of ζ and the matrix modulus in the thickness direction of aged laminates

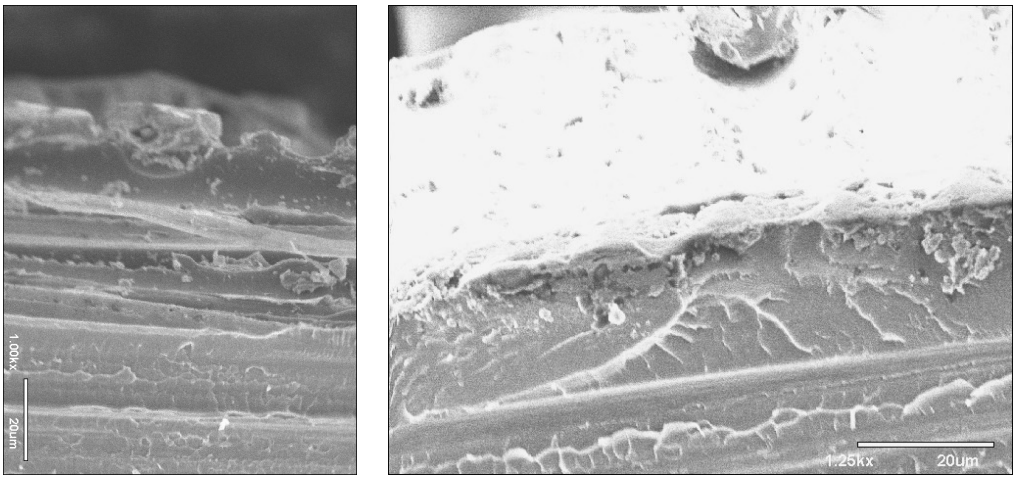

(a) (b)

Figure 3.6: The fracture surface of samples with 90 degree fiber orientations via SEM Microscopy (a) Virgin (b) Aged

3.6 Effective modulus of composites

Here, the composite laminate is considered as a homogenized orthotropic plate with mechanical property variation based on the developed model (see Fig 3.7).

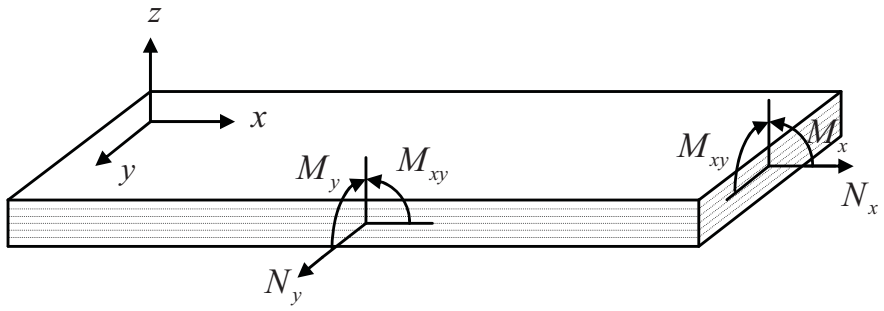

Figure 3.7: Laminated orthotropic plate

From classical laminated theory, the relation between applied force and moments, induced

midplane strain, and curvature can be obtained as:

$$\begin{bmatrix} N \\ M \end{bmatrix} = \begin{bmatrix} A & B \\ B & D \end{bmatrix} \begin{bmatrix} \varepsilon_0 \\ \kappa \end{bmatrix} \tag{3.10}$$

where $N = [N_x, N_y, N_{xy}]^T$ is the applied force and $M = [M_x, M_y, M_{xy}]^T$ is the applied moment. $k = -[w_{0xx}, w_{0yy}, 2w_{0xy}]^T$ is the curvature of the plate and $\varepsilon = [u_{0,x}, v_{0,y}, u_{0,y} + v_{0,x}]^T$ is the midplane strain, consisting of: u_0 , v_0 and w_0, which are the displacement of the midplane in x, y and z direction. A, B, C, and D are given in Appendix A. The $[A/B/B/D]$ matrix is the stiffness matrix of the laminated composite. Equation. 3.10 can be written as:

$$\begin{bmatrix} \varepsilon_0 \\ \kappa \end{bmatrix} = \begin{bmatrix} A^* & B^* \\ B^* & D^* \end{bmatrix} \begin{bmatrix} N \\ M \end{bmatrix} \tag{3.11}$$

The $[A^*/B^*/B^*/D^*]$ is a compliance matrix, which is the inverse of the stiffness matrix. For symmetric laminates, similar to the current composite laminate,

$$\begin{bmatrix} B \end{bmatrix} = 0 \quad \begin{bmatrix} A^* \end{bmatrix} = \begin{bmatrix} A \end{bmatrix}^{-1} \quad \begin{bmatrix} D^* \end{bmatrix} = \begin{bmatrix} D \end{bmatrix}^{-1} \tag{3.12}$$

Substituting $N_y \neq 0$ and $N_x = N_{xy} = 0$ in Eq. 3.11

$$\begin{bmatrix} \varepsilon_{0x} \\ \varepsilon_{0y} \\ \gamma_{0xy} \end{bmatrix} = \begin{bmatrix} A^*_{11} & A^*_{12} & A^*_{16} \\ A^*_{21} & A^*_{22} & A^*_{26} \\ A^*_{16} & A^*_{26} & A^*_{66} \end{bmatrix} = \begin{bmatrix} 0 \\ N_y \\ 0 \end{bmatrix} \tag{3.13}$$

The effective in-plane transverse modulus in y direction can be obtained with:

$$E_y = \frac{\sigma_y}{\varepsilon_{0y}} = \frac{\frac{N_y}{h}}{N_y A^*_{22}} = \frac{1}{hA^*_{22}} \tag{3.14}$$

where h is the thickness of the plate.

To find the effective transverse flexural modulus, $M_y \neq 0$ and $M_x = M_{xy} = 0$ are substituted in Eq. 3.11

$$\begin{bmatrix} k_x \\ k_y \\ k_{xy} \end{bmatrix} = \begin{bmatrix} D^*_{11} & D^*_{12} & D^*_{16} \\ D^*_{21} & D^*_{22} & D^*_{26} \\ D^*_{16} & D^*_{26} & D^*_{66} \end{bmatrix} = \begin{bmatrix} 0 \\ M_y \\ 0 \end{bmatrix} \tag{3.15}$$

The effective flexural transverse modulus in y direction can be obtained with:

$$E^f_y = \frac{12M_y}{k_x h^3} = \frac{12}{h^3 D^*_{22}} \tag{3.16}$$

3.7 Finite element analysis of micro-cracks

The composite laminate is considered as a homogenized orthotropic plate with mechanical property variation based on the developed model. Figure. 3.8 shows the configuration for a three-point bending test on a sample with a crack length, d. As mentioned before, d is the thickness of the thin film on the surfaces of the composite plate degraded by micro-cracking and can be measured with surface microscopy. The initial crack is considered in the midpoint of the laminate, as it is bearing the maximum moment and the failure is initiated at this point. The variation in mechanical properties is in the same direction as crack propagation, thus, mode I crack growth can be observed. The strain energy release rate G_I can be obtained by calculating the J-contour integral when the contour integral approaches the crack tip. This process can be conducted by selecting the element size around the crack tip in the order of 10^{-2} of the crack length and by applying the mechanical property variation to elements in the thickness direction. This reduces the effect of mechanical

property variation on the calculation of the J integral. The J integral and its calculation are further explained in Appendix B. Here, the computation of the J integral is performed with the help of finite element analysis. It is recommended to use the second contour from the crack tip opposed to the first contour used in the calculation of the J integral to avoid the effect of singularities on it [28]. Finite element mesh and different contours around the crack tip are shown in Fig. 3.9.

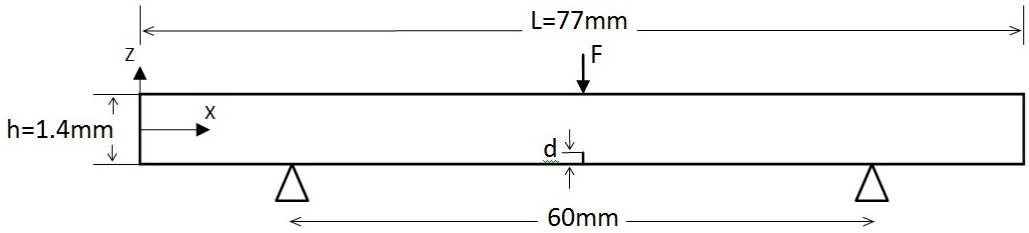

Figure 3.8: Three-point bending test configuration

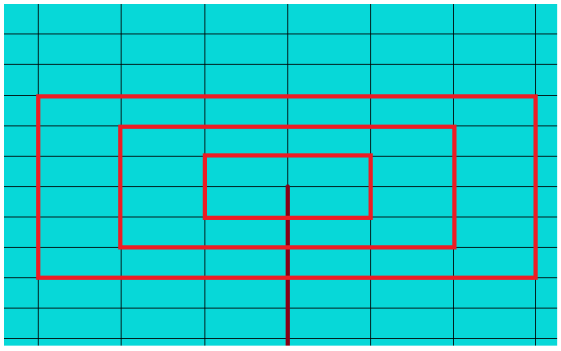

Figure 3.9: Different contours around the crack tip

3.8 Result and discussion

3.8.1 Failure Stress

The transverse modulus of the virgin sample can be obtained by using the Halpin-Tsai equation:

$$E_{0T} = \frac{1+\zeta_0 \eta c}{1-\eta c} E_{0m}$$
$$\eta = \frac{\frac{E_{0f}}{E_{0m}} - 1}{\frac{E_{0f}}{E_{0m}} + \zeta_0} \tag{3.17}$$

where E_{0T} is the transverse modulus, which was measured as 7.01 GPa. Equation (3.12) yields the same value when $\zeta_0 = 0.47$. The transverse modulus of the aged sample after 1000 and 2000 hours of combined UV radiation and moisture exposure is given in Tab. 3.3. The exposure duration is extended here to evaluate the effects of exposure time on the degradation of the transverse modulus. No variation in Poisson's ratio, ν_{LT}, is observed due to environmental exposure. $\nu_{LT} = 0.29$ is obtained by the measurement of both longitudinal and transverse strains during the uniaxial tensile test on samples with 0 degree fiber orientation. From the symmetry of the compliance matrix in orthotropic materials, $\nu_{TL}(z)$ can be obtained with:

$$\nu_{TL}(z) = \frac{E_T(z)}{E_L} \nu_{LT} \tag{3.18}$$

where E_L is a longitudinal modulus, which remains almost unchanged during environmental exposure. The transverse modulus can be obtained by substituting $\zeta(z)$ and $E_m(z)$ from Eqn. (3.5) and Eqn. (3.9) into Eqn. (3.12). With proper selection of the constant parameters in Eqn. (3.5) and Eqn. (3.9), the effective transverse modulus evaluated by applying the developed model in the

laminate theory, yields the same value as the one obtained by experiments. These values are given in Tab. 3.3. The plane stress condition is assumed here.

Table 3.3: Constant parameters

Duration of exposure	transverse modulus	c_1	c_2
1000	6.53 GPa	13	55
2000	6.15 GPa	1.5	55

The predicted ζ and matrix modulus in the thickness direction of aged laminates are given in Fig. 3.10 and Fig. 3.11. The profile of the transverse modulus in the thickness direction is provided in Fig. 3.12. Figure 3.13 shows the distribution of the axial stress in the laminate at the failure point. The results suggest that a stable crack initially grows at the surface of the aged specimen until the bending stress reaches the same level as the failure stress of the specimen. The failure stress is the maximum value of the axial stress profile in the Fig. 3.13. At this point, an uncontrolled fracture can be observed. Simply, in environmentally-aged samples, the failure stress is not defined based on the surface bending stress, but by the maximum stress in the thickness direction. Table 3.4 gives the failure stress of both virgin and aged samples for different exposure times. For virgin samples, $\alpha's$ and $\beta's$ are, respectively, 1 and 0 in the Eqns. (3.2) and (3.6). The failure stress of the environmentally-aged samples is substantially smaller than that of the virgin sample. This is due to the weaker fiber-matrix interface and damaged matrix near the surface of the aged sample, which is a product of the combined exposure to UV radiation and moisture. The failure stress evaluated by the model is smaller than the one estimated by the laminate theory and the assumption of uniform degradation.

It should be noted that, at the onset of failure, after 1000 hours of exposure, the stress in the damaged area is much less than the value predicted using the effective lamina properties assump-

tion (61.81 MPa). However, the maximum stress inside the aged specimen (64.66 MPa) is in line with the 61.81 MPa value, though it exists inside the specimen and not along the surface.

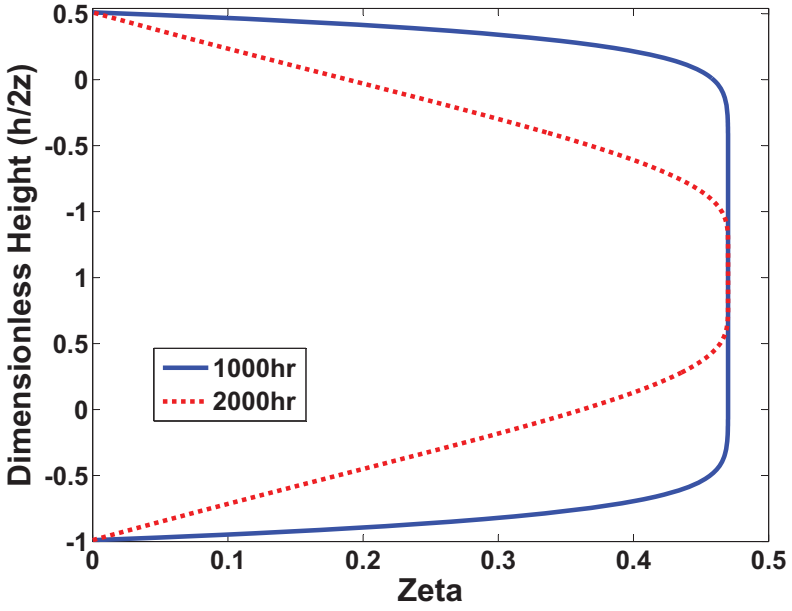

Figure 3.10: ζ in the thickness direction of aged specimens

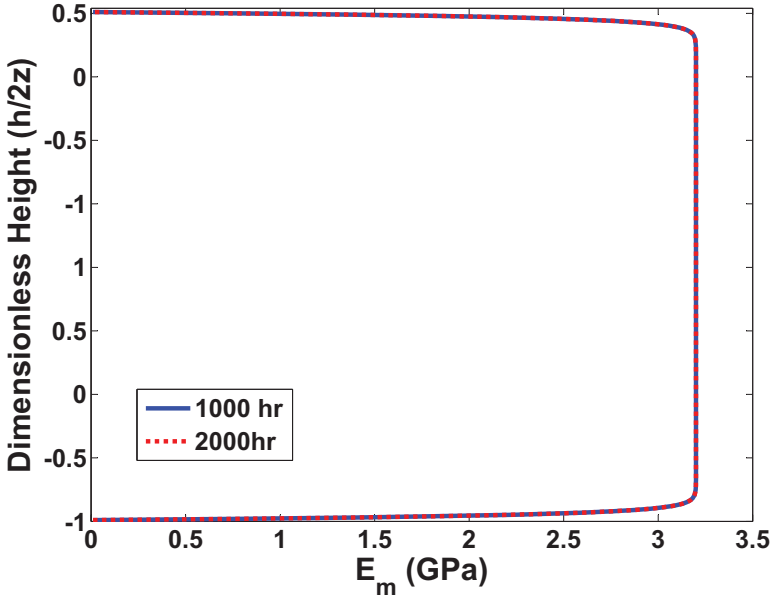

Figure 3.11: Matrix modulus in the thickness direction of aged specimens

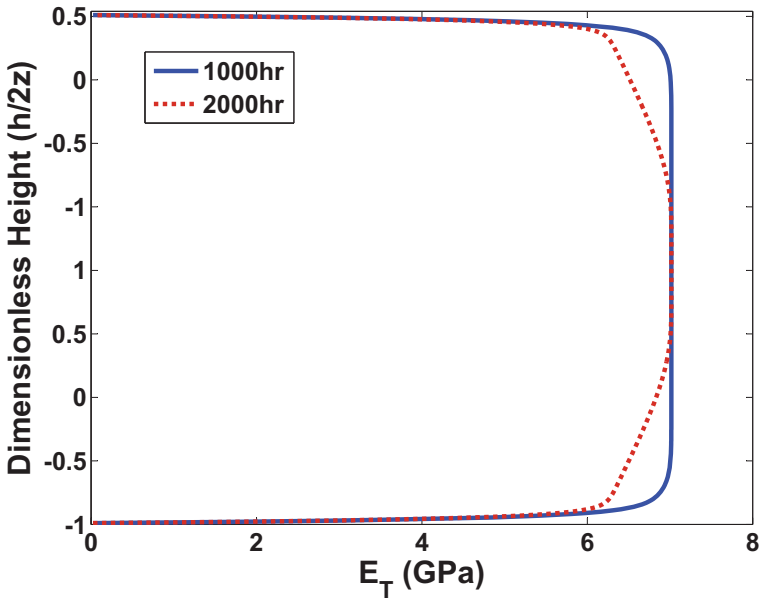

Figure 3.12: Transverse modulus in the thickness direction of aged specimens

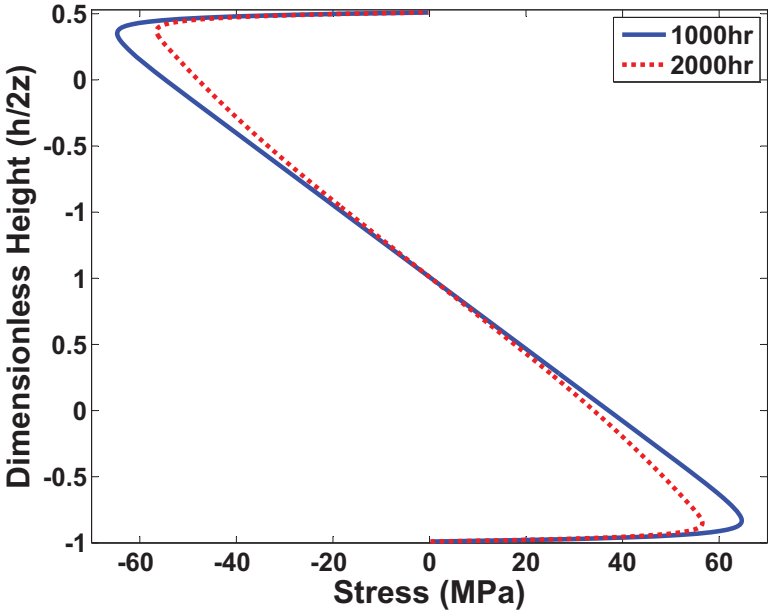

Figure 3.13: Distribution of bending stress in the aged laminate at the failure point

Table 3.4: Failure stress

Fracture stress (MPa)	Virgin	Aged 1000 hr	Aged 2000 hr
Estimation based on the uniform degradation	101.73	72.66	65.43
Evaluated by the model	101.73	64.66	56.50

3.8.2 Work of fracture

The work of fracture γ_F can be defined as:

$$\gamma_F = \frac{\text{Energy under load deflection curve}}{\text{2 specimen cross sectional area}} \tag{3.19}$$

The schematic load-deflection curve for specimens with 0 and 90 degree fiber orientations is given in Fig.3.14.

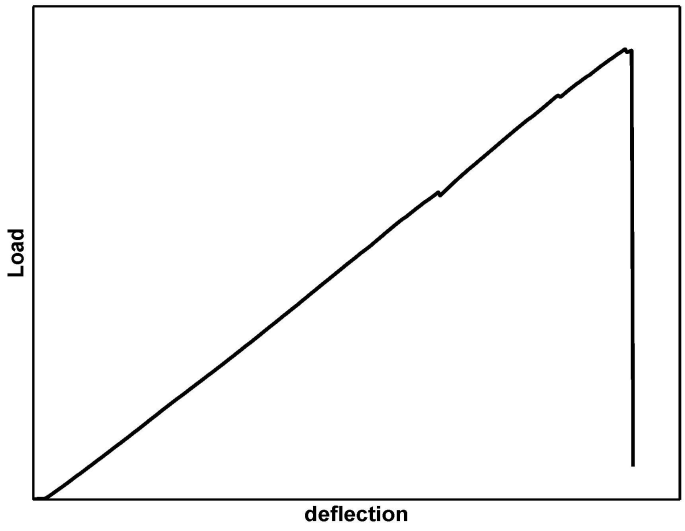

Figure 3.14: The schematic load-deflection curve

This figure indicates an unstable crack growth at the end of the test. This is due to the absence of a dominant crack in samples, which prevents uncontrolled fractures. A small change in the work of a fracture can be observed between virgin and aged samples with 0 degree fiber orientations (see Tab. 3.5). However, for samples with 90 degree fiber orientations, aged samples have lower fracture energy than virgin ones. This is due to the loss in fiber-matrix interface toughness through the thickness of the laminate and extensive micro-cracking on the surface of aged specimens. Typically, the fracture toughness in 0 degree samples is a fiber-dominated property and, in 90 degree specimens, is a matrix-dominated property. The fracture surfaces of virgin and aged samples with 0 and 90 degree fiber orientations are shown in Fig. 3.15 and Fig. 3.16.

Table 3.5: Work of fracture

Fracture energy(KJm^{-2})	Virgin 0	Aged 0	Virgin 90	Aged 90
Work of fracture	47.02	46.85	2.56	1.24

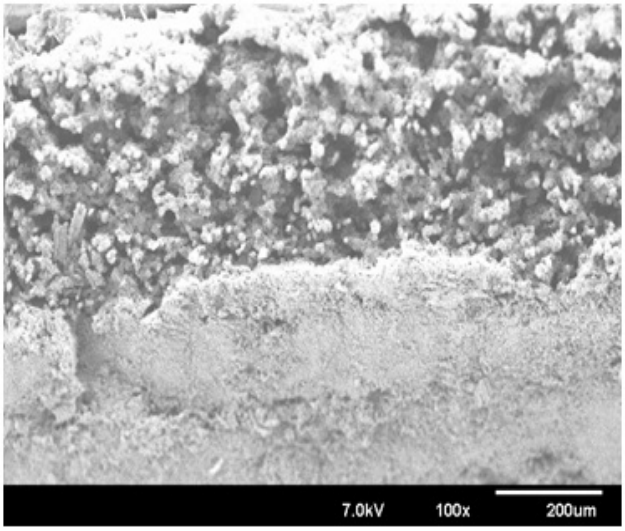

(a)

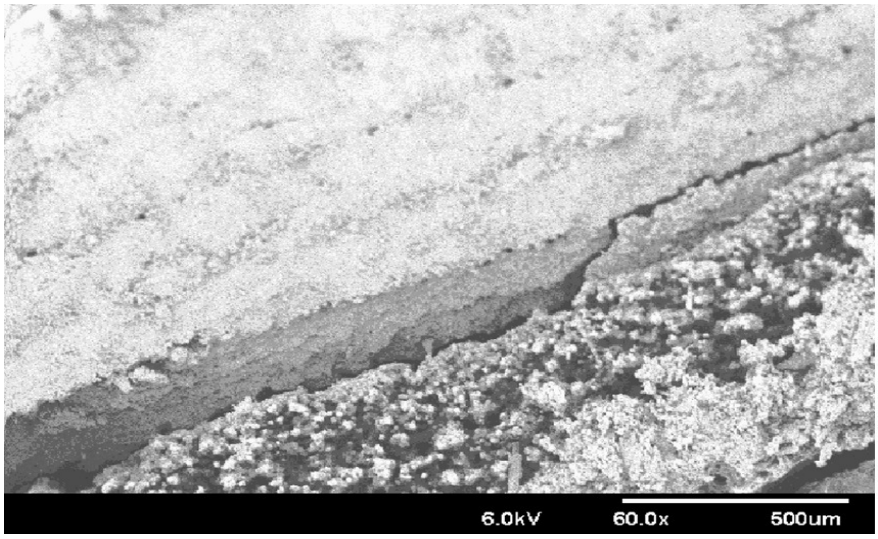

(b)

Figure 3.15: Fracture surface of [0°] fiber orientation samples (a) Virgin (b) Aged

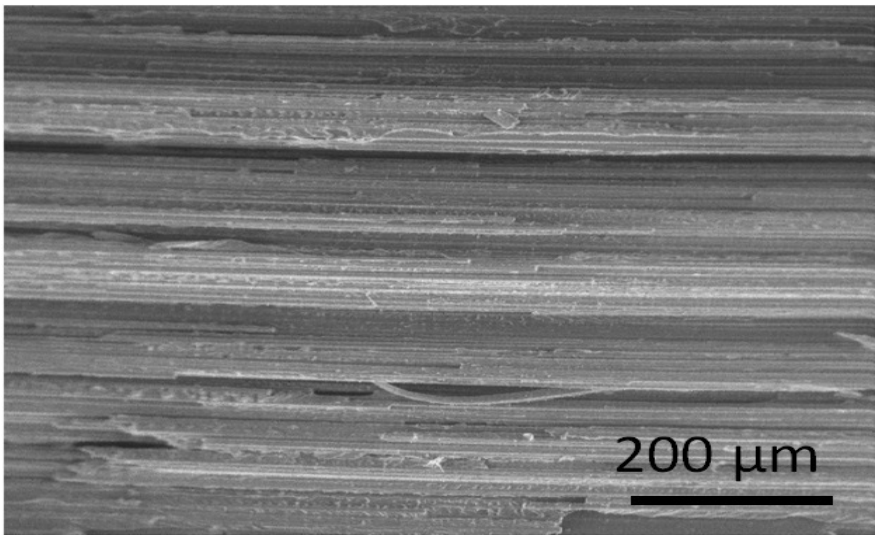

(a)

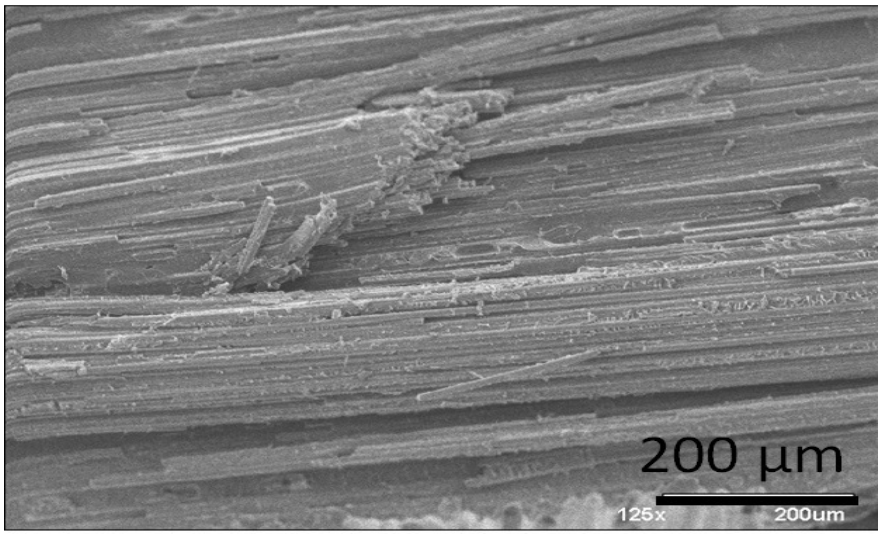

(b)

Figure 3.16: Fracture surface of [90°] fiber orientation samples (a) Virgin (b) Aged

3.8.3 Fracture initiation energy

The fracture initiation energy, γ_I, is defined as the energy required to create a unit area of new fracture surface. Using linear elastic fracture mechanics, γ_I can be related to the critical strain

energy release rate, G_{Ic}, by:

$$2\gamma_I = G_{Ic} \tag{3.20}$$

The fracture initiation energy can be obtained by computing the strain energy release rate at the failure load using finite element analysis described in the section 3.7 of this chapter. There are some invisible flaws in virgin samples, which might occur in the manufacturing stage. The size of these flaws are usually smaller than the size of micro-cracks in degraded samples. However, for the sake of comparison, the initial crack length in both degraded and virgin samples will be assumed to be the same. The fracture initiation energy for degraded and virgin samples with 0 and 90 degree fiber orientations are given in Table 3.6. Similar to the work of fractures, a small change in the fracture initiation energy can be observed between virgin and degraded samples with 0 degree fiber orientations. In samples with [0°] fiber orientations, a small fiber pull-out can be observed in the beginning of the failure at the fracture surface (see Fig. 3.15). This implies that the fracture initiation energy predicted by the model gives a lower estimation of the true value since it does not consider the fiber pull-out. In the case of 90 degree fiber orientations, environmentally-aged specimens exhibit lower fracture initiation energy compared to virgin samples. This is due to the existence of UV-induced micro-cracks on the surfaces of aged specimens.

Table 3.6: Fracture initiation energy

Fracture energy(KJm^{-2})	Virgin 0	Aged 0	Virgin 90	Aged 90
Fracture Initiation Energy	9.32	9.171	0.126	0.063

3.9 Conclusion

The current study shows that the exposure of unidirectional carbon fiber- vinyl ester composite laminates to UV radiation and moisture has minimal effects on the fiber-dominated properties. However, the matrix-dominated properties, including the transverse bending modulus, and transverse and longitudinal bending strength have been diminished significantly. This might be due to the degradation of the fiber-matrix interface, which deteriorates the load transfer mechanism between matrices and fibers. Extensive UV-induced micro-cracking on composite laminate surfaces is another factor in reducing the flexural properties of aged specimens. The maximum degradation is observed in the transverse flexural strength of samples exposed to the combination of UV radiation and condensation. The profiles of contribution of matrix modules and fiber reinforcement to the transverse modulus of aged samples are defined and presented in the thickness direction. The distribution of the transverse modulus based on the above profiles is obtained through the thickness of the laminate. The failure stress of specimens can be, subsequently, obtained by using the profile of the transverse modulus at the failure point. The predicted failure stress by the model is smaller than the one estimated based on the laminate theory and the assumption of uniform degradation. The work of fracture and fracture initiation energy decrease substantially in aged samples with 90 degree fiber orientations. This is due to the loss in the fiber-matrix interface toughness through the thickness of the aged laminates and extensive micro-cracking on the surface of specimens.

Chapter 4

Fatigue Damage in Composites

4.1 Introduction

Fiber-reinforced polymer (FRP) composites are increasingly being considered as practical alternatives to conventional metallic materials for structural load-bearing roles in new classes of naval crafts and warships (e.g., Zumwalt-Class Destroyer [72]). This growing trend towards the use of fiber polymer composites by marine industries has been motivated by their unique and practical properties, such as lower density, higher specific strength and stiffness, reduced radar signatures, better corrosion resistance [17], and their potential for exhibiting application-tailored properties through polymer synthesis, functionalization and nano-reinforcing (e.g.[73]). These unique properties are particularly useful for naval and military industries in their continuous efforts toward developing naval crafts with better maneuverability, fuel economy, structural and operational performance (e.g. increased payload, stability, and stealth) as well as economic efficiency (with decreased capital and maintenance costs) [74]. Composites in naval crafts can be exposed to harsh marine environmental elements, such as UV radiation, moisture, sea water, and temperature extremes (high and frigid). In addition, naval ships are frequently subjected to cyclic hydrodynamic loads due to water slamming [75, 76]. Such harsh marine environmental elements and cyclic hydrodynamic forces can individually and synergistically affect the structural properties

and load-bearing capacity of fiber-reinforced composites, which in turn, can affect and reduce the long-term structural integrity and reliability of composite naval crafts. To protect against such an outcome and shield composites from negative environmental effects, protective coatings (epoxy- or ester-based [77, 113]) are almost always utilized. However, these coatings are susceptible to wear, corrosion, environmental degradation and can become damaged due to normal use or inadvertent activities, leaving the protected composites exposed to marine environmental elements. Therefore, even with protective coatings, to ensure the structural integrity of composite naval crafts, it is instrumental to: I) establish a detailed understanding of the individual and cooperative effects of cyclic loadings and harsh marine environmental elements on the mechanical properties of FRP composites, and II) establish experimental-based models capable of predicting degradation in the properties of FRP composites due to the effects of cyclic loadings and marine environments. Along these two aforementioned fronts, multiple efforts have explored and modelled the degradation in mechanical properties due to marine environmental elements and cyclic (fatigue) loading (e.g., [63, 64, 47, 2]). The effect of fatigue (cyclic) loading on composite materials has been extensively studied in recent decades (e.g., [34, 39, 31, 35]) due to its importance in aerospace, marine and infrastructural composite applications. These efforts provided multiple experimental-based observations and damage accumulation models. Experimental observations regarding fatigue-based damage processes, mechanisms and fracture modes in unidirectional laminates indicate that the process of fatigue in composite laminates, include four damage mechanisms: fiber breakage, matrix cracking, fiber-matrix decohesion, and delamination [39]. In addition, they highlighted that fatigue-grown cracks, regardless of the initial flaw direction or loading direction, evolve during the fatigue process and align with the fiber direction. These cracks propagate through the matrix, along matrix-fiber interfaces when the interfaces are weak or have been compromised, and

across fibers due to fiber breakage when loads are aligned with weak fibers and possess strong matrix-fiber interfaces [52, 53, 54, 55, 56]. The process of damage accumulation regarding effective properties, in unidirectional FRP composite laminates, has been observed to pass through three stages, similar to the ones associated with Pariss law for homogeneous materials. During the first stage, extensive but localized matrix cracking and delamination occur. In the second steady stage, damage accumulates at a relatively slow and steady rate due to stable crack growth along fiber-matrix interfaces. In the final stage, damage accumulates at an exponential and rapid rate due to fiber breakage, coalescence of the localized matrix cracks, excessive delamination and significant fiber-matrix debonding. The third stage culminates with failure and loss of load-carrying capacity. Cumulative damage models representing fatigue-based damage in unidirectional laminates often utilizes reduction in stiffness or strength with elapsed loading cycles as fatigue damage representative parameters [42, 43, 44, 45, 46, 62]. However, stiffness was found to be a more practical, fundamental parameter as its measurement utilizes non-destructive tests. As such, a single specimen can be used to describe damage accumulation during fatigue life, which significantly reduces the number of needed tests and minimizes data scatter [62]. Cumulative fatigue damage models vary in terms of complexity, but fundamentally, they are either defined directly in terms of monitored residual stiffness or strength [47, 48, 78, 79] or in terms of load level and history [34, 42, 46, 80]. Both types of models show good potential for fitting experimental data, but to capture the classical three fatigue phases, fitting functions with many parameters are needed. In addition to being prone to fatigue damage, FRP composites generally exhibit degradation in their structural properties and load-carrying capacity due to exposure to UV radiation, moisture, temperature and chemicals. These elements are abundantly available in marine environments and their adverse effects can be more severe and harder to anticipate when they act in an interactive

manner [81, 82, 16, 83, 84, 85]. Moisture once defused in FRP composites can, through plasticization, hydrolysis and microcracking, damage the matrix and cause fiber-matrix debonding, reducing the composites strength (e.g. CFRP [86, 87, 88]). The adverse effect of moisture is heightened at elevated temperatures due to the increase in water diffusion and ingress (e.g., with an increase in temperature from 50C to 70C, moisture absorption by carbon epoxy composites can increase by more than 100% [89]). Moreover, cyclic exposure to salt water and hot-freeze-thaw temperature cycles was observed to result in significant physical and chemical (e.g., chloride [90] and alkaline solutions [91]) changes as well as reduction in the strength of FRP composites [92, 93, 94, 95, 96, 97, 98, 99, 100, 101, 102, 103, 104, 105, 106, 107, 108, 109]. UV radiation, which is always present as part of the sun spectrum, was observed to cause a reduction in strength [81, 97, 98, 10], increase creep strain [81, 97], and increase brittleness [10] and surface micro-cracks due to photo-oxidation and molecular chains sessions [10, 16]. These micro-cracks can act as sources for stress concentrations and can promote crack initiation and propagation [10, 16]. Also, micro-cracks caused by UV radiation can facilitate moisture diffusion, thus, amplifying the adverse effect of moisture [81, 97]. Enhanced moisture absorption due to UV radiation and elevated temperatures also exacerbates the effect of any chemicals present in sea water, as enhanced moisture absorption allows for deeper chemical penetration and increased concentration. In the case of carbon fibers, moisture in the presence of metals and salt water can damage the fibers through a galvanic reaction [110]. In a marine environment, the aforementioned environmental elements (UV radiation, moisture, and temperatures extremes) can act simultaneously with cyclic fatigue loads. In such scenarios, the adverse effects of environmental elements and cyclic loadings can interact cooperatively, amplifying the total damaging effect (e.g.[63, 64, 47, 2, 65]). For instance, the loss of strength and stiffness due to the cyclic loading in aqueous environments is

greater than what is observed in air [65, 2]. Commonly, the synergistic effects are non-linear in nature (e.g., [89]) and are difficult to anticipate.

Aforementioned efforts illustrate that marine environments and cyclic loadings, when simultaneously acting on FRP composites, can result in significant deleterious effects and unexpected drops in the structural reliability and load-carrying capacity of the composites. However, so far, a fundamental understanding of the synergistic effects of marine environmental elements and fatigue loading, their associated mechanisms, and models capable of predicting this deleterious synergy are lacking.

Therefore, with respect to these synergistic effects, this work aims to:

-Provide experimental data that can lead to a better understanding of the synergistic effects,

-Establish models with few fitting parameters that can model and predict synergistic effects,

-Provide a better understanding of the synergistic effects

In the following sections, the approach, experimental details, modeling, and analysis are provided. Finally, discussion and conclusions are presented.

4.2 Experimental approach

The employed approach is highly experimental, tailored to address the aforestated objectives and is implemented around two main elements: I) In-lab degradation under simulated marine environments, and II) Cyclic loading of environmentally degraded specimens. In this approach, unidirectional carbon fiber-vinyl ester composite laminates are subjected to well-defined, monitored, quantified and repeatable environmental conditions that mimic marine environments with UV radiation, sea water, moisture and typical outdoor temperatures. Subsequently, the environmentally degraded specimens are cyclically loaded until failure. During cyclic loading, the stiffness of the

composite specimens is monitored in terms of elapsed loading cycles. Finally, experimental results are used to illustrate the effect of environments and fatigue on the stiffness of the composite and are used to establish predictive models of the cooperative degradation effects.

4.2.1 Degradation and marine environments simulation

A Q-Lab QUV/se UV radiation/condensation accelerated environmental chamber is used to simulate the individual and combined exposure to the marine elements: UV radiation, humidity and condensation. The UV components of solar radiation, which are not absorbed by the ozone layer and reach the surface of the earth are in the 290-400 nm band [111]. The photons possess the same energy as the covalent bonds in polymers, which are able to break the chemical bonds and alter the mechanical properties of the polymers (see Tab. 4.1 [111]). The UV light with a wavelength of 325 nm is believed to have the most deleterious effect on polymers. The environmental chamber simulates natural sunlight using fluorescent UV bulbs with 340 nm wavelengths and simulates condensation via evaporating water, which, subsequently, condenses on specimens. This particular chamber can simulate combined and individual exposure to UV radiation and condensation. Using this chamber, composite specimens are exposed to 1000 hours of combined and individual accelerated aging. The UV irradiation was set to 0.6 W/m2 at 60 C, and the condensation cycle was set to a temperature of 45 C. To simulate the synergistic exposure, specimens must be cycled every few hours between two conditions [112]. Based on the primary study, the 3-hour intervals between the UV irradiation and condensation cycles yield the maximum damage in the mechanical properties of the carbon fiber-vinyl ester specimens [82].

Table 4.1: Wavelength producing bond excitation

Bond Type	Bond Energy(KJ/mol)	UV Absorption Wavelength(nm)
C-H	380-420	290
C-C	340-350	300
C-O	320-380	320
C-Cl	300-340	350
C-N	320-330	400

4.2.2 Material and cyclic loading

Carbon fiber-reinforced vinyl ester unidirectional composite laminates (Graphtek LLC) were used in these experiments. The type of carbon fiber is 33 M.S.I. and the flexural strength is 1875 MPa. The tensile strength is 2689 MPa, which is based on the failure of fibers in the unidirectional test. Composite laminate sheets with nominal thickness of 1.4 mm were machined using a diamond wet saw into (12.5×152mm) coupons, following the ASTM D790 standard. Two sets of unidirectional specimens were prepared to represent the two material principal directions of the composite laminate. The two sets are referred to, based on their fiber orientation, as [0] and [90]. Cyclic loading was limited to few scenarios, as the process of environmental degradation is time-consuming and the accelerated weathering chamber has a low throughput volume. Accordingly, a tension-tension fatigue loading test was performed at 62% and 67% UTS loading levels with a minimum to maximum stress ratio R =0.2 in an Instron 1332 servohydraulic machine under load control (see Fig. 4.1). This load level is used to perform the test in a reasonable time and obtain

meaningful results. Loading cycles followed a sine form with a frequency of 5Hz for samples with [90] fiber direction and 2Hz for samples with [0] fiber direction. These frequencies are used to give the smooth sine waves and minimize the heat generation during the test. Aluminum tabs were epoxied to the specimen surfaces to facilitate gripping and prevent grips from damaging specimens. Tabs prevented stress concentrations and failure near the grips. Specimens were gripped with mechanical locking wedge grips. The strain was measured by means of extensometer with a gauge length of 25 mm. The stiffness was evaluated from the cyclic load data and the strain, which was stored simultaneously by the Instron data acquisition system. Stiffness in the desired cycles of the fatigue life was obtained by averaging the stress-strain slopes of 10-100 consecutive load cycles. The latter reduced data scatter.

Figure 4.1: Uniaxial loading frame

4.3 Experimental results

Figure. 4.2 shows the stress-strain relationship for unidirectional carbon fiber-vinyl ester composites under 62% loading level for the first and last three cycles. The slope of stress-strain decreases during the fatigue life, which demonstrates the loss in stiffness. Figure. 4.3 shows the transverse modulus of unidirectional carbon fiber-vinyl ester composites during fatigue life under 62% loading level. The experimental data are averaged and reported here. A rapid decrease in the transverse modulus can be observed during the first few cycles of the fatigue life. In the intermediate stage, the modulus decreases in a relatively slow and steady rate until the failure cycle. A similar behavior is observed in Fig. 4.4 for specimens under a 67% loading level, and in Fig. 4.5, for environmentally-aged specimens. The transverse modulus of virgin and environmentally-aged specimens versus the logarithm of the number of loading cycles is shown in Fig. 4.6. The slope of the transverse modulus logN curve is small at the beginning of the fatigue life and increases when it approaches the end of the fatigue life.

Figure. 4.7 shows the longitudinal modulus of unidirectional carbon fiber-vinyl ester composites versus the logarithm of the number of cycles. The longitudinal modulus decreases slowly at the beginning of the fatigue life and reduces rapidly during the final cycles. The longitudinal modulus versus the number of loading cycles for aged and virgin samples are given in Fig. 4.8 and Fig. 4.9. A rapid decrease in the longitudinal modulus is observed at the beginning of the fatigue life. The modulus decreases relatively slowly in the intermediate stage, and further declines at a rapid rate when it approaches the failure cycle.

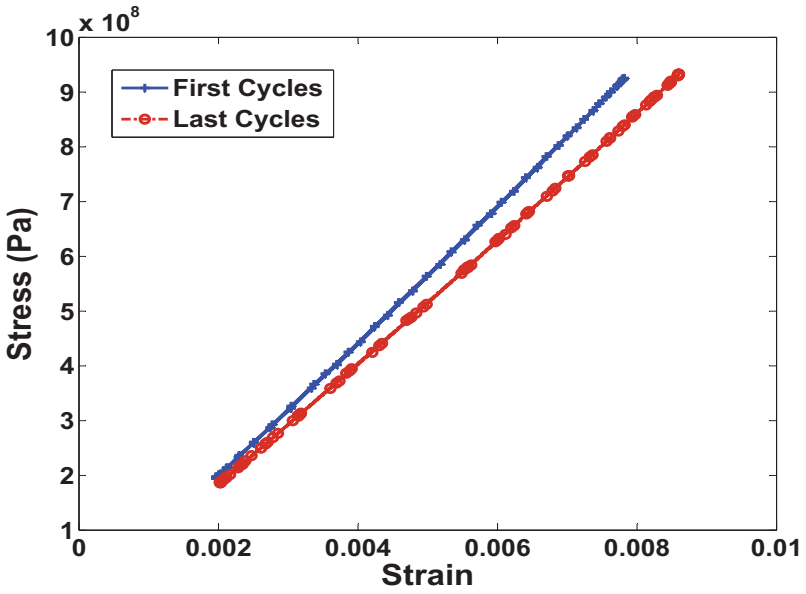

Figure 4.2: Stress-strain relation

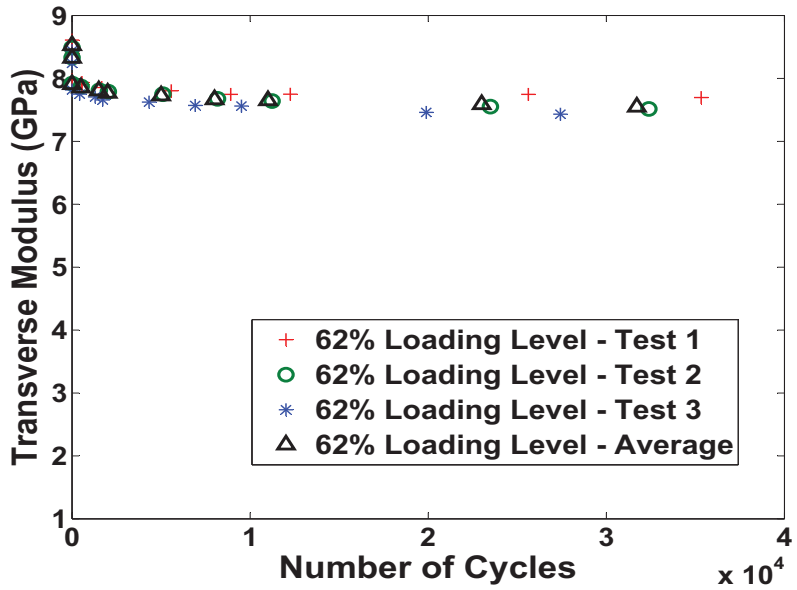

Figure 4.3: Averaging the transverse modulus of virgin samples during the fatigue life at a 62% loading level

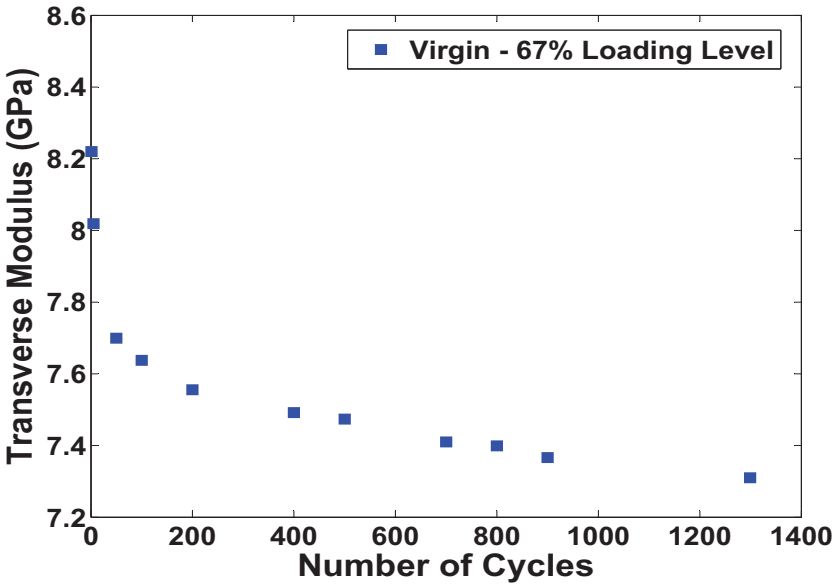

Figure 4.4: Transverse modulus of virgin samples during the fatigue life at a 67% loading level

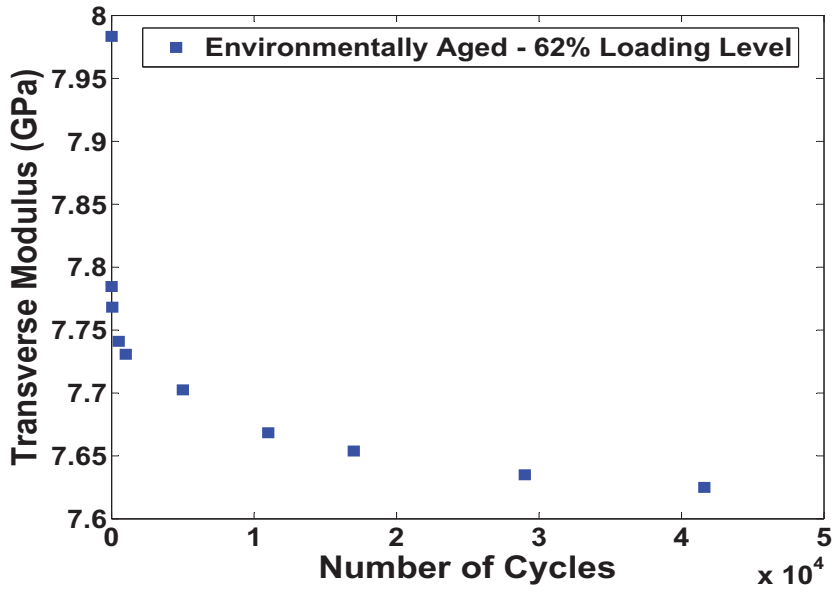

Figure 4.5: Transverse modulus of aged samples during the fatigue life at a 62% loading level

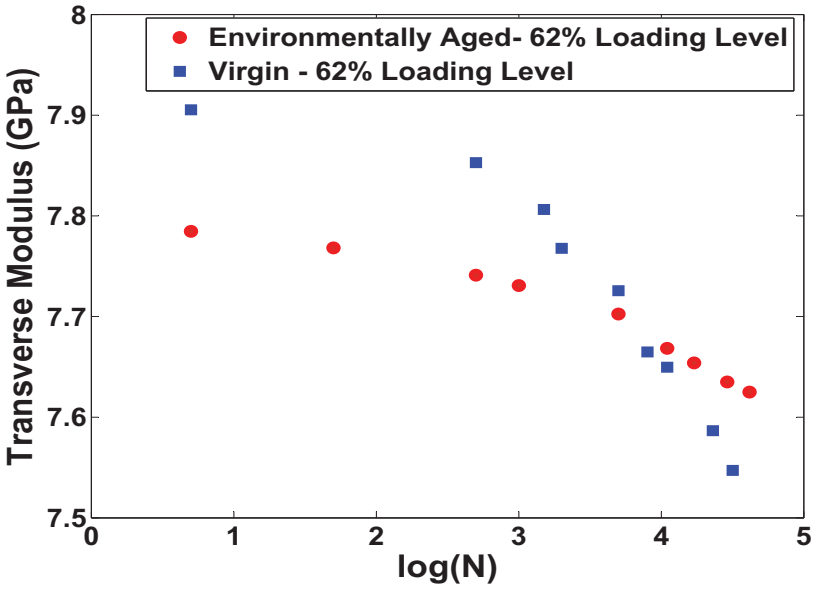

Figure 4.6: Transverse modulus versus logarithmic number of loading cycles

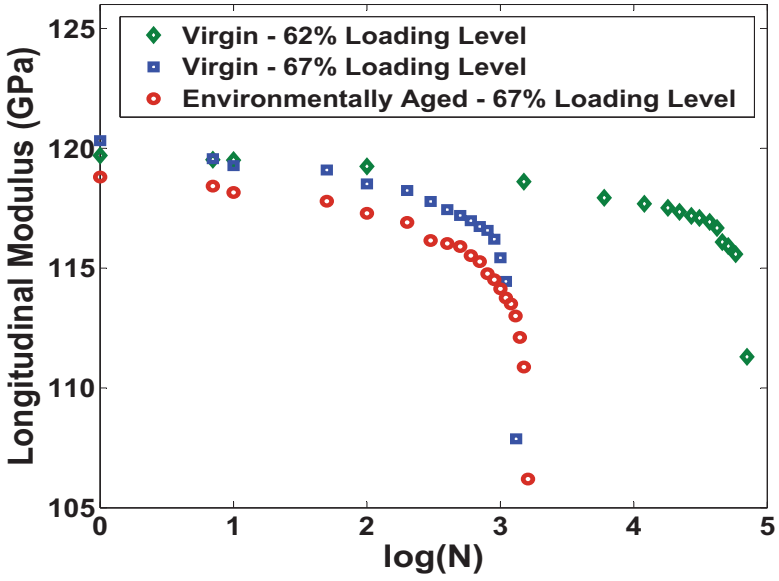

Figure 4.7: Longitudinal modulus versus logarithmic number of loading cycles

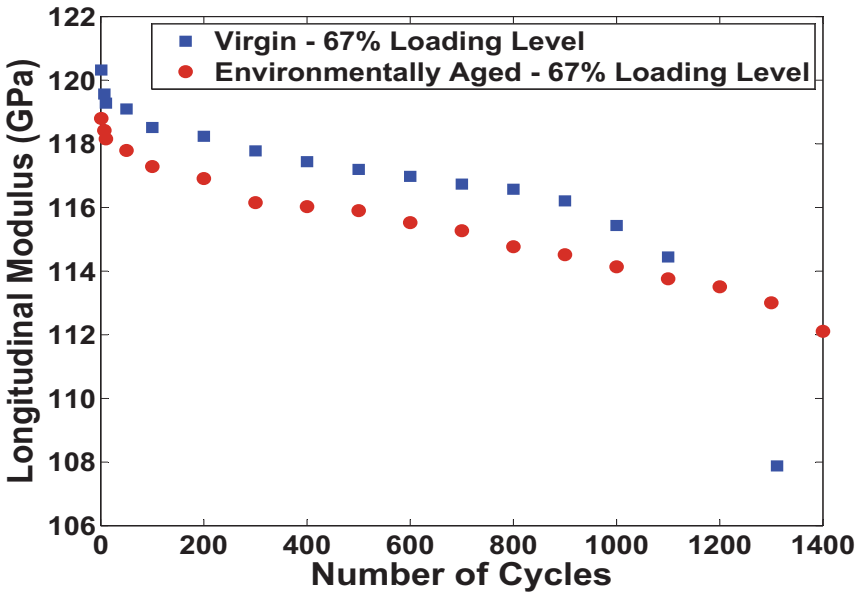

Figure 4.8: Longitudinal modulus during the fatigue life at a 67% loading level

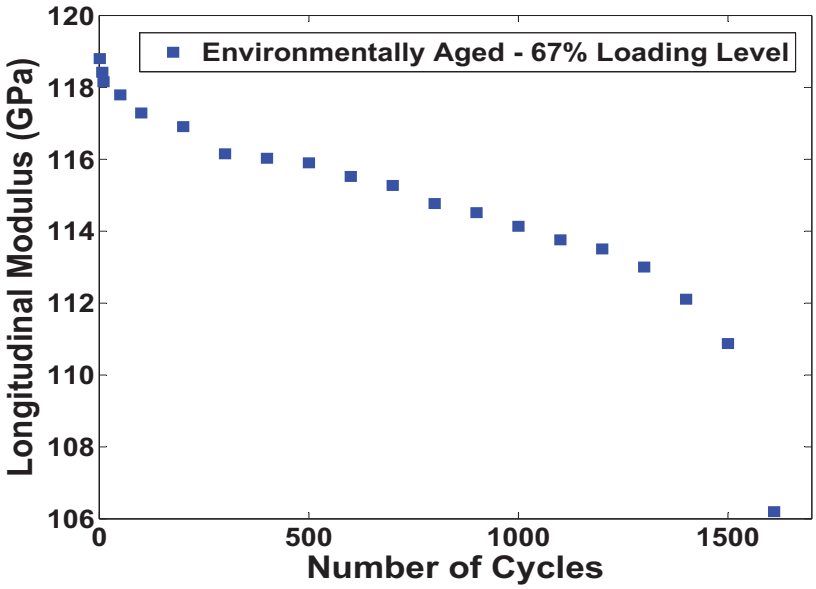

Figure 4.9: Longitudinal modulus during the fatigue life at a 62% loading level

4.4 Modelling fatigue damage in stiffness

Typically, major modes of damage in unidirectional composite laminates under fatigue loading can include: matrix cracking, fiber-matrix debonding, fiber breakage and matrix splitting. These modes of damage reduce the stiffness of fiber-reinforced composites. The damage in the stiffness during the fatigue life can be determined by [78, 79]

$$D = 1 - \frac{E(N)}{E_0} \tag{4.1}$$

where E_0 denotes the initial stiffness. The experimental results show that the stiffness is far from zero at the final cycle of the fatigue life, and therefore, the cumulative damage value is not equal to one at failure. To obtain a damage index that yields a value in the range of 0 to 1, and also, magnifies the damage, a new cumulative damage index is defined here as:

$$D = 1 - \frac{E(N) - E(N_f)}{E_0 - E(N_f)} \tag{4.2}$$

where $E(N_f)$ is the modulus at the final cycle.

The cumulative damages in longitudinal and transverse modulus versus $logN$ during the fatigue life are shown in Fig. 4.10 and Fig. 4.11

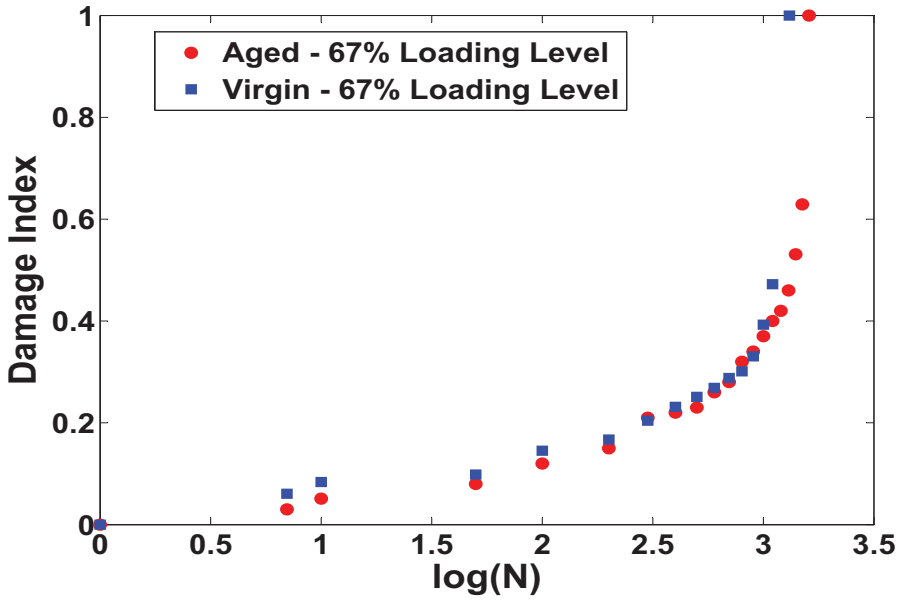

Figure 4.10: Damage accumulation in longitudinal modulus versus logN

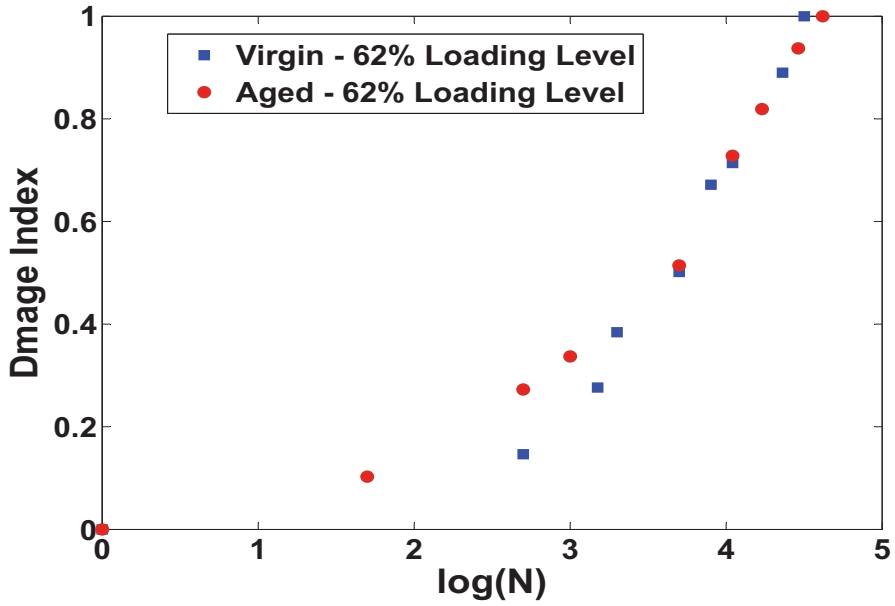

Figure 4.11: Damage accumulation in transverse modulus versus logN

It can be seen that the schematic damage accumulation versus *logN* for typical carbon fiber-

vinyl ester composites can be demonstrated as

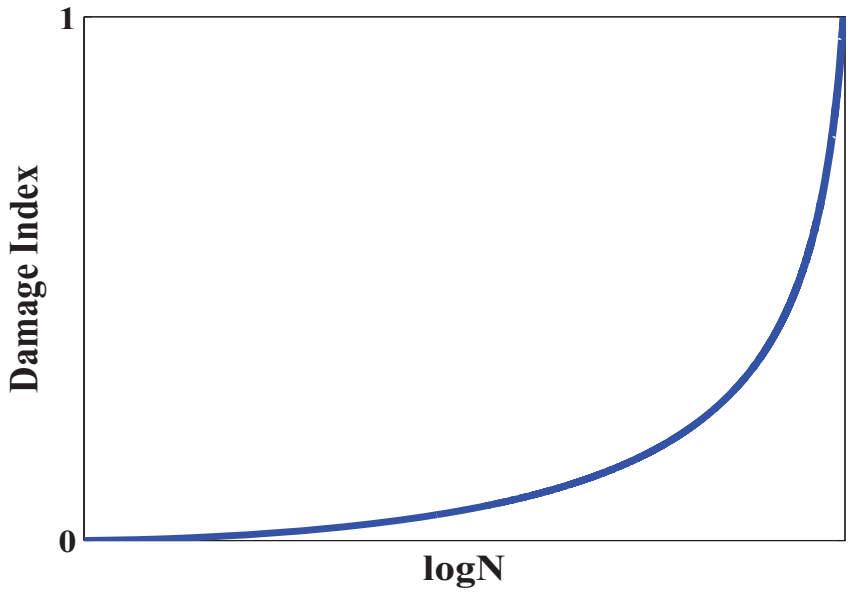

Figure 4.12: Schematic Damage accumulation versus logN

At the early stage of the fatigue life, the slope of the $D/logN$ curve is small and gradually increases when the curve approaches the end of the fatigue life. To fulfill the above conditions of the $D/logN$ curve, a progressive damage function can be defined as:

$$\frac{dD}{dlogN} = \bar{C}e^{nD} \tag{4.3}$$

where n is a constant, which together with $\bar{C}$, determines the shape of the curve. As mentioned earlier, the presentation of the fatigue damage in the stiffness of fiber-reinforced polymeric composites, as a function of $logN$, can disguise the true character of the damage accumulation during the fatigue life. Usually, extensive damage occurs during the first few cycles of the fatigue life, but this damage might not be distinguished in a logarithmic scale. The derivative of the damage index in Eq. 4.3 is computed, with respect to the logarithm of the number of cycles to graphically

preserve and differentiate this abovementioned feature of the event. $\bar{C}$ in Eq. 4.3 is a function of maximum stress, stress amplitude, frequency and temperature. As all the experiments were performed with a low frequency, ($f \leq 5$), and at room temperature, the effects of frequency and temperature on the experimental data can be ignored. Using a power form to describe the damage growth during fatigue loading [42], $\bar{C}$ may be expressed as

$$\bar{C} = \bar{C}(f, T, \sigma_{max}, \sigma_{amp}) \approx \bar{C}(\sigma_{max}, \sigma_{amp}) = C\frac{\sigma_{max}^m \sigma_{amp}^m}{\sigma_{ult}^{2m}} = C(\frac{\sigma_{max}^2(1-R)}{\sigma_{ult}^2})^m \tag{4.4}$$

where σ_{max}= maximum stress; σ_{min}= minimum stress, and $\sigma_{amp} = \sigma_{max} - \sigma_{min}$. R is the ratio of minimum to maximum stress. σ_{ult} is the ultimate strength of the material and C and m are constants. Integration of the Eq.(4.3) yields

$$-\frac{1}{n}e^{-nD} = C(\frac{\sigma_{max}^2(1-R)}{\sigma_{ult}^2})^m logN + A \tag{4.5}$$

where A is a constant of the integral. Since D=0 when N=1, the Eq.(4.5) can be written as

$$-\frac{1}{n}e^{-nD} = C(\frac{\sigma_{max}^2(1-R)}{\sigma_{ult}^2})^m logN - \frac{1}{n} \tag{4.6}$$

Rearranging Eq.(4.6), the damage function can be written in a closed-form as

$$D = -\frac{1}{n}\ln[1 - Cn(\frac{\sigma_{max}^2(1-R)}{\sigma_{ult}^2})^m logN] \tag{4.7}$$

The schematic damage accumulation versus the number of cycles are shown in Fig. 4.13. Three distinctive stages can be observed in the fatigue life of polymeric composites. At the first stage, damage grows rapidly due to the initiation and propagation of micro-cracking in the matrix. In the intermediate stage, damage grows relatively slowly and at a steady rate. In this stage, the

matrix cracks reach the vicinity of fibers and a stable crack growth occurs along the fiber-matrix interface. A rapid damage growth can be observed again in the third stage, and before a sudden failure of the samples. Failure of samples occurs in two different modes. In on-axis samples with stronger fiber-matrix interfaces, the final failure is due to the rupture of fibers. On the other hand, matrix splitting along the fiber direction can be observed in the final stage of the fatigue life of on-axis samples with weaker fiber-matrix interfaces or off-axis samples.

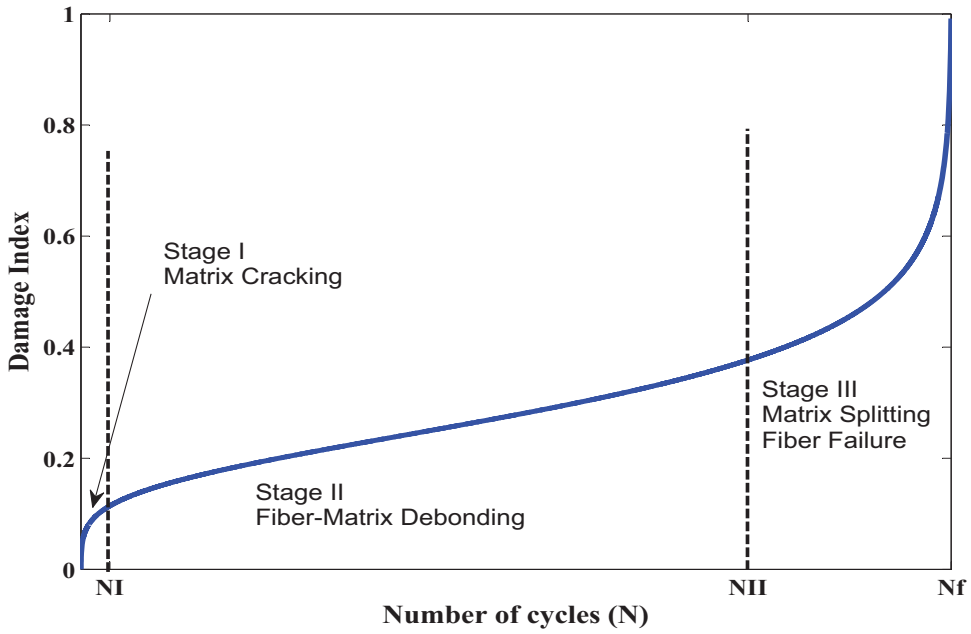

Figure 4.13: Schematic damage accumulation versus N

Using Eq. (4.7), a ratio of normalized residual stiffness to initial stiffness can be obtained with

$$\frac{E(N)}{E_0} = 1 + \frac{1}{n}\left(1 - \frac{E(N_f)}{E_0}\right)\ln[1 - Cn(\frac{\sigma_{max}^2(1-R)}{\sigma_{ult}^2})^m logN] \tag{4.8}$$

It should be noted that n, m and C are constant parameters and can be determined by curve-fitting of the experimental data. D approaches 1 when the number of loading cycles approaches the maximum number of life cycles, N_f. Under this condition, and using the corresponding constant parameters, the stiffness-based S-N curve can be derived from Eq.(4.6):

$$\sigma_{max} = \frac{\sigma_{ult}}{\sqrt{1-R}} \sqrt[2m]{\frac{1-e^{-n}}{CnlogN_f}} \qquad N_f > 1 \tag{4.9}$$

4.5 Modelling modes of fatigue damage

In this section, a model is presented to predict different modes of fatigue damage in carbon fiber-vinyl ester composites with 90° fiber orientations with respect to the loading direction.

The transverse modulus of virgin samples can be obtained via a modified Halpin-Tsai equation:

$$\begin{aligned} E_T(N) &= \frac{1+\zeta(N)\eta c}{1-\eta c} E_m(N) \\ \eta &= \frac{\frac{E_f}{E_m(N)} - 1}{\frac{E_f}{E_m(N)} + \zeta(N)} \end{aligned} \tag{4.10}$$

where $E_T(N)$ is the residual transverse modulus of composites at the Nth cycle. $E_m(N)$ and $\zeta_(N)$ are defined as the contribution of matrix and fiber-reinforcement in the transverse modulus of the composite plate at the Nth cycle.

Degradation in the transverse modulus of carbon fiber-vinyl ester composites by cyclic loading and based on the developed model can be expressed as:

$$\frac{E_T(N)}{E_{0T}} = 1 + \frac{1}{n}\Big(1 - \frac{E_T(N_f)}{E_{0T}}\Big) ln[1 - Cn(\frac{\sigma^2_{max}(1-R)}{\sigma^2_{Tult}})^m logN] \tag{4.11}$$

where E_{0T} is the initial transverse modulus of samples. m, n and C can be obtained by curve-fitting of the experimental data.

Matrix-fiber debonding and matrix cracking are major components of transverse modulus degradation of fiber-reinforced composites. The damage in the fiber-matrix interface can be modelled by decreasing the contribution of fiber-reinforcement in the transverse modulus of composites in Eq.(4.10). Similarly, the damage in the matrix is modelled by reducing the contribution of the matrix modulus in the transverse modulus of specimens. Since matrix cracking is a dominant factor in the degradation of the transverse modulus during the first stage of fatigue life ($\sim 10\%$ of the fatigue life), it can be assumed

$$\zeta(N) = \zeta_0 \qquad N \leq N_I \tag{4.12}$$

where ζ_0 is the initial value of ζ. Using equation Eq.(4.10), $E_m(N)$ can be obtained with

$$E_m(N) = -B + \frac{\sqrt{B^2 - 4AD}}{2A} \qquad N \leq N_I \tag{4.13}$$

where

$A = \zeta_0(1-c)$

$B = E_f(1+\zeta_0 c) - E_T(N)(\zeta_0 + c)$

$D = E_f E_T(N)(c-1)$

$E_T(N) = E_{0T}\left[1 + \frac{1}{n}\left(1 - \frac{E_T(N_f)}{E_{0T}}\right)\ln[1 - Cn(\frac{\sigma^2_{max}(1-R)}{\sigma^2_{ult}})^m logN]\right]$

During the second stage, fiber-matrix decohesion is a main factor in the degradation of carbon fiber-vinyl ester composites' transverse modulus. Therefore, it can be assumed that

$$E_m(N) = E_m(N_I) \qquad N_I < N \leq N_{II} \tag{4.14}$$

where $E_m(N_I)$ is the contribution of the matrix modulus to the transverse modulus of the composite at the $N_I th$ cycle. Using equation Eq.(4.10), $\zeta(N)$ can be calculated with:

$$\zeta(N) = \frac{\frac{E_f E_T(N)}{E_m(N_I)}(1-c) - E_f + E_T(N)c}{cE_f - E_T(N) + E_m(N_I)(1-c)} \qquad N_I < N \leq N_{II} \tag{4.15}$$

For samples with a 90° fiber orientation, the damage in the matrix during the fatigue life can be defined with:

$$D_m(N) = 1 - \frac{E_m(N)}{E_{0m}} \tag{4.16}$$

Similarly, the damage in the fiber-matrix interface can be determined with:

$$D_f(N) = 1 - \frac{\zeta(N)}{\zeta_0} \tag{4.17}$$

The third stage is not observed in the fatigue life of specimens with 90° fiber orientations.

4.6 Result and discussion

In this section, the fatigue damage in the longitudinal and transverse stiffness of unidirectional carbon fiber-vinyl ester composite laminates are evaluated. The damage evolution in virgin and environmentally-aged samples are compared, and corresponding constant parameters of the proposed model are obtained. The constant parameters of the proposed damage model are determined by curve-fitting of the experimental data. The proposed model should fit the experimental data very well when the coefficient of determination nears $r^2 = 1$. r can be calculated with the following:

$$r = \frac{n\sum xy - (\sum x)(\sum y)}{\sqrt{n(\sum x^2) - (\sum x)^2}\sqrt{n(\sum y^2) - (\sum y)^2}} \tag{4.18}$$

where x's are experimental values and y's are predicted values by the model. n represents the number of data pairs. The coefficient of determination, r^2, yields a value between 0 an 1 ($0 \leq r^2 \leq 1$), defining how well the model predicts the experimental data. If the proposed model passes through every point of the experimental data, $r^2 = 1$. However, if the model does not perfectly fit the experimental data, it will not be able to capture the trend variation ($r^2 << 1$). Predicting the fatigue damage at different loading levels can be employed as a measure of accuracy for the predetermined constant parameters. The stiffness-based S-N curve and different modes of fatigue damage are also discussed here. It should be noted that for measuring the fatigue damage in the longitudinal modulus, the direction of fibers should be parallel to the loading direction. Also, to determine the fatigue damage in the transverse modulus, the direction of the fiber has to be perpendicular to the loading direction.

4.6.1 Fatigue damage in longitudinal modulus

Figure. 4.8 displays the longitudinal modulus of virgin and environmentally-aged carbon fiber-vinyl ester composites during fatigue life. The maximum loading level is set to 67% of the corresponding longitudinal tensile strength. Three distinctive stages can be observed in the fatigue life of the longitudinal modulus. A small reduction in the modulus, observed in the first stage, is due to the initiation of micro-cracks inside the matrix and breakage of weak fibers at the first few cycles of fatigue life. In the intermediate stage, a relatively slow and stable damage growth can be observed. During this stage, micro-cracks grow along the fiber-matrix interface, decreasing the contribution of fibers in the load transfer mechanism. A rapid damage growth can be observed at

the final stage of fatigue life. In this stage, the existing micro-cracks and interface debondings link up, leading to an initiation of matrix splitting and propagation of a visible crack along the fiber direction. A visible crack grows along the fibers, causing a redistribution of fiber loads, leading to excessive loads in fibers adjacent to the crack. Breakage of the overloaded fibers causes the crack to progress in the fiber direction until it reaches the aluminium tabs and the specimen fails [55]. The final failure of the composite occurs in the form of matrix splitting, indicating the existence of a weak fiber-matrix interface in the presence of strong fibers.

The cumulative damage in the longitudinal modulus for virgin and environmentally-aged samples are evaluated from the experimental data and given in Fig. 4.14. The constant parameters of the proposed model for both virgin and aged specimens are obtained by curve fitting of the experimental data and given in Table 4.2. The proposed model fits the experimental results well with the coefficient of determination, $r^2 = 0.9939$ for virgin and $r^2 = 0.9937$ for aged samples. Degradation of matrix and fiber-matrix interfaces by environmental exposure prior to fatigue loading leads to faster damage growth in the aged specimens compared to that in virgin ones.

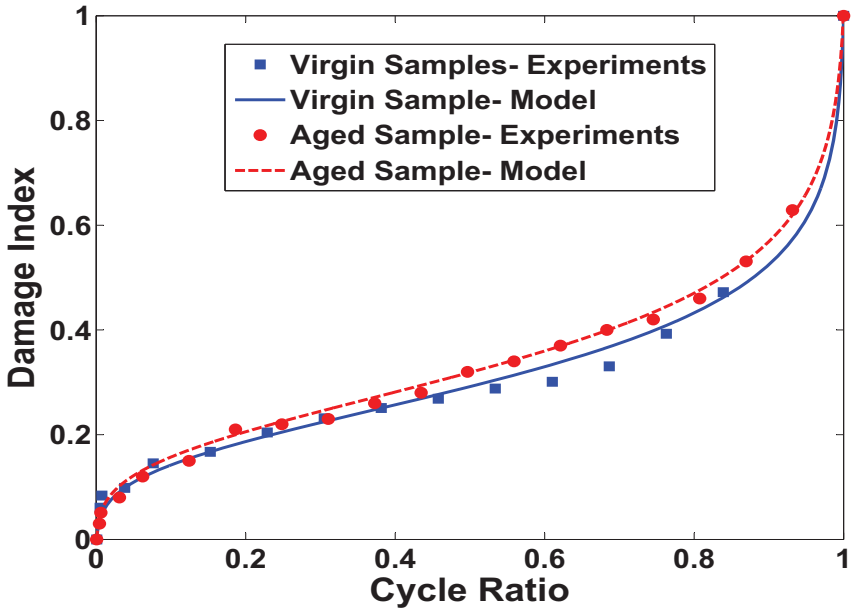

Figure 4.14: Damage in the longitudinal modulus during the fatigue life.

Table 4.2: Constant parameters

Material Constants	Tensile Strength	C	n	m
[0°] Virgin Sample	1492 MPa	0.865	8.00	3.00
[0°] Aged Sample	1387 MPa	1.005	7.40	3.10
[90°] Virgin Sample	60 MPa	5.86	0.32	2.9
[90°] Aged Sample	51.4 MPa	9.63	0.15	3.2

The fatigue damage accumulation in the longitudinal modulus of virgin samples under 62% and 67% loading levels are given in Fig. 4.15. The proposed model with the constant parameters obtained from curve fitting under a 67% loading level provide a good prediction of the failure cycle and damage evolution under a 62% loading level. Figure. 4.16 exhibits damage accumu-

lation for 62% and 67% loading levels versus the normalized number of cycles. The coefficient of determination is 0.9659 for a loading level of 62%. It is worth noting that the damage in the longitudinal modulus grows more slowly for high loading levels than for low loading levels during corresponding fatigue lives.

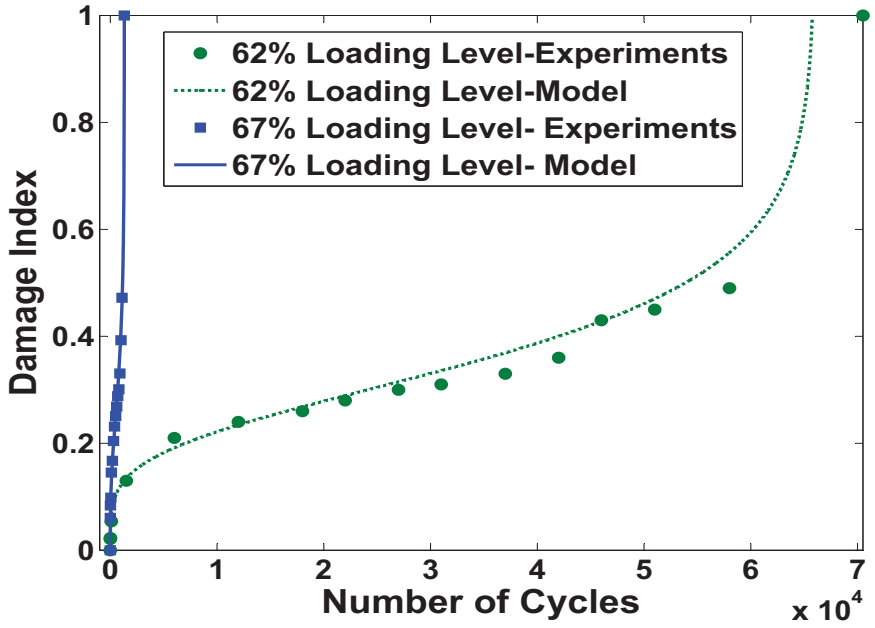

Figure 4.15: Damage evolution in the longitudinal modulus for different loading levels versus the number of cycles.

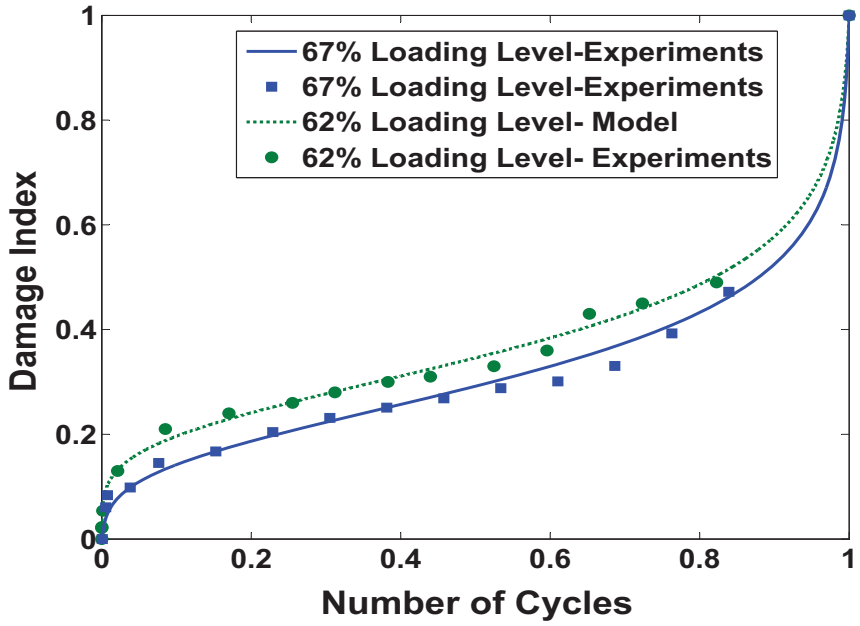

Figure 4.16: Damage evolution in the longitudinal modulus for different loading levels versus the normalized number of cycles.

4.6.2 Fatigue damage in transverse modulus

Figure. 4.17 displays the transverse modulus of virgin and environmentally-aged carbon fiber-vinyl ester composites during fatigue life. The maximum loading level is set to 62% of the corresponding transverse tensile strength. Two distinctive stages can be observed in the fatigue life of the transverse modulus. Since the extensive matrix cracking occurs in the first few cycles of the fatigue life, a large damage is accumulated during the first stage. During the second stage, fiber-matrix decohesion is a main factor in carbon fiber-vinyl ester composites' transverse modulus degradation. A steady and relatively slow damage growth can be observed in this stage. The third stage occurs when a dominant crack starts to grow in the fiber direction. Unlike the longitudinal modulus, a sudden rupture occurs at the beginning of the third stage and this stage can not be

distinguished from previous stages for the transverse modulus. The constant parameters of the developed model are obtained by curve fitting the experimental data and given in Table 4.2. The coefficient of determination is 0.9964 for virgin and 0.9837 for aged specimens. Similar to the longitudinal modulus, the damage grows slightly faster in the aged specimens, in comparison to the virgin specimens, during fatigue life.

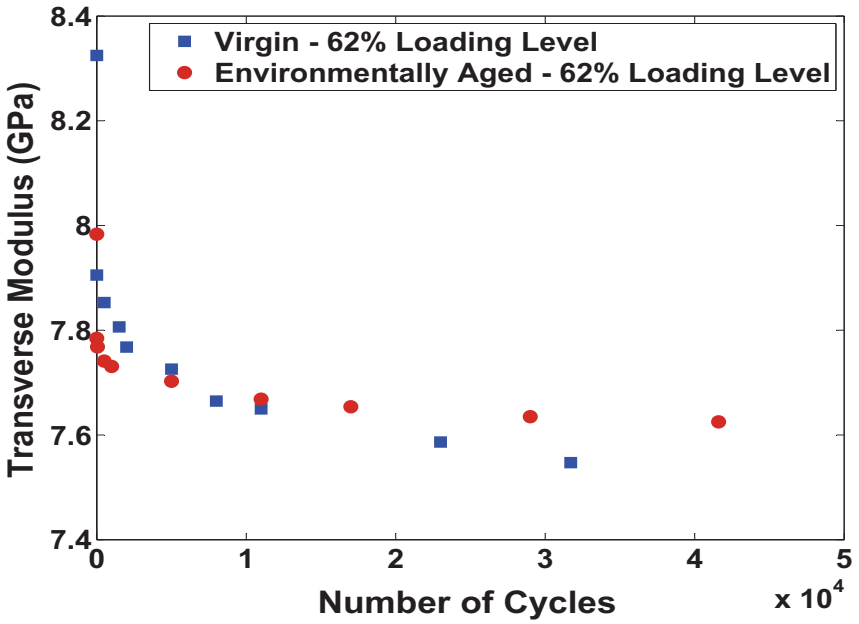

Figure 4.17: The transverse modulus during fatigue life.

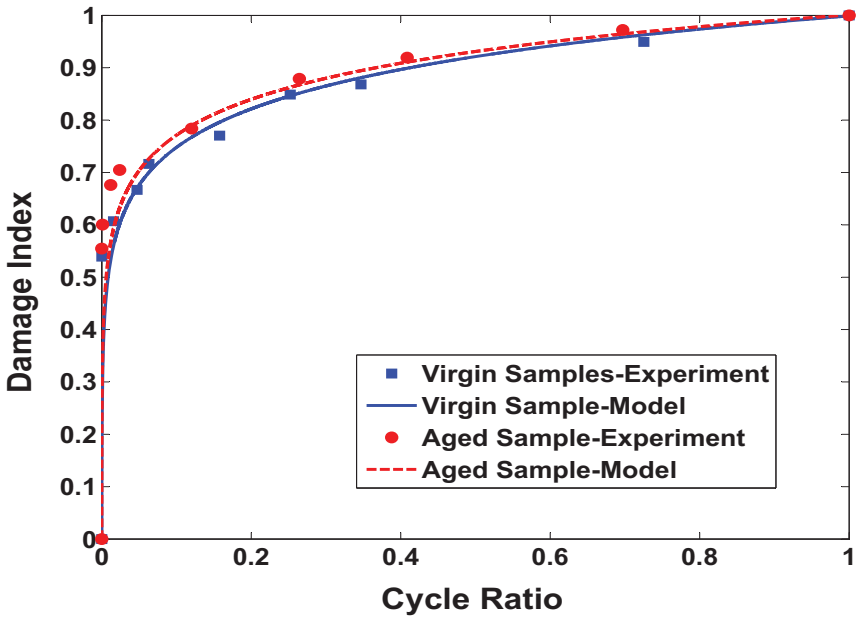

Figure 4.18: Damage in the transverse modulus during fatigue life.

The accumulated fatigue damage in the transverse modulus of virgin samples with 62% and 67% loading levels are given in Fig. 4.19. The final cycle and damage evolution under a 67% loading level were predicted using the proposed damage function. Figure. 4.20 shows the damage accumulation in the transverse modulus for the given loading levels versus the normalized number of cycles. The model fitted the experimental data with the coefficient of determination $r^2 = 0.9716$ for a loading level of 67%. It can be seen that the damage in the transverse modulus grows more slowly for high loading levels than for low loading levels during the corresponding fatigue life.

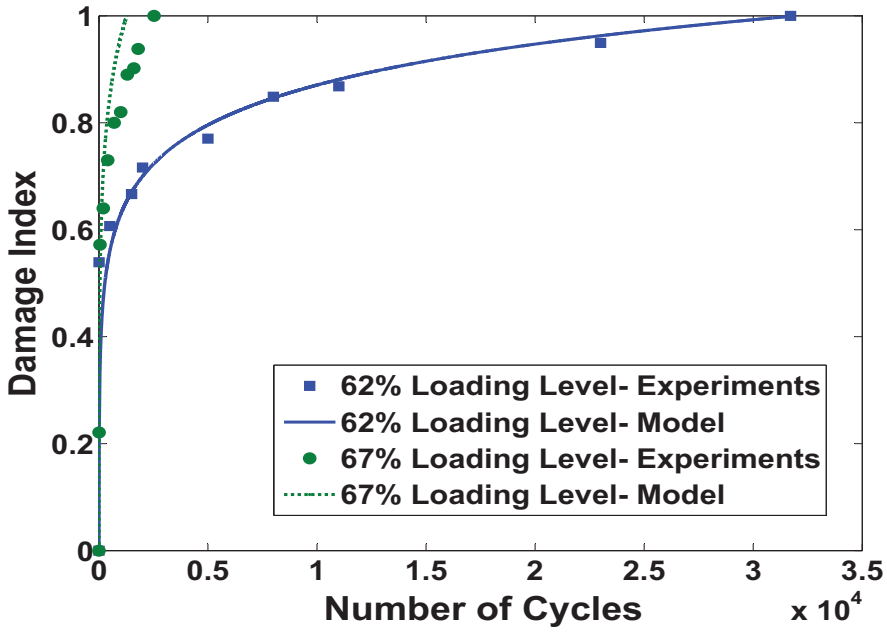

Figure 4.19: Damage evolution in the transverse modulus for different loading levels versus the number of cycles.

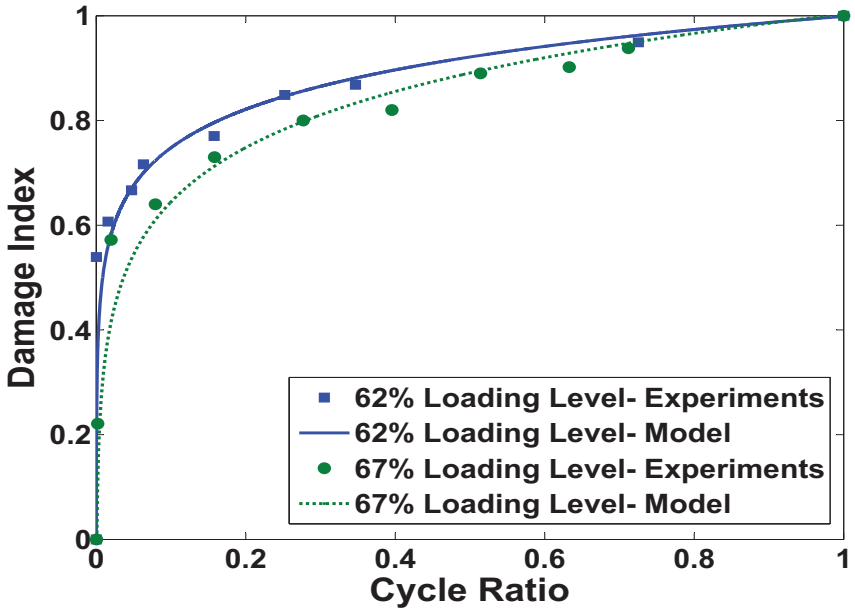

Figure 4.20: Damage evolution in the transverse modulus for different loading levels versus the normalized number of cycles.

4.6.3 Stiffness-Based S-N curve

Using table 4.2 and Eq.(4.9), the stiffness-based S-N curve can be obtained for the specimens. Figure. 4.21 and Fig. 4.22 show the longitudinal and transverse strengths for both virgin and environmentally-aged carbon fiber-vinyl ester composite laminates during fatigue life. The evaluated S-N curves are well-fitted to the experimental data. Both virgin and aged specimens experience a great reduction in strength during the first few cycles. This phenomenon may be due to the fatigue-induced micro-cracking inside the matrix during the first stage of fatigue life. The similar shape of S-N curves for virgin and aged specimens indicates a similar fatigue failure mechanism in both samples.

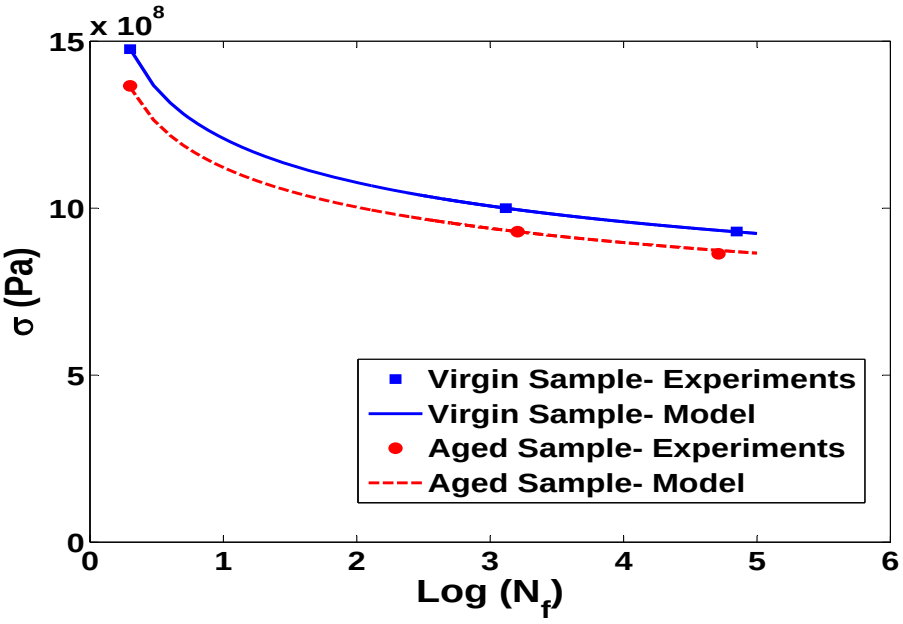

Figure 4.21: Stiffness-based S-N curve for longitudinal strength.

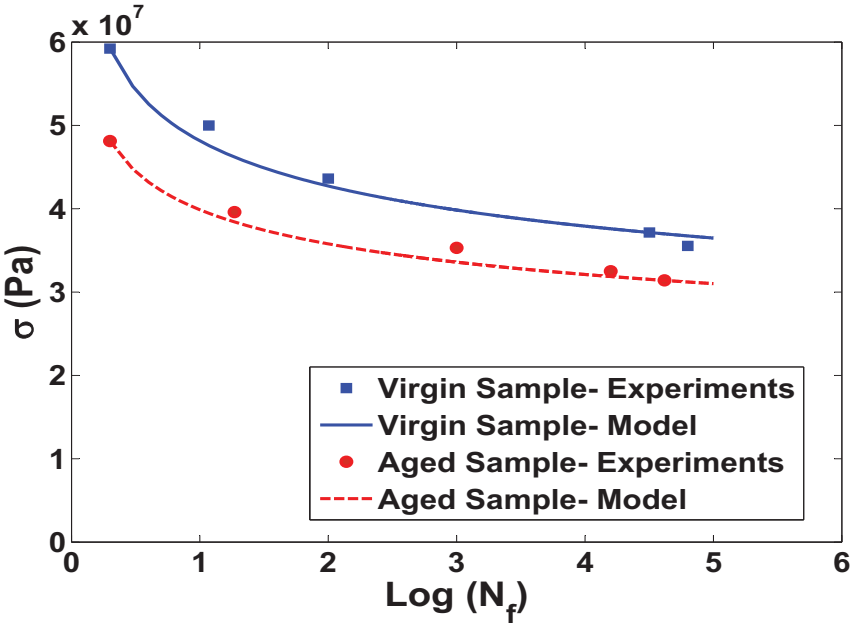

Figure 4.22: Stiffness-based S-N curve for transverse strength.

4.6.4 Modes of fatigue damage

The damage evolution in the matrix of virgin and environmentally-aged specimens can be evaluated by Eq.(4.16) and is given in Fig. 4.23

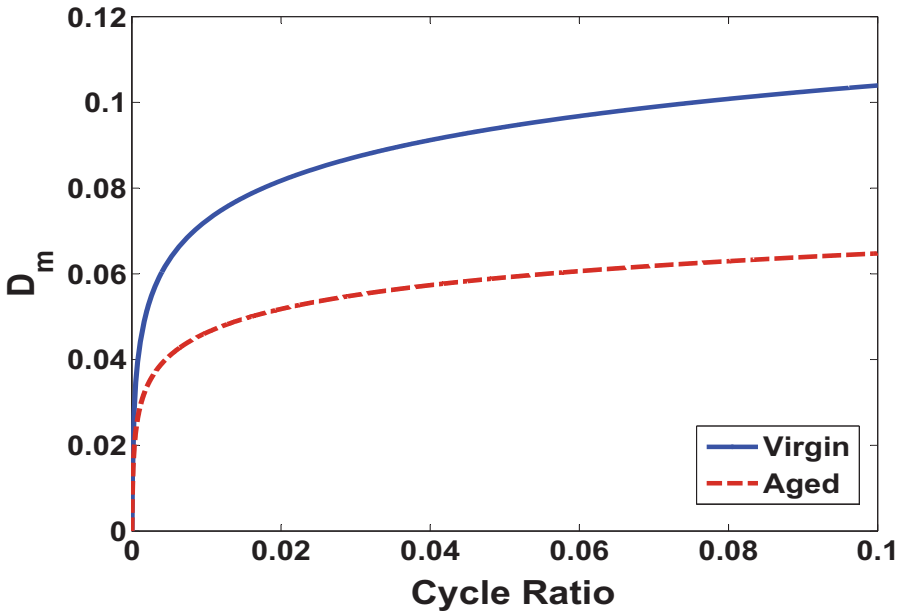

Figure 4.23: Damage in the matrix.

It is assumed that the damage in the matrix due to environmental exposure is limited to the surface of the exposed specimens; therefore, deeming the damage negligible. Figure. 4.23 shows that the damage in the matrix of virgin samples grows faster than in aged specimens during the first stage of fatigue life. This indicates that the matrix is less sensitive to micro-cracking after exposure to differing environmental conditions.

Using Eq.(4.17), the cumulative damage in the fiber-matrix interface of virgin and environmentally-aged specimens is obtained and given in Fig. 4.24

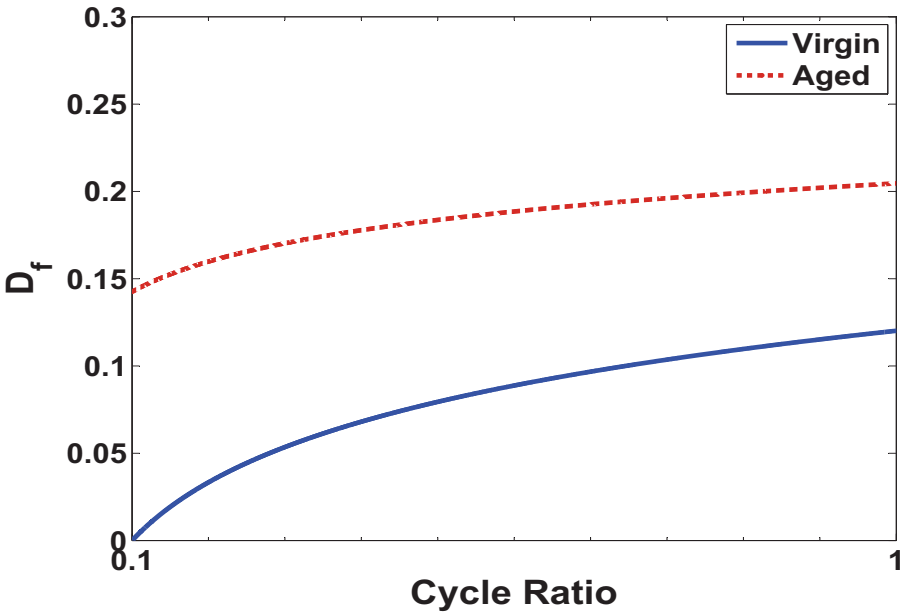

Figure 4.24: Damage in the fiber-matrix interface.

The fiber-matrix interface of environmentally-aged specimens is primarily degraded by environmental exposure and the damage in the interface evolves slowly during fatigue life. The overall damage in the fiber-matrix interface of environmentally-aged specimens was substantially higher than in virgin samples. It seems that the overall damage in the matrix and fiber-matrix interface must reach a critical point before the final failure of specimens.

4.7 Conclusion

The model presented here is able to predict the fatigue damage in the longitudinal and transverse stiffness of unidirectional carbon fiber-vinyl ester composites. The proposed model uses minimum constant parameters to capture all stages of fatigue life of fiber-reinforced composite laminates. The damage in the stiffness of environmentally-aged specimens grows slightly faster than in virgin samples. This is due to the existence of prior damage in the matrix and fiber-matrix

interface, caused by environmental exposures, which accelerate the damage mechanism during fatigue life. The damage in the stiffness grows more slowly for higher loading levels, when compared to that in lower loading levels, during their corresponding fatigue lives. The strength of both virgin and aged samples exhibit a great reduction during the first few cycles of fatigue life due to fatigue-induced micro-cracking inside the matrix during the first stage. The parallel shape of S-N curves of virgin and aged samples indicates that there is a similar fatigue failure mechanism for both specimens.

Chapter 5

Fatigue and Flexural Response

5.1 Introduction

Fiber-reinforced polymer composites are used as exterior top-layers for foam core sandwich panels and as lightweight structural materials, which can undergo cyclic loading during application. Exposure to outdoor environments subjects composites to ultraviolet (UV) and moisture conditions that cause degradation and weakening of composites during service. Here, accelerated aging of carbon fiber-reinforced vinylester composites is performed using UV radiation and condensation to ascertain its effect on fatigue response. Uniaxial cyclic loading is applied to composite coupons after environmental condition exposure, where the effect of the environment will be determined by modulus evolution and post-fatiguing three-point bending.

5.2 Experimental setup

Carbon fiber-reinforced vinylester unidirectional composite laminates (Graphtek LLC) were used in these set of experiments, Table 2.1. Composite laminate sheets with nominal thickness of 1.4 mm were machined (using a diamond wet saw) into 25 x 152 mm coupons with [90°] fiber direction for the fatigue test.

A tension-tension cyclic loading test has been performed on virgin and environmentally aged

samples for 50000 cycles at a minimum to maximum stress ratio $R = 0.2$ with sine wave form and 5 Hz frequency. The maximum load was set to 25% and 45% of ultimate tensile strength of the samples. The flexural properties of virgin and environmentally aged specimens will be determined after fatigue loading and compared with the non-fatigued samples to determine the effect of cyclic loading on the mechanical properties of carbon fiber/vinyl ester composites.

Three-point bending tests were performed on the composite samples following the ASTM D790 standard using a screw-driven mechanical loading frame (TiraTest 26005) with a 0.5 kN load cell. The three-point bending test determines the flexural modulus and flexural strength of samples. Support geometry followed ASTM D790, with the support span set for 60 mm, resulting in a span/thickness ratio of ~ 43. A cross-head rate of 4.25 mm/min was employed to produce a strain rate of 0.01 mm/min.

5.3 Exposure condition

[90°] Fiber direction samples will be exposed to different environmental conditions, including 500 hours of UV irradiation, 500 hours of moisture in the form of condensation, 500 hours of salt spray, and 1000 hours of combined UV irradiation and condensation cycled every 3 hours in the QUV chamber.

5.4 Result and discussion

5.4.1 Tensile modulus during cyclic loading

During cyclic loading of the 90 degree composite coupons (loading is perpendicular to the fiber direction), the transverse tensile modulus of the composites were computed through the measurement of the strain by clip-on extensometer. The modulus was computed from the cyclic load

data and the strain, which was measured simultaneously by data acquisition. Measurements were taken at intervals of 10000 cycles throughout the 50,000 cycle test duration. Data was collected for 1000 cycles, and then, individual slopes of the load cycles and strain responses were calculated for 50 cycles taken at 200 cycle intervals. The computed slopes allow direct calculation of the tensile modulus of the specimens, which were then averaged over the 50 values. The averaged modulus values are plotted against the number of loading cycles in Fig. 5.1 for composites exposed to different environmental conditions and for virgin (as-received) samples. The modulus of samples decrease rapidly during the few first loading cycles. The rapid decrease is due to the extensive micro-cracking within the matrix. Though the initial decrease in modulus is largest after the first 50 cycles for the unconditioned specimens, the overall modulus decrease is largest for the UV/condensation-exposed composites when compared to the non-fatigued undegraded specimens. The UV/condensation specimen modulus decrease was 11% after combined environmental exposure and cyclic loading, for which the virgin specimens' decrease was 8%. These results demonstrate the importance of the fatigue role in the evolution of combined environmental effects, even for the low fatigue levels (0.45) used in these experiments.

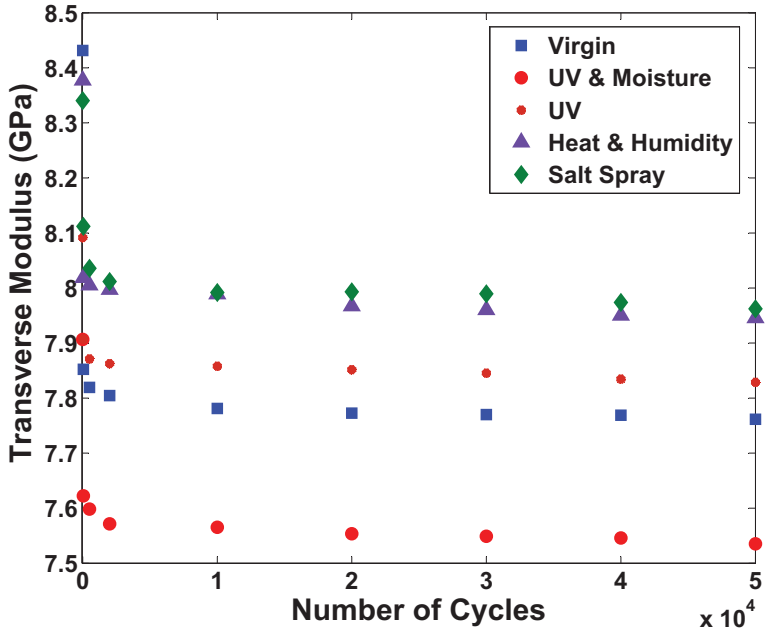

Figure 5.1: Transverse tensile modulus during cyclic loading.

5.4.2 Mechanical flexural response of fatigued specimens

The flexural modulus of virgin and environmentally aged samples before and after the fatigue loading is given in Fig. 5.2. A slight decrease in the flexural modulus of samples due to the environmental exposure can be seen in Fig. 5.2 (Gray colors). The effect of fatigue with different loading levels, 0.25 UTS and 0.45 UTS, is also shown in Fig. 5.2 (blue and red colors). For each condition, a small change can be observed in the transverse modulus of samples subjected to different loading levels. Samples exposed to salt spray showed the minimum transverse modulus (13.5%) after fatigue loading (0.45 UTS loading level).

The flexural strength of aged and virgin samples before and after fatigue loading is shown in Fig. 5.3. A drastic change can be seen in the flexural strength of samples exposed to the combined UV radiation and condensation (29%). The load level of 0.45 UTS causes more degradation in the

flexural strength than that of 0.25 UTS. Samples exposed to UV radiation and moisture, which were subjected to 0.45 UTS fatigue loading levels suffered the greatest reduction in flexural strength (31.5%).

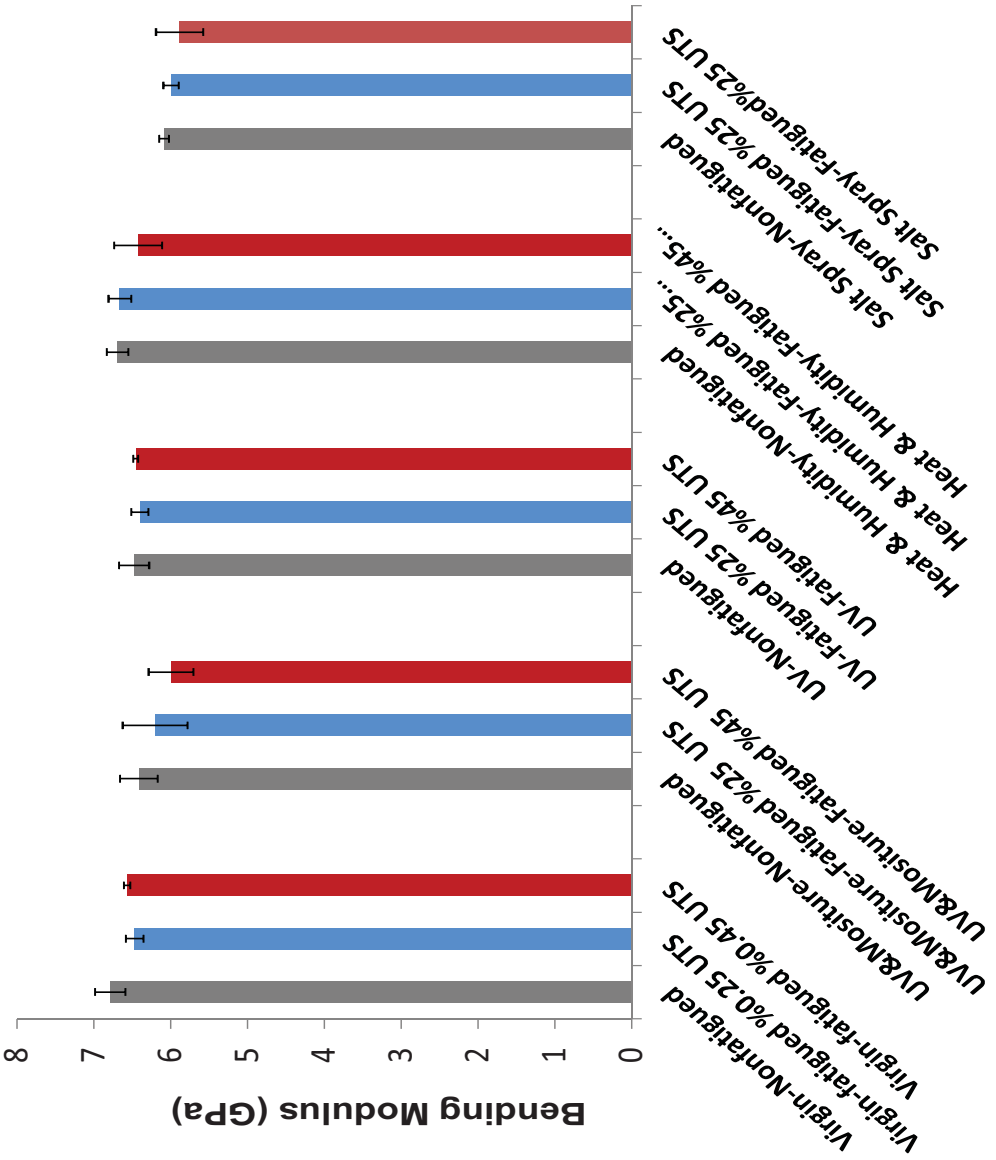

Figure 5.2: Flexural strength degradation in environmental chamber

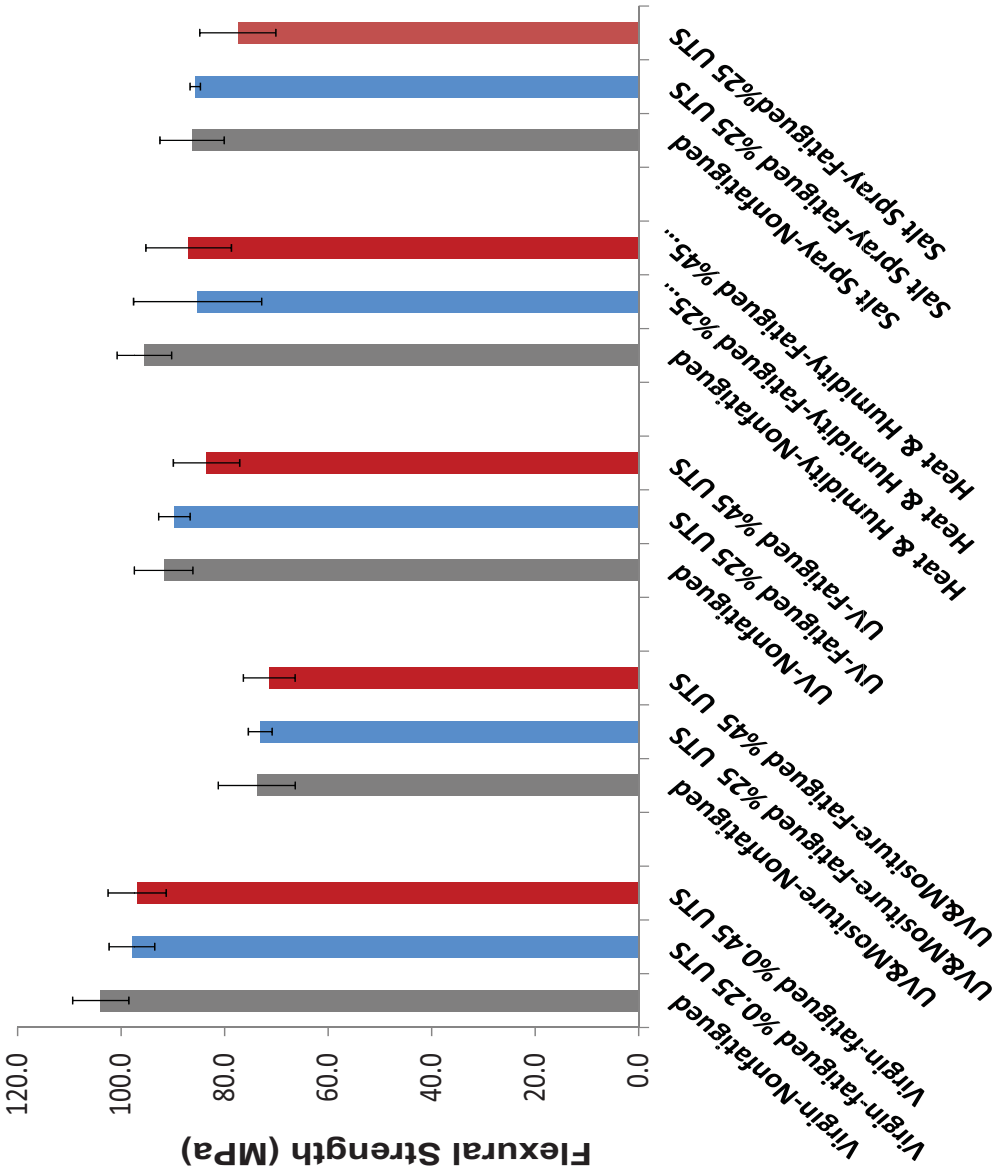

Figure 5.3: Flexural strength degradation in environmental chamber

5.5 Conclusion

The effect of tensile fatigue loading on the mechanical properties of environmentally aged carbon fiber-vinyl ester composite laminates has been characterized by the post-fatiguing flexural test. It can be observed that the greatest portion of damage on the mechanical properties were inflicted on composite coupons during environmental exposure. Additionally, post-exposure fatigue loading had a small effect on further degradation of the mechanical properties. In the next chapter, we will discuss the cyclical rotation of samples between environmental chambers and the the flexural fatigue machine, reaching the desired number of loading cycles and exposure time (in hours). This aids us in understanding the synergistic effects of environmental exposure and fatigue loading on composite laminates in the true marine environment.

Chapter 6

Marine Coating

6.1 Introduction

The process of designing reliable and enduring naval composite crafts is instrumentally dependent upon the utilization of protective coatings (e.g. ester or polyurethane-based coating) to shield composites from harsh environments and protect them against environmental-based degradation. However, as coatings can be vulnerable to corrosion and/or erosion in harsh marine environments, with time, they can and are observed to lose their protective abilities, leading to damage accumulation in the coated composites. To demonstrate the critical nature of this process, we subjected coated (utilizing with ester base gel coating) carbon fiber vinyl-ester laminates to simulated marine environments with UV radiation and condensation. Then, we probed the degradation in the composite by measuring its flexural strength. Results show that, after long-term exposure, the composite can lose more than 20% of its strength, which is critical. This loss can even be amplified under cyclic loadings and combined exposure to corrosive and erosive marine environmental elements.

6.2 Marine coating systems

Different exterior areas of a large ship are

1- Superstructures

2- Decks, walkways, and stairs

3- Sides and splash zone

4- Below the water line

Fig. 6.1 shows these areas on a ship.

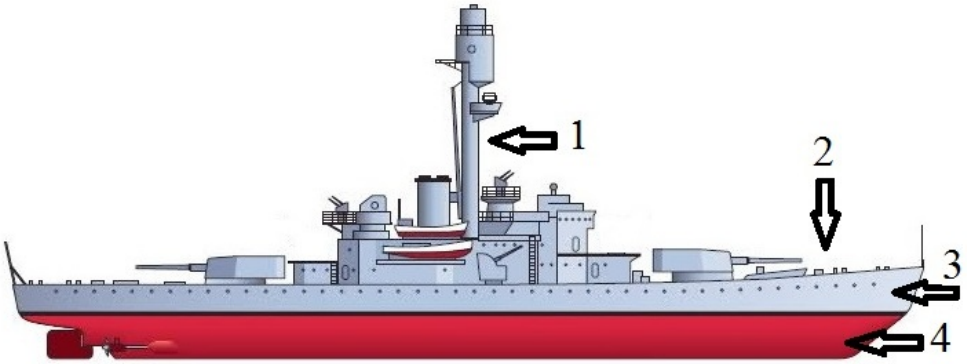

Figure 6.1: Exterior areas of a large ship

Each part of the ship is subjected to different environmental exposures. Top-side and superstructures are exposed to humidity and UV radiation. The splash zone is exposed to sea water and ultraviolet radiation. The ship's hull (below the water line) is fully submerged in the seawater and exposed to different marine organisms. The proper coating should be selected based on the exposure condition of the ship's part. Different types of marine coating used for the splash zone and below the water line will be discussed.

6.2.1 Sides and splash zone

The splash zone is exposed to UV radiation, sea water and atmospheric moisture in the form of dew and rain. The coating of the splash zone needs to be high UV-resistant as well as corrosion-resistant to sea water and moisture. The typical coatings for the splash zone are [113];

1- Pure or modified epoxy primer/epoxy topcoat

2- Aliphatic polyurethane

3- Aliphatic polyurethane/acrylic

4- Polysiloxane/epoxy hybrid (anti-rust stain topcoat may be applied)

Aliphatic polyurethane provides long-term UV protection and excellent resistance to corrosion and weathering. Polysiloxane also has excellent corrosion and chemical resistance and flexibility. It has long-term performance, which is comparable to that of aliphatic urethanes.

6.2.2 Below the water line

Barnacles, mussels, tubeworms, seaweed, other plant life and marine organisms attach themselves to the coating of ships' hulls. This decreases the smoothness of the ship's exterior, resulting in more drag and fuel consumption. To protect the hull of the ship from marine organisms, two different types of coating are applied to the exterior of the hull as follows:

6.2.2.1 Anti-fouling coating

Traditionally, the marine industry provides protection against marine organisms by incorporating biocides, which are released from the coating into the sea water via different mechanisms, such as copper or tributyl tin (TBT) compounds. Although this type of protection has been proven effective, negative environmental concerns were raised by the usage of anti-fouling coating. For

instance, the quantity of tin, copper, and other toxins increased in fish and other marine organisms, inciting harmful effects on the environment and for human health. The use of antifouling with TBT (as a biocide) was banned on September 17, 2008. A great effort has been made by different researchers to produce environmentally friendly antifouling coating. These anti-fouling coatings can be enumerated as tin-free controlled depletion paints (CDPs) and tin-free biocide-containing self-polishing paints (TF-SPCs) or hybrid paints (CDPs and TF-SPCs) [113].

6.2.2.2 Fouling-release coating

Another way to protect the hull system against marine organisms is by using coating systems, which produce very smooth and low energy surfaces. This gives a surface non-stick and easy to clean properties. Since fouling-release coating does not leach toxins into the environment, it is considered environmentally friendly coating. Silicone-based coating is a new technology, which has a fouling-release property [118]. Silicone-based coating surfaces are smooth, non-stick, easy to clean and have low surface energy. The basic features of silicone-based coating are:

1- It is difficult for marine organism to attach to the surface.

2-The attachment of marine organisms is very weak and they are easily removed by vessel movement.

The combination of fouling-release and anti-fouling mechanisms produce self-polishing co-polymers (SPC), which enables vessels to be free of fouling for up to five years.

6.2.3 Coating components

For big structures like ships, coating systems may contain three different layers.

6.2.3.1 Primer

Epoxy primer can be used for immersion and atmospheric services in marine and industrial environments [115, 114]. Epoxy primer might be pigmented with versatile anti-corrosive additives and can be applied to the steel, aluminum and fiberglass laminates, providing superior properties like:

1- Self-polishing

2- Resiliency and toughness of the surface

3- Salt water and fresh water corrosion resistance

6.2.3.2 Tie-coat

Tie-coat is a coating that provides adhesion between the surface of the primer and the top coat [116]. It might be used when the top coat does not have good adhesion to the epoxy surface.

6.2.3.3 Top coat

The top coat is used as a finishing coat for exterior metal and structures in marine and industrial environments [114, 117]. It can be used as a surface coat for marine hulls, and typically, offers a good moisture and corrosion resistance. For the splash zone, it may also offer UV-resistance. The top coat provides very smooth, low energy, glossy and easy to clean surfaces, which produce a proper fouling release system.

6.2.4 Gel coat

Gel coat is a material, which is used as a coating to provide resistance to ultraviolet radiation and moisture in fiber-reinforced composite materials. Gel coats are usually based on saturated polyester resins or epoxy chemistry. They are able to produce high quality finish and a glossy appearance for the surface of fiber-reinforced composites. In the marine and aerospace industries, composite materials are usually coated with a finishing layer of gel coat, typically 0.5 mm to 0.8 mm in thickness.

6.3 Sample preparation

The Sea Hawk Clear HI-UV Gel Coat [119] was used for painting the carbon fiber-vinyl ester composite specimens. This paint offers marine-grade properties and is easy to apply. This gel coat is used as a surface coat to provide proper protection to the composite laminates against various environmental conditions and UV radiation levels. HI-UV gel coat is primarily composed of isophthalic-neopentyl glycol (ISO/NPG) polyester resin, which is a flexible polyester and produces resiliency and toughness for the surface. It also may be used to patch and re-gelcoat.

MEKP is used as a catalyst for clear HI-UV gel coat. The catalyst level (MEKP) should be between 1.2% and 3% of the gel coat's total volume for a proper cure. Gel time with 1.8% MEKP is about 10-17 minutes and may vary based on the temperature, humidity, air movement and catalyst concentration.

To fully cure the gel coat, a surfacing agent should be added to the finishing coat. Sea Hawk 8140 Wax Additive is used as a surface agent up to 4oz per gallon of gel coat for producing a non-sticky surface.

Samples with [0°], [45°] and [90°] fiber orientation were painted with Clear HI-UV Gelcoat. The final thickness of the coating is about 0.15 mm (see Fig. 6.2).

(a) (b)

Figure 6.2: Surface of carbon fiber-vinyl ester composites painted by gelcoat (a) top view (b) side view

Environmentally-aged samples were exposed to radiation/condensation in a Q-Lab QUV/se environmental chamber. In the chamber, the UV radiation and condensation conditions cycled every 3 hours. For the UV cycle, the UV irradiation was set at $0.6W/m_2$ at 60 C, and the condensation cycle was set at a temperature of 45 C. All samples were exposed to radiation/condensation for 600, 1200 and 2200 hours.

6.4 Experimental setup

To understand the synergistic effects of fatigue loading and environmental exposure, the environmental degradation and fatigue loading should be performed simultaneously. To do so, samples are rotated between the environmental chamber and the fatigue test machine. The 24 hour

exposure in the environmental chamber is followed by 4000 loading cycles, a good representation of synergistic environmental exposure and repeated mechanical loading in the marine environment.

Displacement-controlled bending fatigue tests with the minimum to maximum stress ratio R = 0.1 were conducted with a 3 hertz frequency and a $\sim$ 40% Ultimate Flexural Strength loading level for [90°] and $\sim$ 50% for [0°] specimens. R was chosen non-zero to prevent loss of contact between the cross-head and specimens during the test. The support span was set for 110 mm for [0°] and 140 mm for [90°] specimens. The maximum deflection was set to 12 mm.

The home-made flexural fatigue test machine is shown in Fig. 6.3.

Figure 6.3: Flexural fatigue test machine.

To characterize flexural properties of post-fatigue specimens, three-point bending tests were performed on the composite samples following the ASTM D790 standard using a screw-driven

mechanical loading frame (MTS) with a 1 kN load cell (see Fig. 6.4). The three-point bending test determines the flexural modulus and flexural strength of samples. Support geometry followed ASTM D790, with the support span set to 60 mm, resulting in a span/thickness ratio of ~ 43. A cross-head rate of 4.25 mm/min was used to produce a strain rate of 0.01 mm/min.

Figure 6.4: MTS machine.

6.5 Result and discussion

The surface of coated samples before conditioning and after 600, 1200 and 2200 combined UV and moisture exposures is given in Fig. 6.5

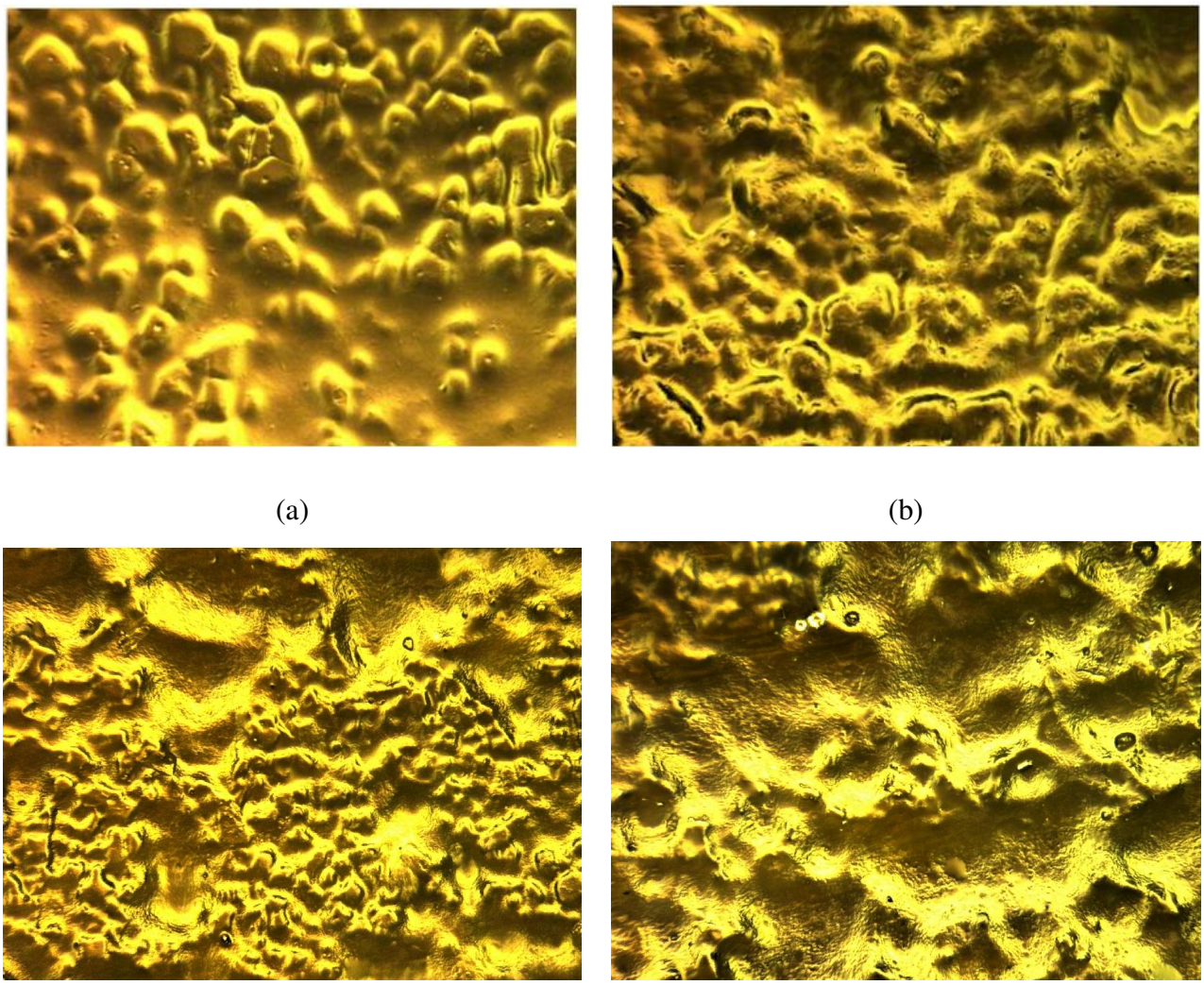

(a) (b)

(c) (d)

Figure 6.5: Coated surface after :(a) 0 hours exposure (b) 600 hours exposure

(c) 1200 hours exposure (d) 2200 hours exposure

Gel coat loses its appearance and gloss during combined exposure to UV radiation and moisture. The coating system is mostly damaged after 1200 hours of exposure time, which implies that the coating system may not be effective in protecting composite materials after long-term exposure. This can be examined by measuring the mechanical properties of composite specimens through a

wide range of exposure time.

The degradation in the flexural modulus and flexural strength of coated and uncoated carbon fibres/vinyl ester composites with 0° fiber orientation are given in Fig. 6.6 and Fig. 6.7.

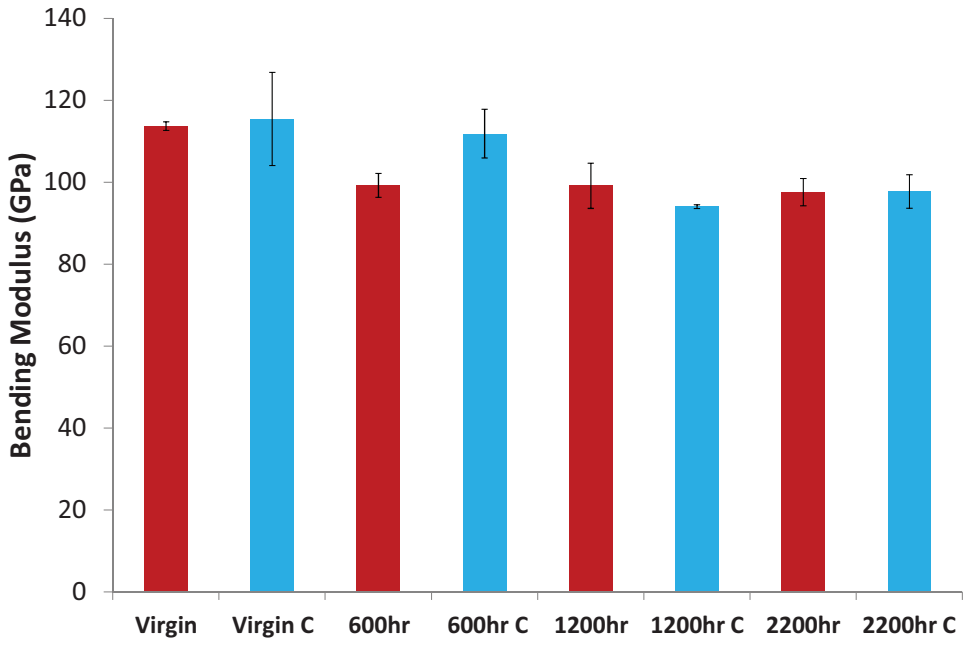

Figure 6.6: Flexural modulus of virgin and coated [0°] samples after different exposure times

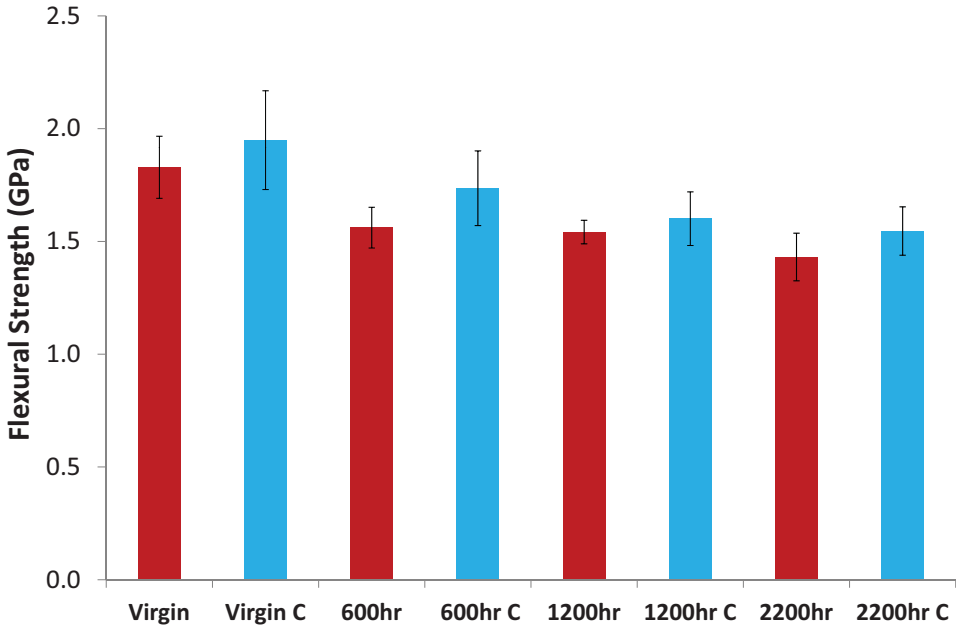

Figure 6.7: Flexural strength of virgin and coated [0°] samples after different exposure times

The longitudinal flexural modulus and longitudinal flexural strength of coated samples were decreased gradually due to the combined exposure of UV radiation and moisture. The loss in flexural properties of uncoated samples are faster than coated specimens. This indicates that the coating system is effective in shielding composite materials against the environmental elements during short-time exposure. For longer exposure times, the protective effect of the coating system is minimal. The same behaviour is observed for the flexural strength of specimens with [45°] and [90°] fiber directions, as shown in Fig. 6.8 and Fig. 6.9.

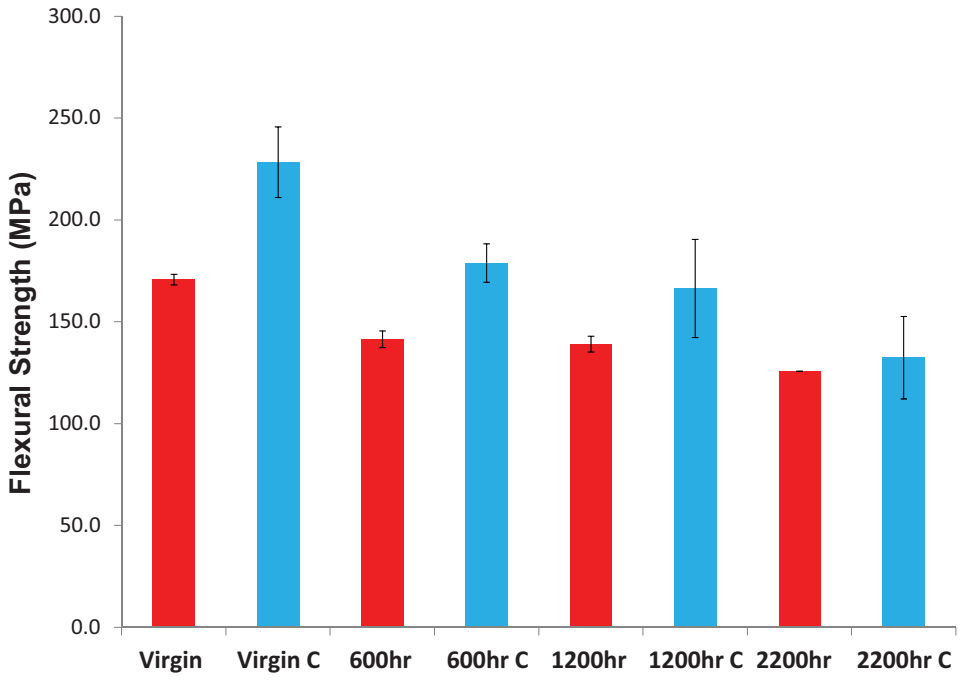

Figure 6.8: Flexural strength of virgin and coated [45°] samples after different exposure times

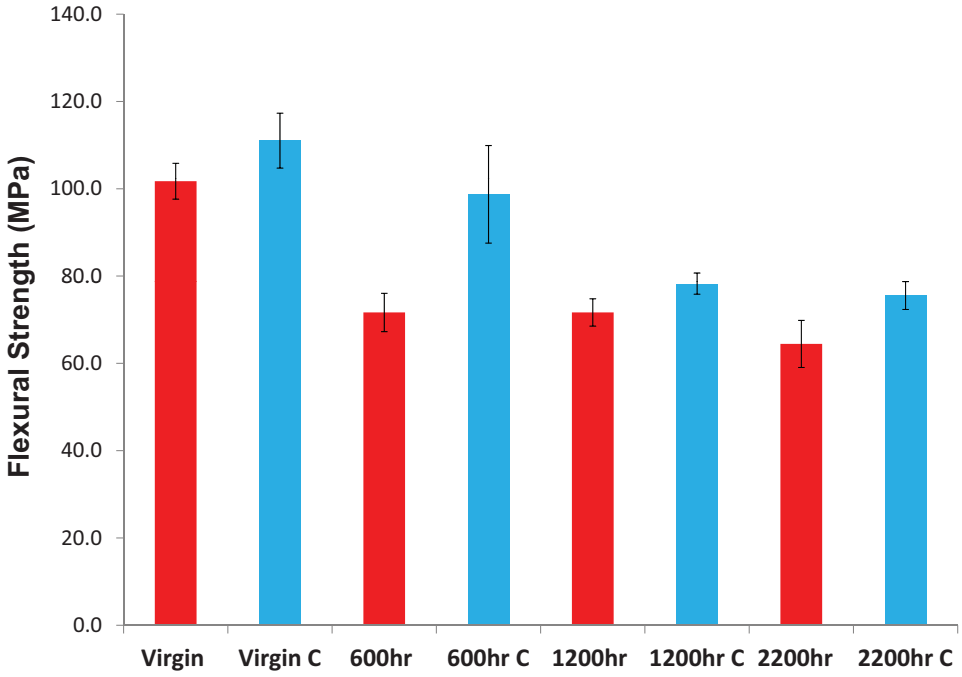

Figure 6.9: Flexural strength of virgin and coated [90°] samples after different exposure times

To investigate the combined effect of flexural fatigue loading and environmental exposure, the specimens are cyclically subjected to 4000 loading cycles followed by 24 hours of combined exposure to UV radiation and moisture. The overall exposure time is 300 hours and the total number of loading cycles is 50000. The tests were performed on coated and uncoated specimens with 0° and 90° fiber orientations. Fig. 6.10 and Fig. 6.11 show the synergistic effects of fatigue loading and environmental exposure on longitudinal flexural properties of uncoated and coated specimens. It can be observed that for both cases, the fatigue damage is accelerated by the environmental exposure. It should be noted that applying gel coat on composite specimens has minimal effects on protecting composite specimens exposed to synergistic fatigue loading and marine environments, even for a short-term exposure (300 hours one-side exposure).

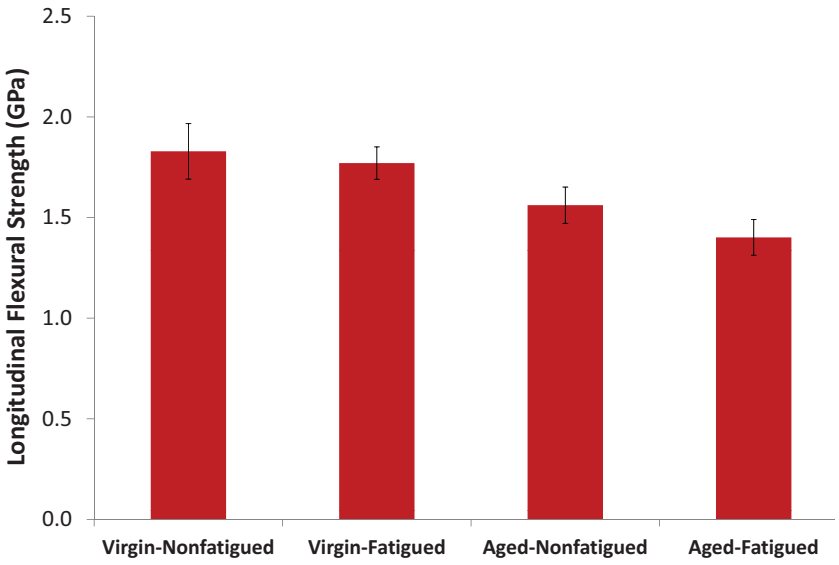

Figure 6.10: Flexural strength of uncoated virgin and aged [0°] samples before and after fatigue loading

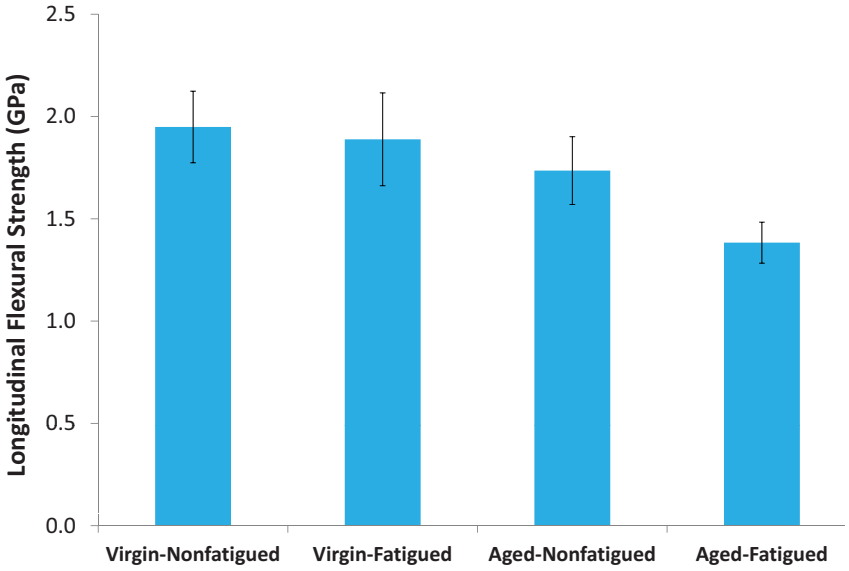

Figure 6.11: Flexural strength of coated virgin and aged [0°] samples before and after fatigue loading

Fig. 6.12 and Fig. 6.13 show the combined effects of fatigue loading and environmental exposure on transverse flexural properties of uncoated and coated specimens. Similar to the longitudinal flexural property, an accelerated fatigue damage can be observed in the transverse flexural property of unidirectional carbon fiber-vinylester composite laminates in the presence of the marine environmental elements.

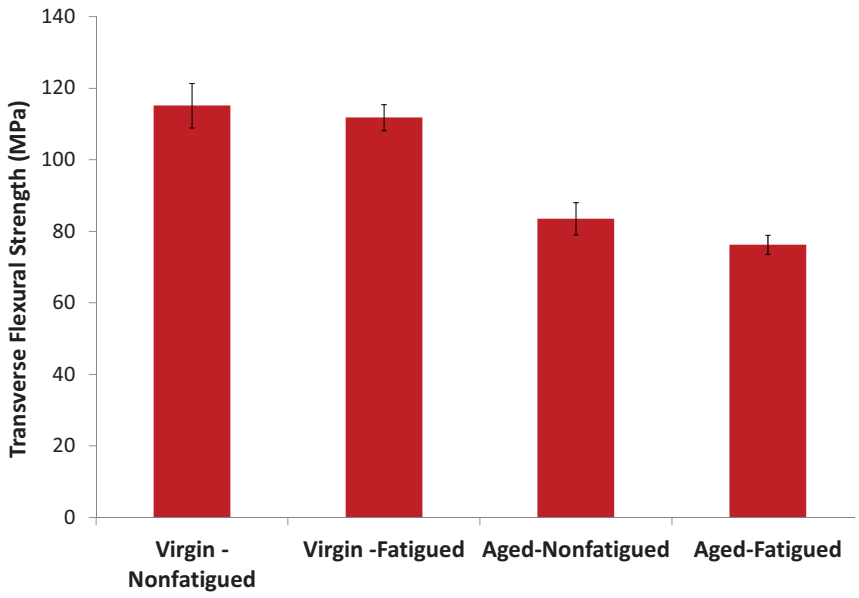

Figure 6.12: Flexural strength of uncoated virgin and aged [90°] samples before and after fatigue loading

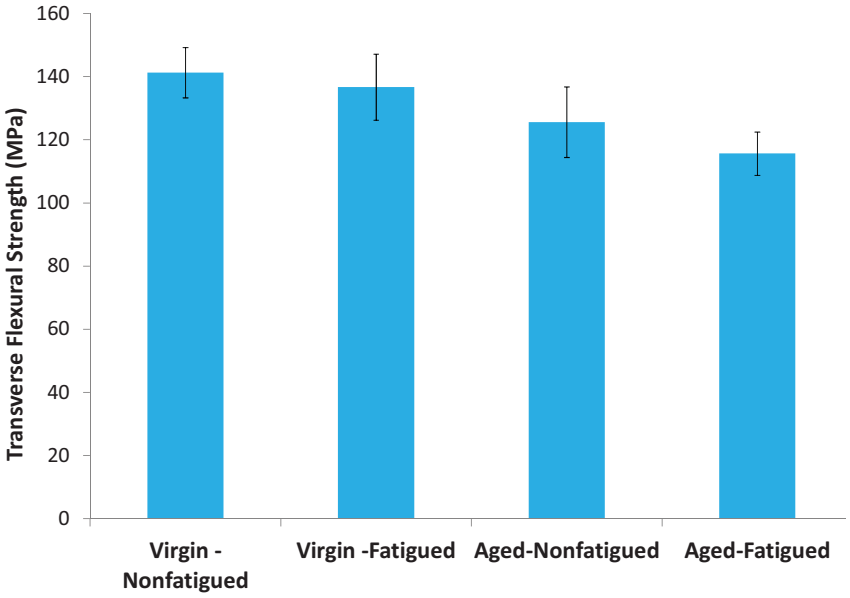

Figure 6.13: Flexural strength of coated virgin and aged [90°] samples before and after fatigue loading

6.6 Conclusion

In the marine industry, coating is being used to shield composite materials from environmental exposure. Our results demonstrate that coating is very effective for short-term exposure to marine environments, but less effective for long-term exposure. The synergistic effects of fatigue loading and environmental conditions can deteriorate the mechanical properties of carbon fiber-vinyl ester composites during a short exposure time, even in the presence of coating.

Bibliography

[1] T. S. Grant and W. L. Bradley, "In-Situ Observations in SEM of Degradation of Graphite/Epoxy Composite Materials due to Seawater Immersion," Journal of Composite Materials, Vol. 29, pp. 852-867, 1995.

[2] F. McBagonluri, K. Garcia, M. Hayes, K. N. E. Verghese, J. J. Lesko , "Characterization of fatigue and combined environment on durability performance of glass/vinyl ester composite for infrastructure applications," International Journal of Fatigue, Vol. 22, pp. 53-64, 2000.

[3] Y. Weitsman, M. Elahi, "Effects of fluids on the deformation, strength and durability of polymeric composites-an overview," Mech Time-Dependent Mater, Vol. 4, pp. 107-126, 2000.

[4] Y. Weitsman, A. In Kelly, C. Zeben (eds.), "Effects of fluids on polymeric composites-a review," Comprehensive Composite Materials, R. Talreja , J.-A.E. Manson (eds.), Polymeric Matrix Composites, Elsevier, Amsterdam, Vol. 2, pp. 369-401, 2000.

[5] Y. Guo, Y. Weitsman, "A correlation between fluid-induced damage and anomalous fluid sorption in polymeric composites," Compos Sci Technol, Vol. 62, pp. 889-908, 2002.

[6] J. P. Komorowski, "Hygrothermal effects in continuous fibre reinforced composites. Part I: Thermal and moisture diffusion in composite materials," National Aeronautical Establishment, National Research Council, Canada. Aeronautical Note NAE-AN-4, NRC No. 20974; January 1983.

[7] Ricky S.C. Woo, Yanghai Chen, Honggang Zhu, Jing Li, Jang-Kyo Kim, Christopher K.Y. Leung, "Environmental degradation of epoxyorganoclay nanocomposites due to UV exposure. Part I: Photo-degradation," Composites Science and Technology, Vol. 67, pp. 34483456, 2007.

[8] Ricky S.C. Woo, Honggang Zhu, Christopher K.Y. Leung, Jang-Kyo Kim, "Environmental degradation of epoxy-organoclay nanocomposites due to UV exposure: Part II residual mechanical properties," Composites Science and Technology, Vol. 68, pp. 2149-2155, 2008.

[9] Andrew W. Signor, Mark R. VanLandingham, Joannie W. Chin, "Effects of ultraviolet radiation exposure on vinyl ester resins: characterization of chemical, physical and mechanical damage," Polymer Degradation and Stability, Vol. 79, pp. 359-368, 2003.

[10] W.B. Liau and F. P. Tseng, "The Effect of Long-Term Ultraviolet Light Irradiation on Polymer Matrix Composites," Vol. 19, pp. 440-445, 1998.

[11] B. Ranby and J.F. Rabek, "Photodegradation, Photo-Oxidation and Photostabilization of Polymers," John Wiley and Sons, London, 1975.

[12] A. Blaga and R.S. Yamasaki, Journal of Materials Science, Vol. 8, pp. 654-666, 1973.

[13] J.W. Chin, T. Nguyen and K. Aouadi, "Effects of environmental exposure on Fiber-Reinforced Plastic (FRP) materials used in construction," Journal of Composites Technology and Research, Vol. 19, pp. 205-213, 1997.

[14] Bhavesh G. kumar, Raman P. Singh and Toshio Nakamura, "Degradation of Carbon Fiber-reinforced Epoxy Composites by Ultraviolet Radiation and Condensation," Journal of Composite Materials, Vol. 36, No. 24, pp. 2713-2733, 2002.

[15] Raman P. Singh, Mikhail Khaitb, Suraj Zunjarrao, Chad S. Korach, and Gajendra Pandey, "Environmental Degradation and Durability of Epoxy/Clay Nanocomposites," Journal of Nanomaterials, Vol. 2010, ID:352746, 2010.

[16] Korach C.S., Liao H.T., Wu D., Feka P., Chiang F.P. "Combined Effects of Moisture and UV Radiation on the Mechanics of Carbon Fiber Reinforced Vinylester Composites," in Proceedings of 2012 Society of Experimental Mechanics International Congress XII, Costa Mesa, CA, USA, 2012.

[17] C.S. Korach and F.P. Chiang, "Characterization of Carbon Fiber-Vinylester Composites Exposed to Combined UV Radiation and Salt Spray," in Proceedings of the 15th European Conference on Composite Materials, Venice, Italy, 2012.

[18] Bernard Budiansky, John W. Hutchinson and Anthony G. Evanst, "Matrix fracture fiber-reinforced ceramics," Journal of the Mechanics and physics of solids, Vol. 34, No. 2, pp. 167-189, 1986.

[19] Yu-Chen Gao, Yiu-Wing Mai and Brian Cotterell, "Fracture of fiber-reinforced materials," Journal of Applied Mathematics and Physics, Vol. 39, 1988.

[20] F. Pars, E. Correa, J. Canas, "Micromechanical view of failure of the matrix in fibrous composite materials," Composites Science and Technology, Vol. 63, pp. 1041-1052, 2003.

[21] Federico Pars, Elena Correa and Vladislav Mantic, "Kinking of Transversal Interface Cracks Between Fiber and Matrix," Journal of Applied Mechanics, Vol. 74, pp. 703-716, 2007.

[22] F. Paris, J.C. Cano and J. Varna, "The fiber-matrix interface crack - A numerical analysis using Boundary Elements," International Journal of Fracture, Vol. 82, pp. 11-29, 1996.

[23] E.S. Folias, "On the Prediction of Failure at a Fiber/Matrix Interface in a Composite Subjected to a Transverse Tensile Load," Journal of Composite Materials, Vol. 26, 1991.

[24] Z.C. Xia, R.R. Carr and J.W. Hutchinson, "Transverse Cracking in Fiber-Reinforced Brittle Matrix," Cross-Ply Laminates, Acta Metall. Mater., Vol 41, No. 8, pp. 2365-2376, 1993.

[25] D.C. Phillips, "The fracture energy of carbon-fibre reinforced glass," Journal of Material Science, Vol. 7, pp. 1175-1191, 1972.

[26] R.W. Davidge and G. Tappin, ibid3, 165, 1968.

[27] F. Erdogan, "Fracture mechanics of functionally graded materials," Composite engineering, Vol. 5, No.7, pp. 753-770, 1995.

[28] G. Anlas, M. H. Santare and J. Lambros, "Numerical Calculation of Stress Intensity Factors in Functionally Graded Materials," International Journal of Fracture, Vol. 104, pp. 131-143, 2000.

[29] Pei Gu and R.J. Asaro, "Cracks in functionally graded materials," Int. J. Solid Structures, Vol. 34, No. 1, pp. l-17, 1997.

[30] Z.H. Jin and R.C. Batra, "Some basic fracture mechanics concepts in functionally graded materials," J. Mech. Phys. Solid., Vol. 44, No. 8, pp. 1221-1235, 1996.

[31] J. Yang, "Fatigue and residual strength degradation for graphite/ epoxy composite under tension-compression cyclic loading," J. Compos. Mater., Vol. 12, No.1, pp. 19-39, 1978.

[32] N. Himmel, M. Kienert, M. Maier, "Fatigue characterization of general purpose thermoplastic composites subject to elementary mechanical loading," In: A.H. Cardon, H. Fukuda, K. Reifsnider, editors. Progress in durability analysis of composite systems. Rotterdam: A.A. Balkema Publisher, pp. 81-86, 1995.

[33] B. Harris, N. Gathercole, H. Reiter, T. Adam, "Constant-stress fatigue response and life-prediction for carbon-fiber composites," In: A.H. Cardon, H. Fukuda, K. Reifsnider, editors. Progress in durability analysis of composite systems. Rotterdam: A.A. Balkema Publisher, pp. 63-74, 1995.

[34] H.G. Halverson, W.A. Curtin, K.L. Reifsnider, "Fatigue life of individual composite specimens based on intrinsic fatigue behavior," Int J Fatigue, Vol. 19, No. 5, pp. 269-77, 1997.

[35] K.L. Reifsnider, "Damage and damage mechanics, Fatigue of composite materials," Ed. by K.L. Reifsnider, Vol. 4, pp. 11-77, 1990.

[36] S.T. Lin, Z. Feng and R.E. Rowlands, "Thermoelastic Determination of Stress Intensity Factors in Orthotropic Composites using the J-Integral," Engineering Fracture Mechanics, Vol. 56, No. 4, pp. 579-592, 1997.

[37] Li-Cheng Guo, "Modeling method for a crack problem of functionally graded materials with arbitrary propertiespiecewise-exponential model," International Journal of Solids and Structures, Vol. 44, pp. 6768-6790, 2007.

[38] Jeong-Ho Kim, Glaucio H. Paulino, "Mixed-mode fracture of orthotropic functionally graded materials using finite elements and the modified crack closure method," Engineering Fracture Mechanics, Vol. 9, pp. 1557-1586, 2002.

[39] R. Talreja, "Fatigue of composite materials: damage mechanisms and fatigue-life diagrams," Proceedings of the Royal Society of London. Series A, Mathematical and Physical Sciences, Vol. 378, No. 1775, pp. 461-475, 1981.

[40] P.T. Curtis, "The fatigue of organic matrix composite materials," In: Partridge I.K., editor. Advanced composites, London: Elsevier Science, pp. 331-67, 1989.

[41] P. T. Curtis, "The fatigue behaviour of fibrous composite materials, Journal of Strain Analysis," Vol. 24, No. 4, pp. 235-44, 1989.

[42] Hai C. Tang, Tinh Nguyen, Tze-jer Chuang, Joannie Chin, H. Felix Wu and Jack Lesko, "fatigue model for fiber-reinforced polymeric composites, Journal of Materials in Civil Engineering," Vol. 12, No. 2, pp. 97-104, 2000.

[43] Mahmood M. Shokrieh and Larry B. Lessard, "Multiaxial fatigue behaviour of unidirectional plies based on uniaxial fatigue experiments - I. Modelling, Int. J. Fatigue," Vol. 19, No. 3, pp. 201-207, 1997.

[44] J.N. Yang, D.L. Jones, S.H. Yang and A. Meskini, "A Stiffness Degradation Model for Graphite/Epoxy Laminates," Vol. 24, 1990.

[45] H.A. Whitworth, "A stiffness degradation model for composite laminates under fatigue loading," Composite Structures, Vol. 40, No. 2, pp. 95-101, 1998.

[46] T.P. Philippidis , A.P. Vassilopoulos, "Fatigue design allowables for GRP laminates based on stiffness degradation measurements," Composites Science and Technology, Vol.60, pp. 2819-2828, 2000.

[47] H. Mao and S. Mahadevan, "Fatigue damage modelling of composite materials, Composite Structures," Vol. 58, pp. 405-410, 2002.

[48] T. Adam, R.F. Dickson, C.J. Jones, H. Reiter and B. Harris, "A Power Law Fatigue Damage Model for Fibre-Reinforced Plastic Laminates," Journal of Mechanical Engineering Science, Vol. 200, No. 3, pp. 155-166, 1986.

[49] Alireza Shirazi A. Varvani-Farahani, "A Stiffness Degradation Based Fatigue Damage Model for FRP Composites of $(0/\theta)$ Laminate Systems," Applied Composite Materials, Vol. 17, pp. 137-150, 2010.

[50] S. Subramanian, K.L. Reifsnider, W.W. Stinchcomb, "A Cumulative damage model to predict the fatigue life of composite laminates including the effect of a fiber-matrix interphase," Int J Fatigue, Vol. 17, No. 5, pp. 343-51, 1995.

[51] S. Subramanian, J.S. Elmore, W.W. Stinchcomb and K.L. Reifsnider, "The influence of fiber-matrix interphase on the long-term behavior of graphite/epoxy composites," presented at the 12th Symposium on Composite Materials: Testing and Design, Montreal, Quebec, Canada, 16-17 May 1994.

[52] M. Kawai and H. Suda, "Effects of Non-Negative Mean Stress on the Off-Axis Fatigue Behavior of Unidirectional Carbon/Epoxy Composites at Room Temperature," Journal of Composite Materials, Vol. 38, No. 10, PP. 833-854, 2004.

[53] M. Kawai, S. Yajima, A. Hachinohe and Y. Takano, "Off-Axis Fatigue Behavior of Unidirectional Carbon Fiber-Reinforced Composites at Room and High Temperatures," Journal of Composite Materials, Vol. 35, No. 7, PP. 545-576, 2001.

[54] E. Kristofer Gamstedta, Lars A. Berglund, Ton Peijs, "Fatigue mechanisms in unidirectional glass-fibre-reinforced polypropylene," Composites Science and Technology, Vol.59, pp. 759-768, 1999.

[55] E.K. GAMSTEDT and R. TALREJA, "Fatigue damage mechanisms in unidirectional carbon-fibre-reinforced plastics, Journal of Materials Science," Vol. 34, pp. 2535-2546, 1999.

[56] A. Varvani-Farahani, H. Haftchenari, M. Panbechi, "A fatigue damage parameter for life assessment of off-axis unidirectional glass fiber-reinforced composites," J. Compos. Mater, Vol. 40, No. 18, pp. 1659-1669, 2006.

[57] Jayantha A. Epaarachchi, Philip D. Clausen, "An empirical model for fatigue behavior prediction of glass fibre-reinforced plastic composites for various stress ratios and test frequencies," Composites: Part A, Vol. 34, pp. 313-326, 2003.

[58] M. Salvia, L. Fiore, P. Fournier and L. Vincent, "Flexural fatigue behaviour of UDGFRP experimental approach," Int. J. Fatigue, Vol. 19, No. 3, pp. 253-262, 1997.

[59] M. Salvia L. Vincent, "Modelling of Flexural Fatigue Behaviour in UD Glass-Fiber-Reinforced Polymer," Composites Science and Technology, Vol. 56, pp. 797-802, 1996.

[60] G. Belingardi, M.P. Cavatorta and C. Frasca, "Bending fatigue behavior of glass-carbon/epoxy hybrid composites," Composites Science and Technology, Vol. 66, pp. 222-232, 2006.

[61] Yoshiyuki Tomita, Kojiro Morioka, Masayuki Iwasa, "Bending fatigue of long carbon fiber-reinforced epoxy composites," Materials Science and Engineering, A319-321, pp. 679-682, 2001.

[62] W. Van Paepegem, J. Degrieck, "A new coupled approach of residual stiffness and strength for fatigue of fibre-reinforced composites," International Journal of Fatigue, Vol. 24, pp. 747-762, 2002.

[63] Ying Shan, Kin Liao, "Environmental fatigue behavior and life prediction of unidirectional glasscarbon/epoxy hybrid composites," International Journal of Fatigue, Vol. 24, pp. 847-859, 2002.

[64] E. Vauthier, J. C. Abry, T. Bailliezb A. Chateauminois, "Interactions between hygrothermal ageing and fatigue damage in unidirectional glass/epoxy composites," Composites Science and Technology, Vol. 58, PP. 687-692, 1998.

[65] T. Nakamura R.P. Singh P. Vaddadi , "Effects of environmental degradation on flexural failure strength of fiber reinforced composites," Experimental Mechanics, Vol. 46, pp. 257-268, 2006.

[66] J.C. Halpin and S.W. Tsai, "Effects of Environmental Factors on Composite Materials," Report AFML-TR, pp.67-423, 1969.

[67] R.M. Christensen, "Mechanics of Composite Materials," Wiley, New York, 1979.

[68] C.F. Shih, B. Moran and T. Nakamura, "Energy Release Rate along a Three-Dimensional Crack Front in A Thermally Stressed Body," International Journal Fracture, Vol. 30, pp. 79-102, 1986.

[69] P. Gu, M. Dao, R.J. Asaro, "A simplified Method for Calculating the Crack-Tip Feild of Functionally Graded Materials Using the Domain Integral," Transaction of the ASME, Vol. 66, 1999.

[70] O. Da La Osa, V. Alvarez and A. Avazquez, "Effect of Hygrothermal History on Water and Mechanical Properties of Glass/Vinylester Composites," Journal of Composite Materials, Vol. 40, issue 22, pp. 2009-2023, 2006.

[71] ASTM D790, "Standard Test Method for Flexural Properties of Unreinforced and Reinforced Plastics and Electrical Insulating Materials," West Conshohocken, PA., 2000.

[72] G.V. Galdorisi and S.C. Truver, "The ZUMWALT-Class Destroyer: A Technology "Bridge" Shaping the Navy after Next," DTIC Document 2010.

[73] E.M. Soliman, M.P. Sheyka, and M.R. Taha, "Low-velocity impact of thin woven carbon fabric composites incorporating multi-walled carbon nanotubes," International Journal of Impact Engineering, Vol. 47, pp. 39-47, 2012.

[74] A. Mouritz, E. Gellert, P. Burchill, and K. Challis, "Review of advanced composite structures for naval ships and submarines," Composite structures, vol. 53, pp. 21-42, 2001.

[75] Jason Lavroff, Michael R. Davis ; Damien S. Holloway, Giles Thomas, "The Effect of Slamming and Whipping on the Fatigue Life of a High-speed Catamaran," Australian Journal of Mechanical Engineering, Vol. 3, 2006.

[76] Guoyang Jiao, "Probabilistic prediction of extreme stress and fatigue damage for ships in slamming conditions," Marine Structures, Vol. 9, pp. 759-785, 1996.

[77] H. Du Plessis, "Fibreglass Boats: Construction, Gel Coat, Stressing, Blistering, Repair, Maintenance," AC Black, 2010.

[78] J. Lemaitre and J.-L. Chaboche, "Mechanics of solid materials," London: Cambridge University Press, 1990.

[79] L. Ye, "On fatigue damage accumulation and material degradation in composite materials," Compos. Sci. and Technol., Vol. 36, pp. 339-350, 1989.

[80] A. Thionnet and J. Renard, "Laminated composites under fatigue loading: A damage development law for transverse cracking," Compos. Sci. and Techno., Vol. 52, pp. 173-181, 1994.

[81] E.G. Wolff, "Moisture effects on polymer matrix composites," Sampe Journal, Vol. 29, pp. 11-19, May-June 1993.

[82] C.S. Korach, A. Afshar, H.-T. Liao, and F.-p. Chiang, "Comparison of Sea Water Exposure Environments on the Properties of Carbon Fiber Vinylester Composites," in Challenges In Mechanics of Time-Dependent Materials and Processes in Conventional and Multifunctional Materials, Vol. 2, ed: Springer, pp. 139-144, 2014.

[83] W. Chu and V.M. Karbhari, "Effect of water sorption on performance of pultruded e-glass/vinylester composites," Journal of materials in civil engineering, Vol. 17, pp. 63-71, 2005.

[84] M.A. Abanilla, Y. Li, and V.M. Karbhari, "Durability characterization of wet layup graphite/epoxy composites used in external strengthening," Composites Part B: Engineering, Vol. 37, pp. 200-212, 2006.

[85] V.M. Karbhari and M.A. Abanilla, "Design factors, reliability, and durability prediction of wet layup carbon/epoxy used in external strengthening," Composites Part B: Engineering, Vol. 38, pp. 10-23, 2007.

[86] D. Lefebvre, K. Takahashi, A. Muller, and V. Raju, "Degradation of epoxy coatings in humid environments: the critical relative humidity for adhesion loss," Journal of adhesion science and technology, Vol. 5, pp. 201-227, 1991.

[87] C. Au and O. Bykztrk, "Peel and shear fracture characterization of debonding in FRP plated concrete affected by moisture," Journal of Composites for Construction, Vol. 10, pp. 35-47, 2006.

[88] N.F. Grace and S. Singh, "Durability evaluation of carbon fiber-reinforced polymer strengthened concrete beams: experimental study and design," ACI Structural Journal, Vol. 102, pp. 40-53, 2005.

[89] B. Ray, "Temperature effect during humid ageing on interfaces of glass and carbon fibers reinforced epoxy composites," Journal of Colloid and Interface Science, Vol. 298, pp. 111-117, 2006.

[90] M.J. Chajes, T.A. Thomson Jr., and C.A. Farschman, "Durability of concrete beams externally reinforced with composite fabrics," Construction and building materials, Vol. 9, pp. 141-148, 1995.

[91] J. Chin, M. Haight, W. Hughes, and T. Nguyen, "Environmental effects on composite matrix resins used in construction," Proceedings of CDCC 1998, pp. 229-242, 1998.

[92] S. Cao, Z. Wu, and X. Wang, "Tensile Properties of CFRP and Hybrid FRP Composites at Elevated Temperatures," Journal of Composite Materials, Vol. 43, pp. 315-330, 2009.

[93] E. Bozkurt, E. Kaya, and M. Tanoglu, "Mechanical and thermal behavior of non-crimp glass fiber reinforced layered clay/epoxy nanocomposites," Composites Science and Technology, Vol. 67, pp. 3394-3403, 2007.

[94] M. Alexandre and P. Dubois, "Polymer-layered silicate nanocomposites: preparation, properties and uses of a new class of materials," Materials Science Engineering R-Reports, Vol. 28, pp. 1-63, 2000.

[95] M. El-Hawary, H. Al-Khaiat, and S. Fereig, "Performance of epoxy-repaired concrete in a marine environment," Cement and Concrete research, Vol. 30, pp. 259-266, 2000.

[96] R. Sen, M. Shahawy, G. Mullins, and J. Spain, "Durability of carbon fiber-reinforced polymer/epoxy/concrete bond in marine environment," ACI Structural Journal, Vol. 96, 1999.

[97] K. Liao, C.R. Schultheisz, D.L. Hunston, and L.C. Brinson, "Long-term durability of fiber-reinforced polymer-matrix composite materials for infrastructure applications: a review," Journal of advanced materials, Vol. 30, pp. 3-40, 1998.

[98] J. Hulatt, L. Hollaway, and A. Thorne, "Preliminary investigations on the environmental effects on new heavyweight fabrics for use in civil engineering," Composites Part B: Engineering, Vol. 33, pp. 407-414, 2002.

[99] M.A. Aiello, M. Frigione, and D. Acierno, "Effects of environmental conditions on performance of polymeric adhesives for restoration of concrete structures," Journal of materials in civil engineering, Vol. 14, pp. 185-189, 2002.

[100] L. Tu and D. Kruger, "Engineering properties of epoxy resins used as concrete adhesives," ACI Materials Journal, Vol. 93, 1996.

[101] L. Malvar, N. Joshi, J. Beran, and T. Novinson, "Environmental effects on the short-term bond of carbon fiber-reinforced polymer (CFRP) composites," Journal of Composites for Construction, Vol. 7, pp. 58-63, 2003.

[102] H.A. Toutanji and W. Gomez, "Durability Characteristics of Concrete Beams Externally Bonded with FRP Composite Sheets," Cement and Concrete Composites, Vol. 19, pp. 351-358, 1997.

[103] V.M. Karbhari, M. Engineer, and D.A. Eckel Li, "On the durability of composite rehabilitation schemes for concrete: use of a peel test," Journal of Materials Science, Vol. 32, pp. 147-156, 1997.

[104] C.K.Y. Leung, H.-G. Zhu, J.-K. Kim, and R.S.C. Woo, "Use of polymer/organoclay nanocomposite surface treatment as water/ion barrier for concrete," Journal of Materials in Civil Engineering, Vol. 20, pp. 484-492, 2008.

[105] V.M. Karbhari, J. Rivera, and J. Zhang, "Low-temperature hygrothermal degradation of ambient cured E-glass/vinylester composites," Journal of Applied Polymer Science, Vol. 86, pp. 2255-2260, 2002.

[106] V.M. Karbhari, J.W. Chin, D. Hunston, B. Benmokrane, T. Juska, R. Morgan, J.J. Lesko, U. Sorathia and D. Reynaud, "Durability gap analysis for fiber-reinforced polymer composites in civil infrastructure," Journal of Composites for Construction, Vol. 7, pp. 238-247, Aug 2003.

[107] A. Haque, M. Shamsuzzoha, F. Hussain, and D. Dean, "S2-glass/epoxy polymer nanocomposites: Manufacturing, structures, thermal and mechanical properties," Journal of Composite Materials, Vol. 37, pp. 1821-1837, 2003.

[108] W. Daud, H.E. N. Bersee, S.J. Picken, and A. Beukers, "Layered silicates nanocomposite matrix for improved fiber reinforced composites properties," Composites Science and Technology, Vol. 69, pp. 2285-2292, Nov 2009.

[109] W. Chu, L.X. Wu, and V.M. Karbhari, "Durability evaluation of moderate temperature cured E-glass/vinylester systems," Composite Structures, Vol. 66, pp. 367-376, 2004.

[110] R. H. Jones, Environmental effects on engineered materials: CRC Press, 2001.

[111] Cezar Capanescu, Corneliu Cincu, "Evaluation of UV Inhibitors in Polyester Gelcoats," Journal of Advances in Polymer Technology, Vol. 22, No. 4, pp. 365-372, 2003.

[112] "Practice for Operating Light-and Water-Exposure Apparatus (Fluorescent UV-Condensation Type) for Exposure of Nonmetallic Materials," (Withdrawn 2000).

[113] Elisabete Almeida, Teresa C. Diamantino, Orlando de Sousa, "Marine paints: The particular case of antifouling paints, physical and mechanical damage," Progress in Organic Coatings, Vol. 59, pp. 2-20, 2007.

[114] X.F. Yang, C. Vang, D.E. Tallman, G.P. Bierwagen, S.G. Croll, S. Rohlik, "Weathering degradation of a polyurethane coating, Polymer Degradation and Stability, Vol. 74, pp. 341-351, 2001.

[115] Elaine Armelin, Ramon Oliver, Francisco Liesa, Jose I. Iribarren , Francesc Estrany, Carlos Aleman, "Marine paint fomulations: Conducting polymers as anti-corrosive additives," Progress in Organic Coatings, Vol. 59, pp. 46-52, 2007.

[116] http://www.sherwin-williams.com

[117] Peter Davies, Guy Evrard, "Accelerated ageing of polyurethanes for marine applications, Polymer Degradation and Stability," Vol. 92, pp. 1455-1464, 2007.

[118] "Selecting and Sourcing Marine Coatings," A JPCL eBook, Technology Publishing Company, 2012.

[119] http://www.seahawkpaints.com

[120] J.A. Nairn, "Fracture mechanics of unidirectional composites using the shear-lag model model II: experiment, Journal of Composite Materials," Vol. 22, 1988.

Appendix A

$$A = \sum_{k=1}^{N} \bar{Q}(z_{k+1} - z_k)$$
$$B = \frac{1}{2} \sum_{k=1}^{N} \bar{Q}(z_{k+1}^2 - z_k^2)$$
$$D = \frac{1}{3} \sum_{k=1}^{N} \bar{Q}(z_{k+1}^3 - z_k^3) \tag{A.1}$$

where

$$\bar{Q} = T^{-1} \left[Q\right] T \tag{A.2}$$

T and Q can be defined as

$$T = \begin{bmatrix} c^2 & s^2 & 2sc \\ s^2 & c^2 & -2sc \\ -sc & sc & c^2 - s^2 \end{bmatrix} \tag{A.3}$$

and

$$Q = \begin{bmatrix} Q_{11} & Q_{12} & 0 \\ Q_{12} & Q_{22} & 0 \\ 0 & 0 & G_{12} \end{bmatrix} \tag{A.4}$$

where
$c = \cos\theta \; s = \sin\theta$
and
$Q_{11} = \frac{E_L}{1 - v_{LT} v_{TL}}$
$Q_{22} = \frac{E_T}{1 - v_{LT} v_{TL}}$
$Q_{12} = \frac{v_{TL} E_L}{1 - v_{LT} v_{TL}} = \frac{v_{LT} E_T}{1 - v_{LT} v_{TL}}$

Appendix B

The J integral can be expressed as

$$J = \lim_{\Gamma \to 0} \int_{\Gamma} (W_{1j} - \sigma_{ij} u_{j,1}) n_i dC \tag{B.1}$$

where Γ is a contour integral path, which starts from the lower face of the crack and ends at the upper face of it. n_j is outward normal to the path and W is the strain energy inside the path.

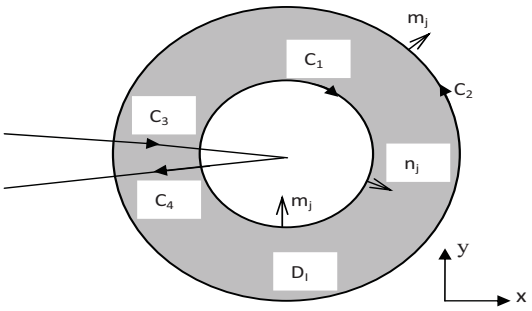

Figure B.1: A simply connected domain around the crack tip

Instead of calculating the contour integral directly , it is possible to write it in the form of a boundary integral and solve it numerically using:

$$J = \int_{C} (\sigma_{ij} u_{i,1} - W_{1j}) q m_j ds \tag{B.2}$$

where C or $C_1 + C_2 + C_3 + C_4$ is the boundary of D_I. m_j is normal to D_I. $m_j = -n_j$ on C_1 and $m_j = n_j$ on C_2. q is a function that smoothly changes from unity on C_1 to zero on C_2.

Assuming the material property changes in the direction of the crack growth, the divergence theorem Eq. B.2 can be written as:

$$J = \int_{D_I} (\sigma_{ij} u_{i,1} - W \delta_{1j}) q_{,j} dD - \int_{D_I} (W_{,1} q dA) \tag{B.3}$$

The second term shows the presence of non-homogeneity, as strain energy density changes in the x direction. The computed J integral is not sensitive to the function q as long as q has the mentioned values on boundaries C_1 and C_2 [68]. q can be defined within an element as:

$$q = \sum_{i=1}^{n} N_i q_i \tag{B.4}$$

where N_i denotes the shape of functions and n is the number of nodes in each element. q_i is the value of q in each node of the element. Taking the derivative of q, with respect to global coordinates, x_i, yields

$$\frac{\partial q}{\partial x_i} = \sum_{i=1}^{n} \sum_{k=1}^{2} \frac{\partial N_i}{\partial \eta_i} \frac{\partial \eta_i}{\partial x_i} \tag{B.5}$$

where η_i is the local coordinate in isoperimetrical space. To obtain the integral in Eq. (B.5) numerically, its value can be calculated at the Gauss integration points [69]

$$J = \sum_{D_I} \sum_{m=1}^{n} \{[(\sigma_{ij} u_{i,1} - W \delta_{1j}) q_{,j} - W_{,1} q] det(\frac{\partial x_k}{\partial \eta_k})]\}_m w_m \tag{B.6}$$

As aforementioned, q is a smooth function from zero on C_1 to unity on C_2. By selecting small elements around the crack tip (about 10^{-2} of the crack length), the term $q_{,j}$ emerges much larger than the term q in the Eq. (B.6). This leads to a reduction in the effect of the additional term in the J integral expression due to non-homogeneity of the system.